NORTHWESTERN UNIVERSITY

Double Phase Slips and Bound Defect Pairs in Parametrically Excited Waves

A DISSERTATION

SUBMITTED TO THE GRADUATE SCHOOL
IN PARTIAL FULFILLMENT OF THE REQUIREMENTS

for the degree of
DOCTOR OF PHILOSOPHY
Field of Applied Mathematics

By
Glen D. Granzow

EVANSTON, ILLINOIS
December 1997

ABSTRACT

Double Phase Slips and Bound Defect Pairs in Parametrically Excited Waves

Glen D. Granzow

Results of numerical simulations of coupled Ginzburg-Landau equations that describe parametrically excited waves are presented. Parametrically excited waves are an example of a pattern forming system. Interest in these systems is due in part to the chaotic dynamics which often develop when the system is sufficiently driven. The particular equations discussed here are studied with the goal of characterizing their solutions (especially those displaying spatio-temporal chaos) and comparing them to earlier results in pattern forming systems.

In one spatial dimension the focus is on a new regime in which the Eckhaus sideband instability does not lead to an overall change in the wavelength via the occurrence of a single phase slip but instead leads to "double phase slips". They are characterized by the phase slips occurring in sequential pairs, with the second phase slip quickly following and negating the first. The resulting dynamics range from transient excursions from a fixed point resembling the dynamics seen in excitable media, to periodic solutions of varying complexity and chaotic solutions. In larger systems localized spatio-temporal chaos is found, where the solution consists of a chaotic region with quiescent regions on each side. The localization is explained using an effective phase diffusion equation which can be viewed as arising from a homogenization of the chaotic state.

In two dimensions the double phase slips are replaced by fluctuating bound defect pairs. To characterize different spatio-temporally chaotic solutions that arise the motion of the defects is traced in detail yielding their life-times, annihilation partners, and distances traveled. In a regime in which in the one-dimensional case the chaotic dynamics are due to double phase slips, the two-dimensional system exhibits an ordered stripe pattern disrupted by the appearance and disappearance of defects. When the parity-breaking instability to traveling waves is approached this order vanishes and the correlation function decays rapidly. In the ordered regime the defects have a typical life-time, whereas in the disordered regime the life-time

distribution is exponential. The probability of large defect loops is substantially larger in the disordered regime.

Contents

List of Figures vi

1 Introduction **1**

1.1 Spatio-Temporal Chaos in Pattern Forming Systems 1

1.2 Parametrically Excited Waves 4

1.3 Highlights of the Dissertation 7

I One-Dimensional system **10**

2 The Model **11**

3 Linear Stability Analysis **14**

4 Phase Slips and Double Phase Slips **21**

5 Dynamics of a Small System **24**

5.1 Transient Solutions 24

5.2 Periodic Solutions 26

5.3 Complex Solutions 35

5.4 Remarks About (Q,b) Space 35

6 Dynamics of a Large System **40**

6.1 Extended Spatio-Temporal Chaos 40

6.2 Localized Spatio-Temporal Chaos 42

6.3 Effective Phase Equation 45

7 Dynamics of a Very Small System **57**

II Two-Dimensional System 64

8 The Model **65**

9 Linear Stability Analysis **67**

10 Defect Pairs and Bound Defect Pairs **73**

11 Ordered and Disordered Defect Chaos **77**

12 Conclusions and Discussion **93**

References **99**

A Amplitude Equations from Symmetries **108**

B Numerical Technique **111**

B.1 Pseudospectral Methods 111

B.2 Runge-Kutta Method 112

B.3 Integrating Factor 113

B.4 Implementation 115

C 2-D Parametrically Excited Wave Program (parallel version) **117**

D Defect Tracking Program **136**

List of Figures

3.1 Linear Stability diagram for $a = -0.05$, $c = -1 + 4i$, $d = 1 + 0.5i$, $s = 0.2$, $g = -1 - 12i$. 16

3.2 The real part of the eigenvalues of the matrix M for $a = -0.05$, $b = 0.2$, $c = -1 + 4i$, $d = 1 + 0.5i$, $s = 0.2$, $g = -1 - 12i$. a) Stable solution, wavenumber $Q = 0.2$. b) Unstable solution, wavenumber $Q = 0.3$. 18

4.1 Space-time diagram illustrating (a) single phase slip observed for small values of the forcing amplitude (e.g. $b = 0.1$), and (b) double phase slip observed for larger values of the forcing amplitude (e.g. $b = 0.6$). 23

5.1 Example values of the forcing amplitude b and wavenumber Q where the three solution types occur. 25

5.2 Phase plane representation of a transient solution involving one double phase slip. The square indicates the initial condition which is the perturbed 5-wave state. The loop is traversed once, with the final state of the solution being the (stable) fixed point indicated by a diamond. ($b = 0.54$, $Q = 5(2\pi)/L = 0.3628$). 27

5.3 Each circle represents the location (in space and time) of a double phase slip for a simple periodic solution ($b = 0.54$, $Q = 5(2\pi)/L = 0.3645$). 29

5.4 Spatial average of the local wavenumber plotted as a function of time for a simple periodic solution ($b = 0.54$, $Q = 5(2\pi)/L = 0.3645$). . . 30

5.5 Phase plane representation of a simple periodic solution ($b = 0.54$, $Q = 5(2\pi)/L = 0.3645$). 31
5.6 Divergence of the period of the simple periodic solutions as the wavenumber Q is decreased ($b = 0.54$). 32
5.7 Location of double phase slips for a periodic solution occurring after a period doubling bifurcation ($b = 0.54$, $Q = 5(2\pi)/L = 0.3653$). . . 33
5.8 Location of double phase slips for $b = 0.81$ and various system sizes; period doubling bifurcation occurs at $L \approx 76.7$. 34
5.9 Location of double phase slips for solutions where a wave of double phase slips propagates through the system. a) $b = 0.54$, $Q = 5(2\pi)/L = 0.3674$; b) $b = 0.81$, $Q = 5(2\pi)/L = 0.4833$. 36
5.10 A complex solution where the double phase slips occur irregularly in space and time ($b = 0.54$, $Q = 5(2\pi)/L = .3692$). 37
5.11 Divergence of the time between the two phase slips which make up a double phase slip as the forcing amplitude is decreased. 38

6.1 Extended spatio-temporal chaos in a large system ($b = 0.6$, $L = 800$): (a) $Q = 50(2\pi)/L = 0.3927$, (b) $Q = 51(2\pi)/L = 0.4006$, (c) Initial wavenumber $Q_0 = 52(2\pi)/L = 0.4084$, after a single phase slip at $t \approx 13000$ the wavenumber is $Q = 0.4006$. 41
6.2 Localized spatio-temporal chaos in a large domain. Each dot represents a double phase slip ($b = 0.6$, $L = 783$, $Q = 47(2\pi)/L = 0.377$). 43
6.3 Temporal evolution of the width of the localized region exhibiting spatio-temporal chaos for two different initial conditions ($b = 0.605$, $Q = 47(2\pi)/L = 0.377$). 44
6.4 Local wavenumber of the time average of $A(X, T)$ for a localized chaotic solution. The local wavenumber in the chaotic region is larger than in the quiescent region. ($b = 0.6$, $L = 783$, $Q = 47(2\pi)/L = 0.377$). 46

6.5 Decay of the magnitude of the coefficient of the time Fourier transform of A corresponding to the frequency ω_0 in the localized advection term v in equations (6.5 ,6.6), for two different values of ω_0 ($b = 0.61$, $L = 800$, $Q = 51(2\pi)/L = 0.4006$, $v_0 = 1.630\omega_0$). 50
6.6 Imaginary part of the ratio of the coefficients of the time Fourier transform of A corresponding to the frequencies $\pm\omega_0$ in the localized advection term v in equations (6.5 ,6.6), for two different values of ω_0 ($b = 0.61$, $L = 800$, $Q = 51(2\pi)/L = 0.4006$, $v_0 = 1.630\omega_0$). 52
6.7 Analytical phase diffusion coefficient D for the stationary solution (solid line) and effective diffusion coefficient $\hat{D}$ for the chaotic solution; Triangles and circles represent numerical results as obtained from α and β (cf. Figures 6.5 and 6.6), the dashed line is the presumed extension of these results ($b = 0.61$). 53
6.8 Space-time diagram shows the real part of a time average of A ($b = 0.61$). a) Effective phase remains almost stationary ($Q = 51(2\pi)/L = 0.4006$). b) Effective phase drifts significantly ($Q = 51(2\pi)/L = 0.4067$). 55
6.9 A set of solutions obtained by incrementally increasing the forcing amplitude b. The extended spatio-temporal chaos breaks up into localized regions before the Eckhaus stability limit is reached ($L = 800$, $Q = 51(2\pi)/L = .4006$). (a) $b = 0.62$, (b) $b = 0.64$, (c) $b = 0.66$. 56

7.1 Phase plane representation including a transient for two types of solutions in a very small system (a) L=11.2, final state is a stationary mixed mode solution; (b) L=11.3, final state is periodic in time. ($a = -0.05$, $b = 1.0$, $c = -1 + 4i$, $d = 1 + 0.5i$, $s = 0.2$, $g = -1 - 12i$) 59

7.2 Final state for the mixed mode solution whose phase plane representation is shown in figure 7.1 a ($L = 11.2$). a) Real and imaginary parts of $A(X)$ (solid symbols) and $B(X)$ (open symbols). b) Magnitude of the Fourier coefficients for either A or B (the magnitudes are equal). 60
7.3 Mixed mode solution for $L = 11.2$ plotted in the complex plane. . . . 61
7.4 Phase plane representations of solutions for $L = 8.0$ to $L = 11.3$. . . 62
7.5 Phase plane representations of solutions for $L = 11.4$ to $L = 12.1$. Note that the scales have changed from the previous figure. 63

9.1 Linear Stability diagram for X direction waves for parameter values $a = -0.05$, $c = -1 + 4i$, $d = d_2 = 1 + 0.5i$, $s = 0.2$, $g = -1 - 12i$. The zig-zag instability reduces the band of stable wavenumbers for $b > 0.15$. 69
9.2 Transitory state which results from an initial condition which is zigzag unstable. Shown is a snapshot of the real part of A. White regions represent high values ($A \approx 0.3$), black regions represent low values ($A \approx -0.3$). The initial condition was vertical rolls perturbed with a small amount of random noise ($b = 0.5$, $Q = 5(2\pi)/L = .2$). 70
9.3 Linearly stable wavevectors for the two-dimensional system. The stable region indicated in Figure 9.1 is a cross section of this volume in the Q, b plane. 71
9.4 Linearly stable wavevectors for standing waves in the two-dimensional system for $b = 0.10, 0.15, 0.20, \ldots, 0.80, 0.85$. The leftmost curve is $b = 0.10$, the smallest closed curve (located near the right end of the figure) is $b = 0.85$. 72

10.1 Standard wavenumber reducing transition in two dimensions. Solid curves represent locations where the real part of the solution is zero. Dashed curves represent locations where the imaginary part of the solution is zero. A *bound defect pair* can be visualized by considering the left column only, progressing from the top to the bottom then returning to the top. 74
10.2 Space-time diagram showing the projection of the location of defects on the x-axis for a simulation of the two-dimensional system. The *loops*, for example the one starting at $x \approx 29$ and $t \approx 2680$, represent bound defect pairs ($b = 1.2$, $L = 62.832$). 76

11.1 Linear stability diagram for $a = 0.25$, $c = -1 + 4i$, $d = 1 + 0.5i$, $s = 0.2$, $g = -1 - 12i$. For details see text. 79
11.2 The real part of the eigenvalues of the matrix M given by equation (3.13) for $a = 0.25$, $b = 0.4$, $c = -1 + 4i$, $d = 1 + 0.5i$, $s = 0.2$, $g = -1 - 12i$, and (unstable) solution wavenumber $Q = 0.45$. Positive growth rates occur for a band of perturbation wavenumbers which is bounded away from zero. 80
11.3 Snapshot of the real part of the wave pattern for $b = 1$ (other parameters as in Figure 11.1). 82
11.4 Snapshot of the real part of the wave pattern for $b = 0.5$ (other parameters as in Figure 11.1). 83
11.5 Time-averaged correlation function of the wave pattern for $b = 1$. The inset shows one-dimensional cuts in the X-direction and Y-direction on a linear scale. The other parameters are as in Figure 11.1 84
11.6 Time-averaged correlation function of the wave pattern for $b = 0.5$. The inset shows a one-dimensional cut in the X-direction of the absolute value of the correlation function on a linear-logarithmic scale. The other parameters are as in Figure 11.1 85

11.7 Relative frequency of defect loops in space-time containing n defect pairs for $b = 1$ (solid squares) and $b = 0.5$ (open squares). The other parameters are as in Figure 11.1 . a) log-log plot, b) linear-log plot. 87
11.8 Relative frequency of defect loops in space-time with life-time τ for $b = 1$ (solid squares) and $b = 0.5$ (open squares). The other parameters are as in Figure 11.1 89
11.9 Relative frequency of defect loops in space-time with extension d_x in the x-direction (top figure) and d_y in the y-direction (bottom figure) for $b = 1$ (solid symbols) and $b = 0.5$ (open symbols). The other parameters are as in Figure 11.1 . The inset in the top figure shows there is a local minimum in the the distribution for $b = 1$ corresponding to half the wavelength of the underlying stripe pattern. 90
11.10 Relative frequency of the number of defects pairs in the system for $b = 1$ (solid symbols) and $b = 0.5$ (open symbols). The other parameters are as in Figure 11.1 91

Chapter 1

Introduction

1.1 Spatio-Temporal Chaos in Pattern Forming Systems

Pattern formation is a striking and interesting phenomenon observed in many physical systems driven far from thermodynamic equilibrium. In addition to parametrically excited waves (which are described in the next section), classic examples include the rolls formed in Rayleigh-Bénard convection when a fluid confined between two horizontal plates is heated from below, the annular Taylor vortices that form in a fluid between rotating concentric cylinders, and rotating spirals (and other patterns) consisting of regions of different chemical concentrations formed in chemical reactions such as the Belousov-Zhabotinsky reaction. A review of pattern forming systems can be found in [15]. Typically, the basic equations that describe these pattern-forming experiments are quite complicated (such as the Navier Stokes equations). However, for pattern-forming systems near onset, the complicated system of equations can often be simplified using asymptotic expansions for small amplitudes. The resulting amplitude equations (e.g. [49, 28]) describe the variation of the pattern on large space and time scales. For example, for plate temperature differences just above the onset of convection, the behavior of the convection rolls in a Rayleigh-Bénard experiment are well described by the Newell-Whitehead-Segel equation [58, 72]

$$\partial_t A = A + (\partial_x - i\partial_y^2)^2 A - |A|^2 A. \tag{1.1}$$

In many systems transitions from simple to chaotic behavior are found when a control parameter (such as the temperature difference in Rayleigh-Bénard convection, the angular velocity of the inner cylinder in Taylor-Couette flow, or the supplied concentration of a particular chemical in a reaction diffusion system) is changed. Studies of chaos began with low-dimensional attractors as found, for instance, in the Lorenz system [48] and have progressed to chaotic behavior in both space and time in spatially extended systems with a large number of degrees of freedom. Examples of extended systems with spatio-temporal chaos which have been studied experimentally include Rayleigh-Bénard convection and variants of this system: convection in a porous medium; convection in a rotating container (which introduces a Küppers-Lortz instability); binary fluid convection systems where a mixture of two fluids are used; and electrohydrodynamic convection where a nematic liquid crystal is driven by an electric field. The Taylor vortex system can also exhibit spatio-temporal chaos as can chemical reaction-diffusion experiments such as the Belousov-Zhabotinsky system. These are just examples of extended systems which exhibit spatio-temporal chaos; this list is not intended to be exhaustive. Most of these systems are discussed in [15] and references therein.

Of particular interest in both experimental and mathematical systems is identifying features that allow the different types of observed chaos to be classified in some way. A well studied example is the complex Ginzburg-Landau equation

$$\partial_t A(x,t) = A + (1+ic_1)\nabla^2 A - (1-ic_3)|A|^2 A, \tag{1.2}$$

for which a number of different chaotic regimes have been reported [74, 1, 22, 10, 50]. These include two-dimensional regimes characterized by fast motion of defects including their pairwise creation and annihilation; regimes where spirals form around the defects and move about regions delineated by shocks; and regimes where regions with many defects appear intermittently on a background of growing spirals. In this context *defect* refers to a location where the magnitude of the solution is zero. Traversing a small closed path that encircles the defect the phase of the solution changes by 2π. Such a defect corresponds to a dislocation where a pair of convection rolls terminate and provides the mechanism for changing the average wavelength in a periodic pattern (this is discussed in more detail in chapter 10). In solutions of the complex Ginzburg-Landau equation (1.2) the defects initiate spirals which appear in regular as well as chaotic solutions. Multiarmed spirals can form if the phase change over the path enclosing the defect is greater than 2π (that is, $\Delta\phi = \pm n 2\pi$, with $n > 1$).

In pattern forming systems in general the word defect refers to a localized disturbance in or at the edges of regions that otherwise approximate well an ideal pattern. Additional examples of defects in two-dimensional patterns include disclinations, target centers, penta-hepta pairs in hexagonal patterns, and grain boundaries. Defects in one-dimensional systems include fronts (where a finite amplitude domain meets a zero amplitude domain), pulses (isolated regions with nonzero amplitude), and domain boundaries (where two different finite amplitude domains meet). Domain boundaries include sources and sinks where traveling waves with opposite directions originate or terminate.

Relevant for the present treatise is the observation that in the complex Ginzburg-Landau equation (and other systems) a distinction can be drawn between a phase-chaotic regime, where there are no defects, and amplitude-chaotic regimes, such as those described above. In one dimension amplitude chaos is characterized by the occurrence of phase slips during which the amplitude of the wave goes to zero and the total phase of the system changes by 2π, that is, a wavelength is inserted or eliminated. In phase chaos there are essentially no phase slips [22, 50] and the system can be described by an equation for the phase of the wave alone [45]. For the complex Ginzburg-Landau equation this phase equation is the Kuramoto-Sivashinsky equation [46]

$$\partial_t \phi = (1 - c_1 c_3)\nabla^2 \phi - \frac{1}{2}(1 + c_1^2)\nabla^4 \phi - (c_1 + c_3)(\nabla\phi)^2, \tag{1.3}$$

which has been the subject of numerous investigations (e.g. [35,32]). Phase equations break down during phase slips so they cannot be used to describe amplitude chaos.

The existence of the phase-chaotic regime in the thermodynamic limit of infinite system size has been questioned and this question remains open to speculation and investigation [22, 50]. Numerical studies of the complex Ginzburg-Landau equation have indicated that there *are* phase-chaotic regimes where no defects occur. However these studies cannot resolve the possibility that the probability of a defect occurring remains nonzero but too small to be realized in the finite simulations.

1.2 Parametrically Excited Waves

In this investigation parametrically excited waves, which are also a classic pattern forming system [25] are considered. Parametrically excited waves arise quite generally in systems exhibiting weakly damped modes that are oscillatory in time and often periodic in space as well, when these modes are forced at twice their natural frequency. While the weakly damped modes are often associated with a Hopf bifurcation, a Hopf bifurcation is not present in every system which can be parametrically excited. A Hopf bifurcation *is* assumed in the derivation of the model equations used in this investigation, however.

Faraday's experiment [25] in which surface waves are formed on a liquid in a vertically oscillated container is probably the most well known example of parametrically excited waves. Stripe, square, and hexagon patterns (e.g. [42]), as well as quasipatterns [21], spirals [36], and chaotic states (e.g. [80, 41, 42]) have all been observed in Faraday experiments with various fluids, forcing amplitudes, and frequencies. Parametrically excited waves have also been observed in magnetic materials (spin waves) [77,23], in electroconvection in nematic liquid crystals [64,17], and in Taylor-Dean flow [78]. The latter two experimental systems undergo a Hopf bifurcation to states that are periodic in space as well as time as is assumed in the amplitude equations described in this dissertation. The Belousov-Zhabotinsky reaction provides an example of a system where a Hopf bifurcation gives rise to a spatially uniform state. Parametric forcing of such a system has been studied using an amplitude equation [12]

$$\partial_t A = (\mu + i\nu)A + (1 + i\alpha)\nabla^2 A - (1 + i\beta)|A|^2 A + \gamma_n (A^*)^{n-1} \qquad (1.4)$$

that is similar to but simpler than the pair of coupled amplitude equations considered here (cf. (2.1,2.2) or (8.2,8.3)). The parameter n in (1.4) is dependent on the forcing frequency; $n = 2$ in the case where the forcing is at approximately twice the Hopf frequency. Remarkably, parametrically excited waves have also been observed in experiments where a container of granular media (similar to sand) is vertically oscillated [81, 52, 53]. In these experiments two dimensional localized states as well as stripes, squares, hexagons, and disordered states have been seen. Incidentally, the name *parametrically* excited waves refers to the imposed variation in one of the parameters in the system, for example the effective gravitational acceleration in Faraday's experiment.

Mathematical treatments of parametrically excited waves include the work of Benjamin and Ursell who did a linear stability analysis of the flat surface of the fluid in a Faraday experiment with an incompressible, inviscid fluid [4]. Writing an expression for the position of the surface of the fluid as a sum of orthogonal eigenfunctions (which depend on the shape of the container) they show that the amplitudes of these normal modes satisfy Mathieu's equation

$$\frac{d^2a}{dt^2} + (p - 2q\cos 2t)a = 0. \tag{1.5}$$

The well known Arnol'd tongues, which represent regions in parameter space with growing solutions of Mathieu's equation, thus give the parameters for which the parametrically excited surface waves arise. The Arnol'd tongues correspond to standing waves with various frequencies with the first tongue corresponding to a wave with half the forcing frequency. Each additional tongue corresponds to a wave whose frequency is an integer multiple of half the forcing frequency. In this inviscid model all of these waves are excited by an arbitrarily small forcing amplitude. Kumar and Tuckermann did a linear stability analysis for a viscous fluid and show that the tongues are modified such that there is a finite forcing for which no waves are excited [43]. For the parameters analyzed in [43] the waves whose frequency is equal to half the forcing frequency is the only mode excited at onset. When the thickness of the viscous boundary layer created at the bottom of the container becomes comparable with the depth of the fluid (this can occur for lower forcing frequencies, smaller fluid depths, or higher viscosities) the harmonic waves or even waves whose frequency is a higher harmonic of half the forcing frequency can be the mode(s) excited at onset [44, 9].

Various boundary conditions and fluid approximations can be considered in the analysis of Faraday's experiment. The goal of such analyses is to understand not only the forcing required to excite the parametrically excited waves but also the nonlinear evolution above onset, including pattern selection and the transition to spatio-temporal chaos. A review of work to 1990 is given in [54]. Important for most of the analyses is that for small viscosity and small deformation of the surface the viscosity may be neglected except in a thin boundary layer at the free surface (e.g. [47]). Kumar and Tuckermann discuss this approximation as applied to the stability analysis of the flat surface in [43] and arrive at a damped Mathieu equation

$$\frac{d^2a}{dt^2} + 2\gamma\frac{da}{dt} + (p - 2q\cos 2t)a = 0 \tag{1.6}$$

(cf. 1.5) whose solution qualitatively agrees with their primary analysis which includes viscosity throughout the fluid. A weakly nonlinear analysis which similarly starts with analysis of an inviscid fluid, subsequently modified to account for the viscous boundary layer (e.g. [55]) results in amplitude equations similar to the model equations considered in this dissertation (2.1,2.2,8.2,8.3), which are derived from symmetries present in the physical system. Ezerski and coworkers [24] use such amplitude equations to explain the observed effects in their (Faraday) experiments using silicon oil. These effects include the threshold for the appearance of square cells seen at onset, their instabilities, and the development of spatio-temporal chaos. A second approach to the weakly nonlinear analysis is to use the "quasi-potential approximation". This approximation incorporates weak viscous effects by introducing modified boundary conditions, which account for the viscous boundary layer, to otherwise inviscid flow. This results in nonlocal amplitude equations [89]. That is, the equations involve integrals over the entire domain as well as derivatives.

1.3 Highlights of the Dissertation

This dissertation describes dynamics arising in numerical simulations of a system of equations that model parametrically excited waves with the focus on solutions which are chaotic in space and time. Part one presents results for a one-dimensional system, part two describes results for the system in two dimensions.

The one-dimensional simulations reveal chaotic solutions which are characterized by a new phenomenon: double phase slips. Double phase slips consist of a sequential pair of phase slips in which the second phase slip quickly follows and negates the first. They are described in chapter 4. In addition to one-dimensional chaotic solutions where double phase slips occur irregularly in space and time, which are described in sections 5.3 and 6.1, transient and periodic solutions involving double phase slips are also described in sections 5.1 and 5.2.

Of central interest in the one-dimensional simulations are localized chaotic states (section 6.2). That is, there are solutions that include a spatial region, bounded by quiescent regions on each side, in which the dynamics are irregular in space and time. Experimentally, a similar phenomenon has been observed in Taylor vortex flow where domains with large turbulent vortices can exist with domains of smaller regular vortices on each side [2]. A localized chaotic state has also been reported in Rayleigh-Bénard convection experiments [11]. In these experiments the underlying state on which there are localized chaotic perturbations is much less ordered than in the Taylor vortex system. Exciting in the present context is that localized spatio-temporal chaos has also recently been found in the Faraday experiment [41, 42]. In the Faraday experiment strongly disordered fluctuating domains can exist simultaneously with a stripe pattern. The localization mechanism in these experimental systems is not well understood. For the system of equations discussed in this treatise the localization can be understood using an effective phase diffusion equation. The validity of this approach is confirmed by explicitly determining the effective phase diffusion coefficient in section 6.3. Some remarks comparing the experimentally observed localized chaotic regimes with the localized spatio-temporal chaos in the numerical simulations are included in chapter 12.

In two dimensions the role of the phase slips is played by the creation and annihilation of defects in the wave pattern. A description of these defects is found in chapter 10.

One possible characterization of the chaotic states in two dimensions is in terms of the dynamics and statistics of the defects. For the complex Ginzburg-Landau equation (1.2) it has been found that the probability distribution for the number of defects observed in numerical simulations is consistent with a stochastic model in which the defects are created randomly in pairs and annihilated by each other at a rate that is proportional to their density [26]. Thus they appear to be statistically independent of each other. This was also found in experiments on electro-convection in nematic liquid crystals [65]. The autocorrelation function of the defect density in numerical simulations of the complex complex Ginzburg-Landau equation was investigated in [71]. There, it was also remarked that the defects are typically not bound in pairs, that is they are usually annihilated by a defect that is not the defect they were created with. No detailed analysis of this question has been performed, however.

In part two of this dissertation two-dimensional spatio-temporal chaos is investigated in a two-dimensional model for parametrically excited waves. The double phase slips seen in one dimension are expected to correspond to 'fluctuating bound defect pairs' in two dimensions, that is to pairs of defects that are created together and are annihilated by each other after a typical time during which the defects remain strongly correlated. Computations reported in chapter 10 indicate such behavior. An interesting question concerns the possibility of an 'unbinding' of these defect pairs resulting in a transition from a more ordered to a less ordered chaotic state. In chapter 11 computations are presented which show a drastic decrease in the order of the chaotic state connected with the disappearance of the typical lifetime of the defects and other signatures in the defect statistics.

The terms bound and unbound defect pairs suggest a similarity to the Kosterlitz-Thouless transition in two-dimensional melting [39, 57, 16]. There bound defect pairs, which occur in the solid phase, become unbound in the melting transition. The Kosterlitz-Thouless transition has been used to explain experimental results in superfluid films (where the "solid" phase is the superfluid state), superconducting films (where the "solid" phase is the superconducting state), liquid crystals, and other systems [56]. That such a transition could occur in a nonequilibrium system such as parametrically excited waves has been conjectured [59, 84, 15] but not established.

Chapter 12 concludes the dissertation with a summary and discussion of the results.

Part I

One-Dimensional system

Chapter 2

The Model

The equations considered here generically describe a system with a uniform state that has a supercritical Hopf bifurcation to a state that is periodic in both space and time when subjected to a uniform, constant forcing. Subjecting the system to an additional spatially uniform, time-periodic forcing at approximately twice the Hopf frequency creates a codimension-three bifurcation point involving the following three parameters: 1) the amplitude of the time-independent forcing, 2) the amplitude of the periodic forcing, and 3) the frequency of the periodic forcing. In the vicinity of this codimension-three bifurcation point the following amplitude equations [69,83,70] are derived by considering the reflection and translation symmetries in space and the weakly broken translation symmetry in time (see appendix A):

$$\begin{aligned} \partial_T A + s\partial_X A &= d\partial_X^2 A + aA + bB + cA(|A|^2 + |B|^2) + gA|B|^2, & (2.1) \\ \partial_T B - s\partial_X B &= d^*\partial_X^2 B + a^*B + bA + c^*B(|A|^2 + |B|^2) + g^*B|A|^2. & (2.2) \end{aligned}$$

The dependent variables A and B are complex, and represent amplitudes of left and right traveling waves that are summed together to yield the solution of the underlying system:

$$u(x,t) = \epsilon A(X,T)e^{i(q_c x - \frac{\omega_e}{2}t)} + \epsilon B(X,T)e^{i(q_c x + \frac{\omega_e}{2}t)} + c.c. + o(\epsilon), \qquad (2.3)$$

where $u(x,t)$ would give, for example, the position of the fluid surface in the Faraday experiment. The amplitudes A and B vary on the slow time and space scales, $T = \epsilon^2 t$ and $X = \epsilon x$. The coefficients in (2.1,2.2) are complex except for s and b, which are real. The real part of the coefficient of the linear term a gives the linear damping of the traveling waves in the absence of the periodic forcing and is proportional to the distance from the Hopf bifurcation. The coefficient of the linear coupling term b gives the amplitude of the periodic forcing. (Note that this term breaks the continuous time translation symmetry $t \to t + \Delta t$, which implies the transformation $A \to Ae^{i\Delta t\omega_e/2}$, $B \to Be^{-i\Delta t\omega_e/2}$). The imaginary part of the coefficient of the linear term a gives the difference between the frequency of the unforced waves and half the forcing frequency ω_e.

While in general a codimension-three bifurcation might be difficult to realize in an experiment, in the above situation (involving a system that undergoes a Hopf bifurcation) each of the three bifurcation parameters are natural control parameters in the system. In the Faraday experiment, however, there is no Hopf bifurcation and the above equations are only valid in the limit of weak damping (small viscosity). In this case the coefficients of the nonlinear terms c and g would be purely imaginary, since their real parts also represent (nonlinear) damping and would be higher order. In addition, for the Faraday experiment the group velocity parameter s would generally be complex, and s in (2.2) would be replaced by its complex conjugate s^*.

There is one caveat concerning (2.1,2.2) when they are used to describe either the Faraday experiment or parametrically excited waves induced near a Hopf bifurcation point. With the scaling $X = \epsilon x$, the group velocity term (involving ∂_X) would generically appear at lower order, so (2.1,2.2) require that the group velocity is small. If it is not small a strict asymptotic analysis would require the introduction of a second slow time scale and would lead to equations in which the cross-coupling between A and B arises through a spatially averaged term [38, 37, 60, 51, 82].

Note that (2.1,2.2) are in one (spatial) dimension. With periodic boundary conditions (as will be imposed in the numerical simulations) these equations would describe (for example) the Faraday experiment in a narrow annular container. Equations in two (spatial) dimensions (8.2,8.3) are discussed in chapter 8.

Solutions of (2.1,2.2) of the form $A = A_0 e^{iQX}$, $B = B_0 e^{iQX}$ include those where A_0 and B_0 are constants of unequal magnitude that correspond to traveling waves in the underlying system (see (2.3)) , and those where A_0 and B_0 are constants with equal magnitude that correspond to standing waves in the underlying system [69, 83]. It is these standing-wave solutions, which are phase locked to the periodic forcing, that are the focus of this study. In particular, the ensuing dynamics when these standing waves are perturbed are discussed. There are also solutions where A_0 and B_0 have equal magnitude but vary periodically in time, which correspond to standing waves that are not phase locked to the external forcing [69]. These standing waves are not treated in this dissertation.

The standing waves which are phase locked to the external forcing are stationary solutions of (2.1,2.2) and are given by [69, 83]

$$A = Re^{i(QX+\phi_A)} \tag{2.4}$$

$$B = Re^{i(QX+\phi_B)} \tag{2.5}$$

where:

$$R^2 = \frac{-(\hat{a}_r n_r + \hat{a}_i n_i) \pm \sqrt{(\hat{a}_r n_r + \hat{a}_i n_i)^2 - (n_r^2+n_i^2)(\hat{a}_r^2+\hat{a}_i^2-b^2)}}{(n_r^2+n_i^2)} \tag{2.6}$$

$$\phi_B - \phi_A = \arctan \frac{\hat{a}_i + n_i R^2}{\hat{a}_r + n_r R^2} \tag{2.7}$$

and:

$$\hat{a} \equiv \hat{a}_r + i\hat{a}_i = a - isQ - dQ^2 \tag{2.8}$$

$$n \equiv n_r + in_i = 2c + g. \tag{2.9}$$

They arise from the trivial solution in a steady bifurcation at the onset $b^2 = \hat{a}_r^2 + \hat{a}_i^2$. Equations (2.4-2.9) actually give a family of solutions for each wavenumber Q since the phase ϕ_A (or ϕ_B) can be chosen arbitrarily. Changing the value of ϕ_A (with $\phi_B - \phi_A$ fixed) corresponds to spatial translations of the solution.

Chapter 3

Linear Stability Analysis

In most pattern forming systems that display solutions which are periodic in space, such as Rayleigh-Bénard rolls, Taylor vortices, or the parametrically excited waves which are the subject of this study, the wavenumber (q) of the pattern that forms will always fall within a limited range of wavenumbers for a given value of the control parameter. In the mathematical models of the experimental systems this range of stable wavenumbers can be found using linear stability analysis.

Linear stability analysis (e.g. [27]) determines the behavior of small perturbations to a given solution of the system of equations of interest. If any perturbation grows with time, the solution is unstable. Since the perturbations are small, nonlinear terms in the resulting differential equations for the perturbations are smaller than the linear terms and are neglected. For example, to perform the linear stability analysis of the trivial solution $A = B = 0$ of equations (2.1,2.2) perturbations of the form

$$A = \tilde{A}e^{iQX} \tag{3.1}$$

$$B = \tilde{B}e^{iQX} \tag{3.2}$$

where $|\tilde{A}|, |\tilde{B}| \ll 1$ are considered. Subsituting (3.1,3.2) into (2.1,2.2) and neglecting nonlinear terms gives

$$\partial_T \tilde{A} + isQ\tilde{A} = -dQ^2\tilde{A} + a\tilde{A} + b\tilde{B} \tag{3.3}$$

$$\partial_T \tilde{B} - isQ\tilde{B} = -d^*Q^2\tilde{B} + a^*\tilde{B} + b\tilde{A}. \tag{3.4}$$

This system of linear ordinary differential equations with constant coefficients has solutions

$$\begin{pmatrix} \tilde{A} \\ \tilde{B} \end{pmatrix} = \begin{pmatrix} E_1 \\ E_2 \end{pmatrix} e^{\sigma t} \tag{3.5}$$

where

$$\sigma = a_r - d_r Q^2 \pm \sqrt{b^2 - (a_i - sQ - d_i Q^2)^2} \tag{3.6}$$

are the eigenvalues of the matrix:

$$M = \begin{bmatrix} a - isQ - dQ^2 & b \\ b & a^* + isQ - d^* Q^2 \end{bmatrix} \tag{3.7}$$

and $\begin{pmatrix} E_1 \\ E_2 \end{pmatrix}$ is the corresponding eigenvector.

For given values of $Q, s, a,$ and d there is a specific value of b above which the small perturbations to the solution $A = B = 0$ will grow (Real(σ) > 0) and below which perturbations will decay (Real(σ) < 0). This value is found by solving Real(σ_+) $= 0$ for b (where σ_+ is given by (3.6) with the $+$ sign), giving [68]

$$b^2 = (a_i - sQ - d_i Q^2)^2 + (a_r - d_r Q^2)^2. \tag{3.8}$$

This gives the "neutral curve" that has been plotted (for given values of s, a, d) as a dashed line in Figure 3.1.

The linear stability analysis of the solutions of equations (2.1,2.2) given by equations (2.4-2.9) can be performed in a similar way. One begins by considering solutions of the form

$$A = A_0 + \tilde{A} \tag{3.9}$$

$$B = B_0 + \tilde{B} \tag{3.10}$$

where A_0 and B_0 are the solution with wavenumber Q given by equations (2.4,2.5). $\tilde{A}$ and $\tilde{B}$ are the perturbations which have the form

$$\tilde{A} = A_1 e^{\sigma T + i(Q+k)X} + A_2 e^{\sigma^* T + i(Q-k)X} \tag{3.11}$$

$$\tilde{B} = B_1 e^{\sigma T + i(Q+k)X} + B_2 e^{\sigma^* T + i(Q-k)X} \tag{3.12}$$

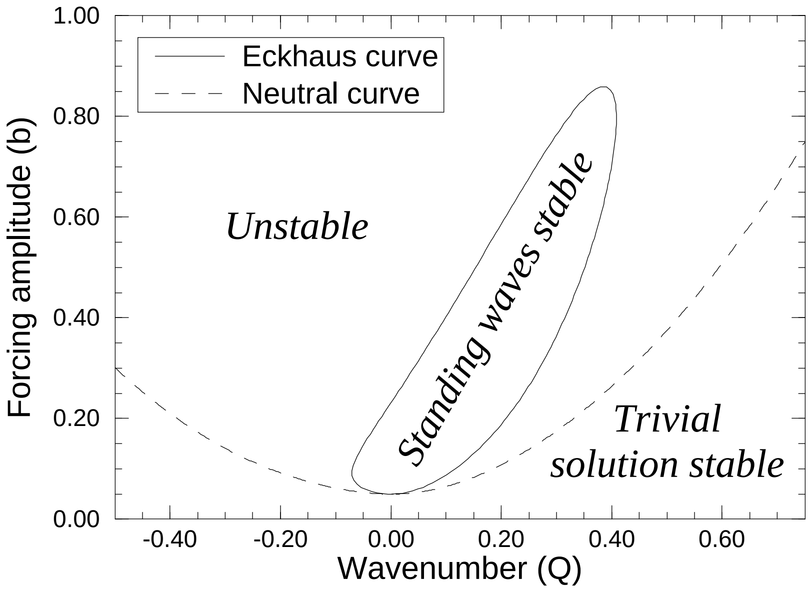

Figure 3.1: Linear Stability diagram for $a = -0.05$, $c = -1 + 4i$, $d = 1 + 0.5i$, $s = 0.2$, $g = -1 - 12i$.

where $|A_1|, |A_2|, |B_1|, |B_2| \ll 1$. The perturbation (3.11,3.12) is appropriate for detection of both amplitude instabilities and sideband instabilities in the wavenumber. Substituting (3.9,3.10) into (2.1,2.2) and neglecting nonlinear terms in A_1, A_2, B_1, B_2 results in the eigenvalue problem $M\mathbf{x} = \sigma\mathbf{x}$ where

$$M = \begin{bmatrix} m_{11} & cR^2e^{i2\phi_A} & b+\hat{g}R^2e^{i(\phi_A-\phi_B)} & \hat{g}R^2e^{i(\phi_A+\phi_B)} \\ c^*R^2e^{-i2\phi_A} & m_{22} & \hat{g}^*R^2e^{-i(\phi_A+\phi_B)} & b+\hat{g}^*R^2e^{i(\phi_B-\phi_A)} \\ b+\hat{g}^*R^2e^{i(\phi_B-\phi_A)} & \hat{g}^*R^2e^{i(\phi_A+\phi_B)} & m_{11}^* & c^*R^2e^{i2\phi_B} \\ \hat{g}R^2e^{-i(\phi_A+\phi_B)} & b+\hat{g}R^2e^{i(\phi_A-\phi_B)} & cR^2e^{-i2\phi_B} & m_{22}^* \end{bmatrix} \tag{3.13}$$

$$\text{and} \quad \mathbf{x} = \begin{bmatrix} A_1 \\ A_2^* \\ B_1 \\ B_2^* \end{bmatrix}. \tag{3.14}$$

Here

$$\hat{g} = c + g \tag{3.15}$$

$$\text{and} \quad m_{11} = a - is(Q+k) - d(Q+k)^2 + (2c+\hat{g})R^2 \tag{3.16}$$

$$m_{22} = a^* + is(Q-k) - d^*(Q-k)^2 + (2c^*+\hat{g}^*)R^2. \tag{3.17}$$

For given values of the parameters a, b, c, d, g, s, the solution wavenumber Q, and the perturbation wavenumber k, the eigenvalues of this matrix can be found numerically [76]. Figure 3.2 shows graphs of the real part of the eigenvalues σ (which are the growth/decay rates of the perturbations) versus the perturbation wavenumber k for two different values of the solution wavenumber Q. In Figure 3.2a the real part of each of the four eigenvalues is negative indicating the solution with $Q = 0.2$ is stable. In Figure 3.2b the real part of one of the eigenvalues is positive for a range of k's indicating the solutions with $Q = 0.3$ is unstable. Note that the real part of this eigenvalue goes through the origin with zero slope but positive curvature. This means the solution is unstable to perturbations with infinitesimally small wavenumbers. As one changes Q corresponding to going from

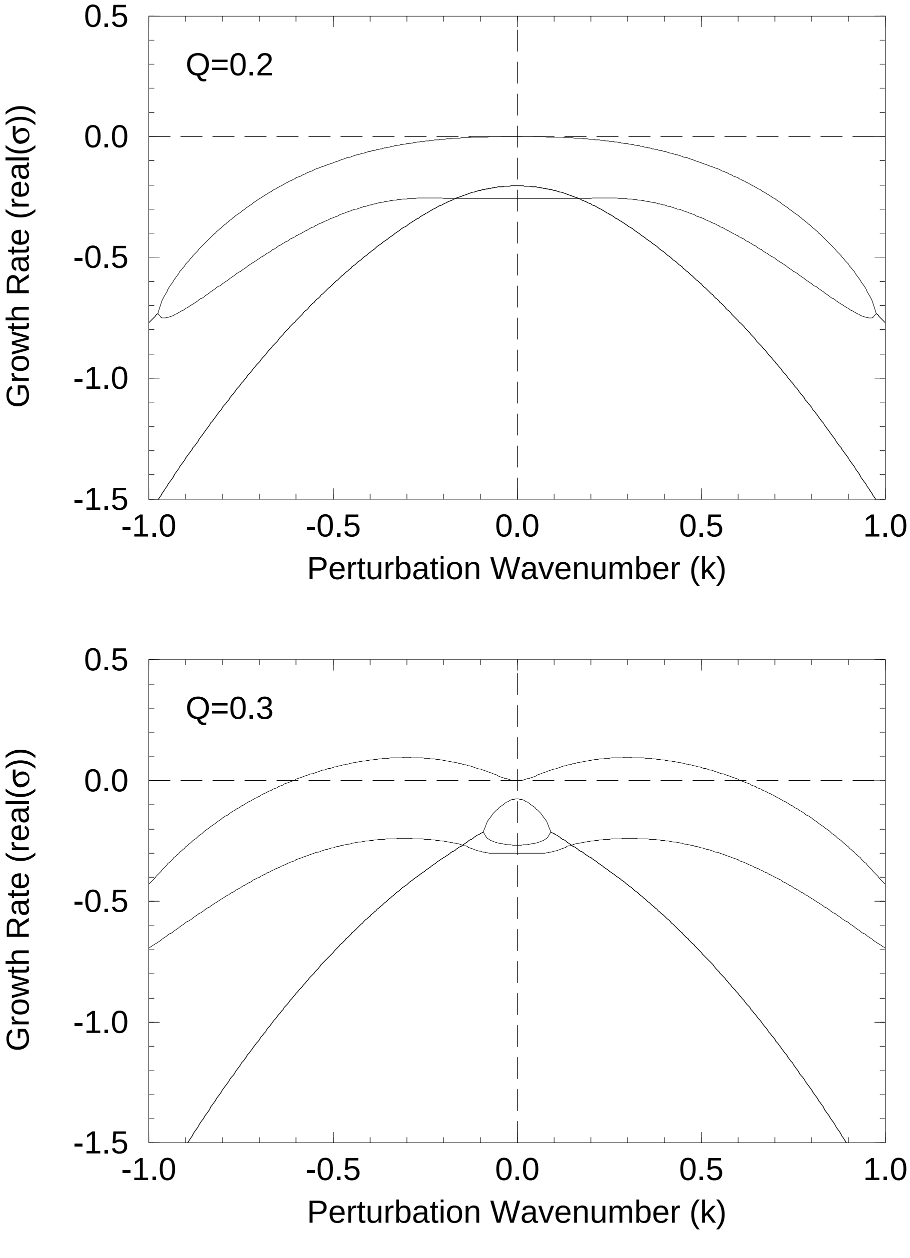

Figure 3.2: The real part of the eigenvalues of the matrix M for $a = -0.05$, $b = 0.2$, $c = -1 + 4i$, $d = 1 + 0.5i$, $s = 0.2$, $g = -1 - 12i$. a) Stable solution, wavenumber $Q = 0.2$. b) Unstable solution, wavenumber $Q = 0.3$.

Figure 3.2a to Figure 3.2b, the infinitesimally small wavenumbers are the first to become unstable. This long wavelength sideband instability is known as an Eckhaus instability. For given values of a, c, d, g, and s, the values of Q and b which separate solutions which are stable (as in Figure 3.2a) from solutions which are unstable to long wavelength perturbations (as in Figure 3.2b) define an Eckhaus curve. The Eckhaus curve for selected parameters has been plotted as a solid line in Figure 3.1.

The Eckhaus instability has been previously studied for many systems including a single Ginzburg-Landau equation with real coefficients. For this equation it is well known that the Eckhaus and neutral curves are parabolic. It can be shown that equations (2.1,2.2) can be reduced to a single Ginzburg-Landau equation with real coefficients near onset [68]. Thus the Eckhaus and neutral curves in Figure 3.1 are parabolic near onset. However, for larger values of b, the Eckhaus curve need not be parabolic. For the parameters used to generate Figure 3.1 the Eckhaus curve closes on itself indicating that for values of the periodic forcing amplitude b larger than 0.86 all wavenumbers are unstable, reminiscent of the Benjamin-Feir instability for traveling waves [3]. Therefore chaotic dynamics might be expected for values of b greater than 0.86 (although other stationary solutions are possible in principle). As it turns out, there are also interesting dynamics (including chaos) for b less than 0.86.

The Eckhaus curve can also be determined from phase dynamics. In reference [68] the Eckhaus curve in Figure 3.1 is found this way. There a WKB ansatz

$$A = Re^{i(\frac{\phi}{\epsilon}+\phi_A)}(1+\epsilon A_1) \tag{3.18}$$

$$B = Re^{i(\frac{\phi}{\epsilon}+\phi_B)}(1+\epsilon B_1) \tag{3.19}$$

leads to a diffusion equation for the phase ϕ

$$\partial_T \phi = D(Q)\partial_X^2 \phi + \ldots \tag{3.20}$$

where $Q = \partial_X \phi$. ($D(Q)$ is also a function of the parameters in equations (2.1,2.2).) When $D(Q) > 0$ perturbations in Q (from a uniform state) will decay diffusively indicating a stable solution. When $D(Q) < 0$ perturbations in Q will grow, indicating an unstable solution. The Eckhaus curve is given by $D(Q) = 0$.

The two different ways of calculating the Eckhaus curve give identical results. They are related in the following way. The phase diffusion coefficient D in equation (3.20) is given by

$$D = -\frac{1}{2}\frac{d^2}{dk^2}[Real(\sigma_o)]\bigg|_{k=0} \tag{3.21}$$

where $Real(\sigma_o)$ versus k is the top curve in Figure 3.2a or 3.2b. If this curve is concave up at the origin (as in Figure 3.2b) D is negative and the solution is unstable. If this curve is concave down at the origin (as in Figure 3.2a) D is positive and the solution is stable.

The long-wave theory in [68] cannot test for instabilities where the perturbation wavelength that is the first to grow is finite instead of being arbitrarily small as in the Eckhaus instability. It was assumed in [68] that there is no finite wavelength instability for the parameters used to generate Figure 3.1. This assumption is verified by the fact that the real(σ) < 0 for all four eigenvalues plotted in Figure 3.2a and in (all) similar plots for other values of Q and b in the Eckhaus stable region indicated in Figure 3.1. Note that although there are only three curves in Figure 3.2a, one of the curves (the bottom one at $k = \pm 0.5$) represents a pair of complex conjugate eigenvalues. This pair splits into two real eigenvalues near $k = \pm 0.1$ in Figure 3.2b.

Chapter 4

Phase Slips and Double Phase Slips

The main questions to be addressed here are: What are the solutions to (2.1,2.2) if started with initial conditions that correspond to unstable standing waves? What features characterize the solutions? How do the solutions differ as one changes the forcing amplitude b and the wavenumber of the initial condition Q? These questions are investigated by calculating numerical approximations to the solutions of (2.1,2.2) using a pseudospectral method in space (periodic boundary conditions) and a fourth-order Runge-Kutta/integrating-factor scheme in time (see appendix B for details).

The one-dimensional dynamics described in this treatise all incorporate a new feature called a "double phase slip". In this chapter this feature is described and contrasted to an ordinary single phase slip, which is a well known feature of many systems (including the solution of a single Ginzburg-Landau equation with real coefficients, e.g. [20]) when started with an initial condition that is Eckhaus unstable. In order to excite the Eckhaus instability, the initial condition typically chosen for the simulations is a wave, perturbed so that the local wavenumber varies slightly throughout the domain such that it has a maximum and a minimum at distinct locations.

Since near onset (2.1,2.2) can be reduced to a single real Ginzburg-Landau equation [68], the solution of (2.1,2.2) for small values of b should resemble the solution of a single real Ginzburg-Landau equation. This is indeed seen in the simulations. For small values of b ($b = 0.1$, say) and an initial condition slightly to the right of the Eckhaus stable region in Figure 3.1, the solution undergoes a phase slip near the location of the initial maximum in the wavenumber that reduces the wave number and moves the solution into the stable region. This behavior is shown in Figure 4.1a. For larger values of b however ($b = 0.6$, say), the behavior of the solution is markedly different, as shown in Figure 4.1b; given an initial condition slightly to the right of the Eckhaus stable region, the solution undergoes a phase slip that reduces the average wave number but a short time later undergoes a second phase slip at essentially the same location in space that restores the wave number to its original value. This *double phase slip* causes the solution to remain in the Eckhaus unstable region, thus allowing persistent dynamics.

In the simulations a phase slip in A is always accompanied by an essentially coincident phase slip in B. Thus a double phase slip in the solution of (2.1,2.2) means that there are double phase slips in both A and B at approximately the same point in space and time.

Double phase slips occur in a variety of solutions to (2.1,2.2) including periodic solutions, chaotic solutions, and nontrivial transients. These solutions are described in the following three chapters. Results for small system sizes are presented first in chapter 5. Then results for large systems are given in chapter 6 and it is shown that they allow a simplified long-wave description. Chapter 7 presents results for a minimal system where the double phase slips move the system between a configuration where the total phase of the system is zero and one where the total phase of the system is 2π.

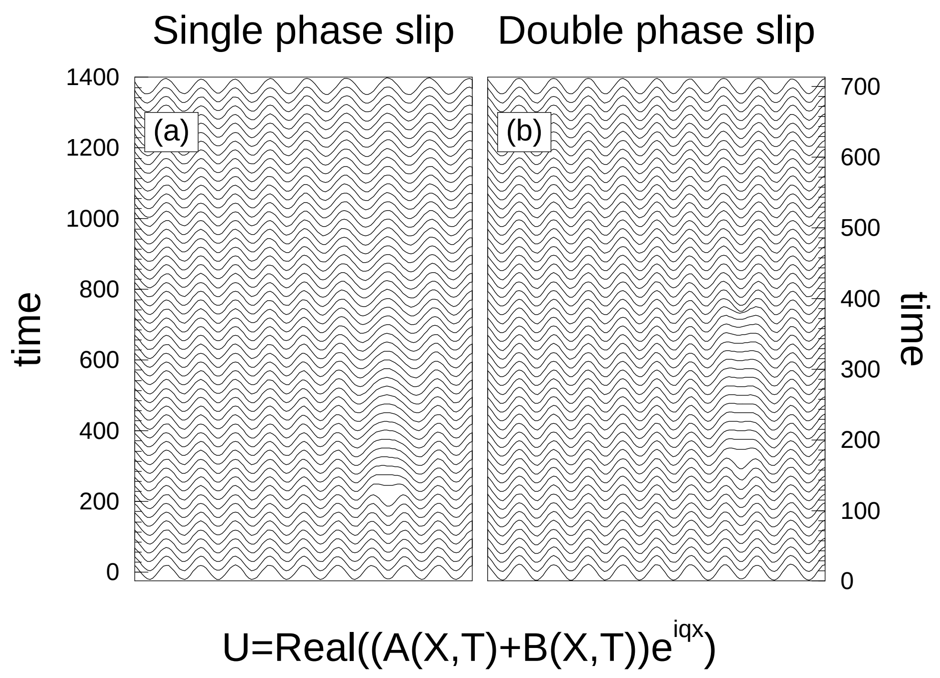

Figure 4.1: Space-time diagram illustrating (a) single phase slip observed for small values of the forcing amplitude (e.g. $b = 0.1$), and (b) double phase slip observed for larger values of the forcing amplitude (e.g. $b = 0.6$).

Chapter 5

Dynamics of a Small System

Typically, the most complex solutions of a continuous system are formed when the spatial dimensions of the system are large. In fact, one is often interested in the "thermodynamic limit" where these spatial dimensions and the time interval considered become infinite. Studies of smaller systems, often interesting in their own right, can also be valuable because their simpler dynamics often provide insight into the dynamics of larger systems. For the simulations presented in this chapter the domain size L has been chosen such that the initial conditions, which have an average wave number in the vicinity of the Eckhaus curve, include only five wavelengths. Three different types of solutions are presented: 1) Transient solutions where there is only one double phase slip, 2) Solutions where double phase slips occur periodically in time, and 3) Complex solutions where double phase slips occur irregularly in space and time. Figure 5.1 shows where examples of these solutions occur in relation to the Eckhaus curve that is shown in Figure 3.1. The initial conditions for these solutions are close to the standing wave solutions but perturbed such that there is a maximum in the local wave number that triggers the first double phase slip and determines its location. Examples of each of the solution types are described in the following sections.

5.1 Transient Solutions

In the transient solutions described here, there is only one double phase slip. After the double phase slip, the solution relaxes to the stationary solution (2.4-2.9)

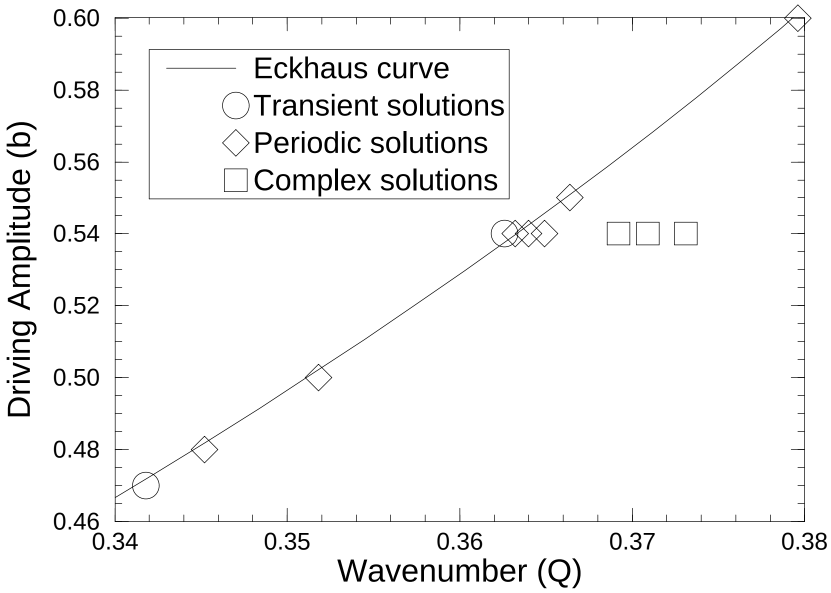

Figure 5.1: Example values of the forcing amplitude b and wavenumber Q where the three solution types occur.

corresponding to the regular standing wave state in the underlying system. These transient solutions resemble the response of an excitable medium; beginning with an initial condition that is in the vicinity of a stable fixed point, the transient solution makes an excursion far away from the fixed point before finally coming to rest there. This is most clearly seen in the phase-plane representation of the solution shown in Figure 5.2. It shows the magnitudes of the (spatial) Fourier modes corresponding to 4 and 5 wavelengths in the domain. Each dot in Figure 5.2 represents an instant in time. The square indicates the initial condition which is the perturbed 5-wave state. The loop in Figure 5.2 is traversed once, with the final state of the solution being the fixed point on the vertical axis (marked by a diamond) corresponding to the (stable) 5-wave solution.

Solutions with only one double phase slip occur only where the initial condition is a perturbation of a *stable* solution. The lowest point on Figure 5.1 appears to contradict this statement since it appears on the outside of the Eckhaus curve. However, this is due to the fact that the Eckhaus curve represents a long-wavelength instability. Since arbitrarily small wavenumbers are not present in a finite domain the true stability curve for the finite system is slightly outside the Eckhaus curve and all of the solutions with only one double phase slip are in fact within the stable region.

At the stability limit an unstable saddle-point solution branches subcritically off the branch of solutions given by (2.4-2.9) [40,79]. The perturbation required to excite a double phase slip must place the initial condition beyond this saddle point in phase space. As the wavenumber is moved further into the Eckhaus stable region, the bifurcated saddle point moves further from the stable stationary solution in phase space, and a larger perturbation is required to excite the system.

5.2 Periodic Solutions

In the periodic solutions, double phase slips occur at the same locations in space, periodically in time. An example of the simplest of these periodic solutions

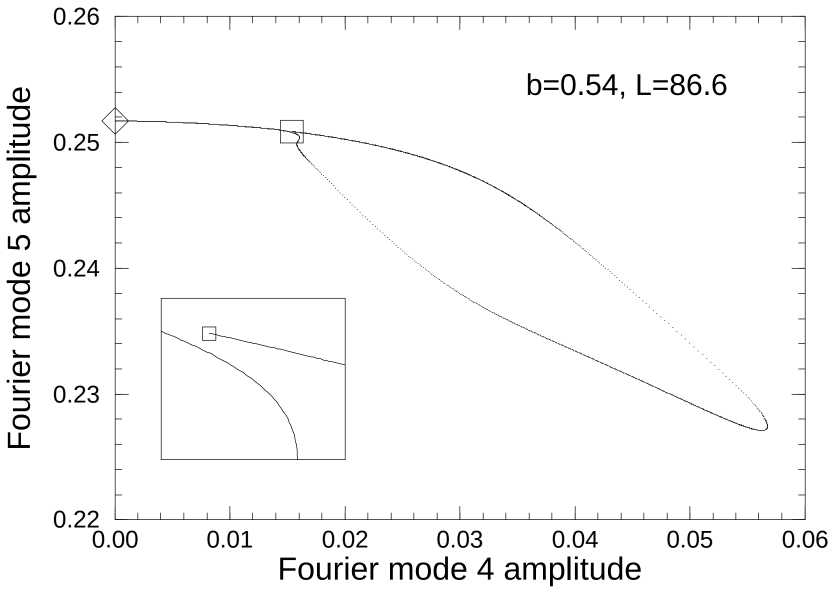

Figure 5.2: Phase plane representation of a transient solution involving one double phase slip. The square indicates the initial condition which is the perturbed 5-wave state. The loop is traversed once, with the final state of the solution being the (stable) fixed point indicated by a diamond. ($b = 0.54$, $Q = 5(2\pi)/L = 0.3628$).

is shown in Figure 5.3 where the location in space and time of each double phase slip is indicated by a circle. The time between each double phase slip is much larger than the time between the individual phase slips which make up a double phase slip. This can be appreciated by looking at Figure 5.4 which shows the (spatial) average of the wavenumber plotted versus time. Each of the downward "spikes" in Figure 5.4 represents a double phase slip; the average wavenumber is reduced by the first phase slip, then restored by the second. Figure 5.5 shows the phase-plane representation of the simple periodic solution. The loop in Figure 5.5 is traversed periodically, with the upper left portion of the loop (where the mode 5 magnitude is large and the mode 4 magnitude is small) being passed between double phase slips, and the lower right portion of the loop (where the mode 5 magnitude is smaller and the mode 4 magnitude is larger) being passed during a double phase slip.

Although the periodic solutions occur for larger wavenumbers (for a given value of b) than the transient solutions where there is only one double phase slip (see Figure 5.1) the periodic solutions can still occur within the Eckhaus stable region indicating that stable stationary solutions and stable periodic solutions can coexist.

As the wavenumber is decreased the period of the simple periodic solutions diverges as shown in Figure 5.6. This appears to be due to the unstable saddle-point solution which branches subcritically off the branch of solutions given by (2.4-2.9) at the Eckhaus stability limit. Inside the Eckhaus stable region, as the average wavenumber of the initial condition is decreased by increasing the size of the system L, the saddle point moves away from the stable fixed point and towards the periodic orbit in phase space. This causes the periodic orbit to pass closer to the saddle point, increasing its period (cf. Figure 5.6). Our simulations suggest that the divergence of the period occurs when the periodic orbit becomes a homoclinic orbit of the saddle point. Beyond this point the periodic solutions no longer exist and the excitable transient solutions occur.

Increasing the wavenumber from those which produce simple periodic solutions results in a period doubling bifurcation which leads to the solution shown in Figure 5.7. Figure 5.8 shows the period doubling bifurcation in more detail for

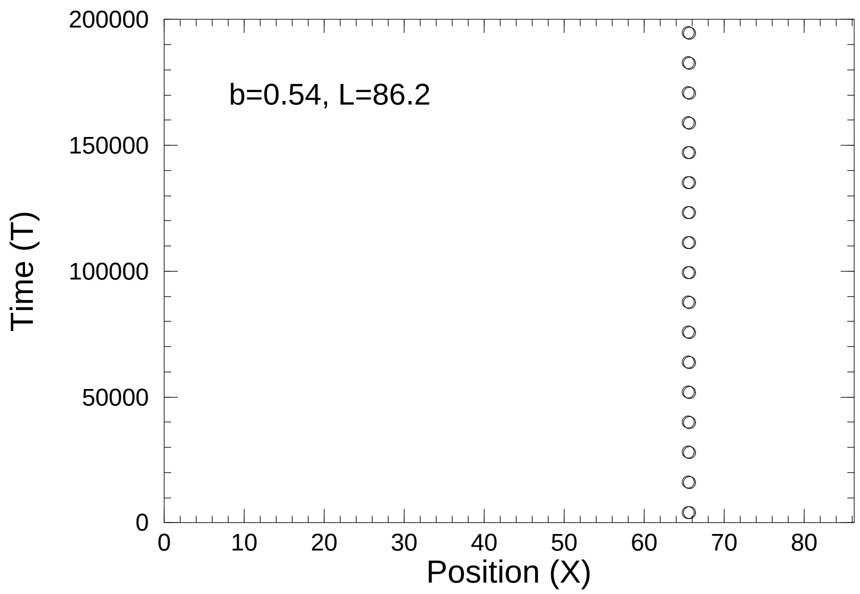

Figure 5.3: Each circle represents the location (in space and time) of a double phase slip for a simple periodic solution ($b = 0.54$, $Q = 5(2\pi)/L = 0.3645$).

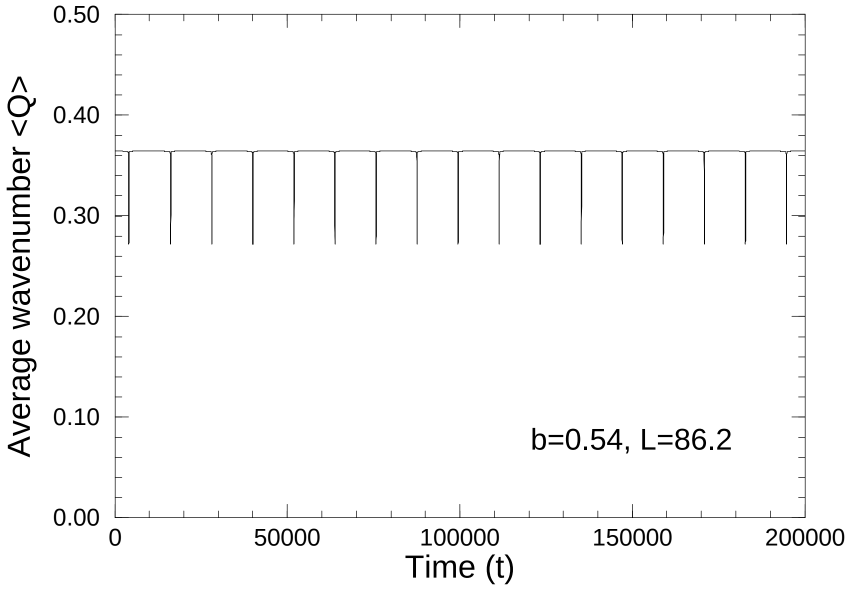

Figure 5.4: Spatial average of the local wavenumber plotted as a function of time for a simple periodic solution ($b = 0.54$, $Q = 5(2\pi)/L = 0.3645$).

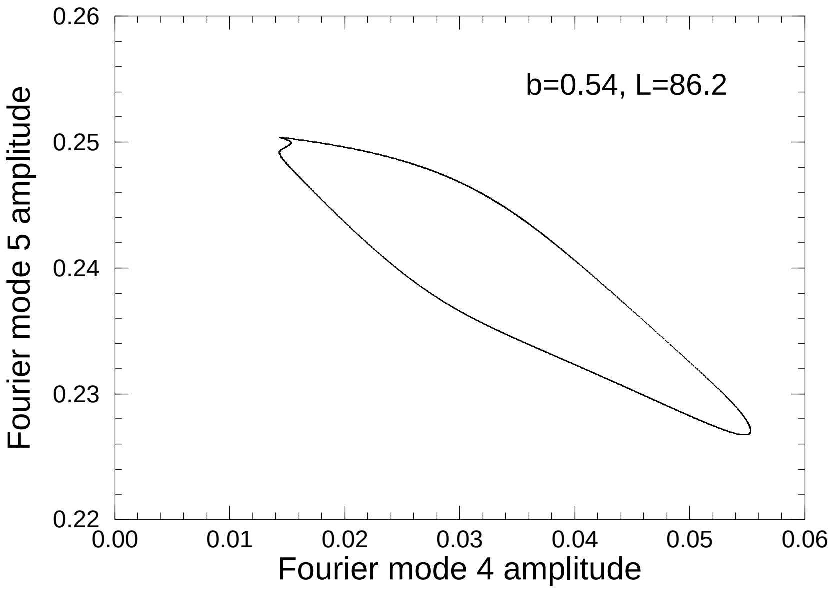

Figure 5.5: Phase plane representation of a simple periodic solution ($b = 0.54$, $Q = 5(2\pi)/L = 0.3645$).

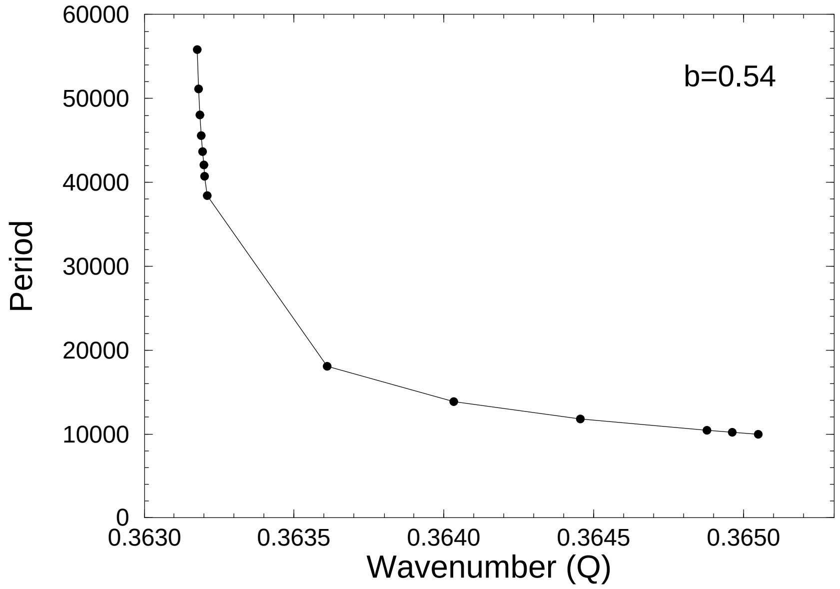

Figure 5.6: Divergence of the period of the simple periodic solutions as the wavenumber Q is decreased ($b = 0.54$).

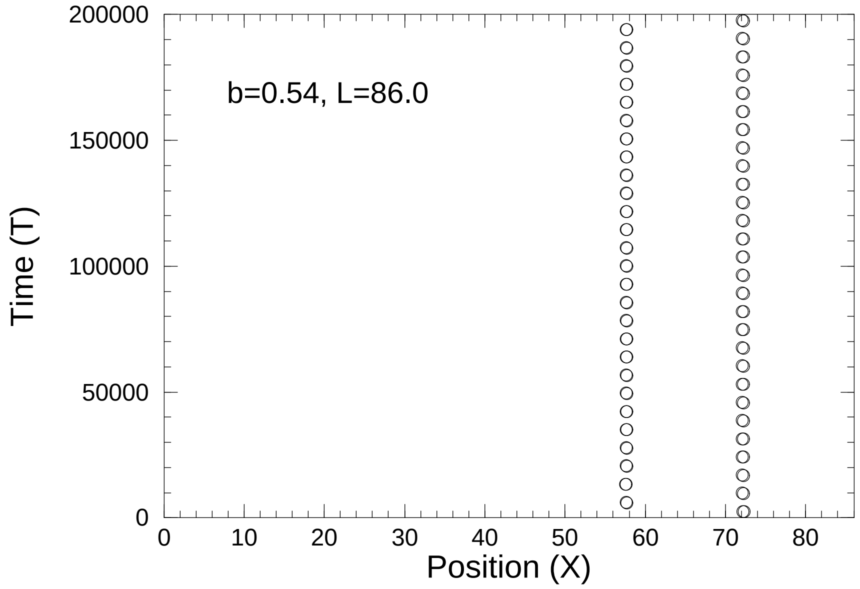

Figure 5.7: Location of double phase slips for a periodic solution occurring after a period doubling bifurcation ($b = 0.54$, $Q = 5(2\pi)/L = 0.3653$).

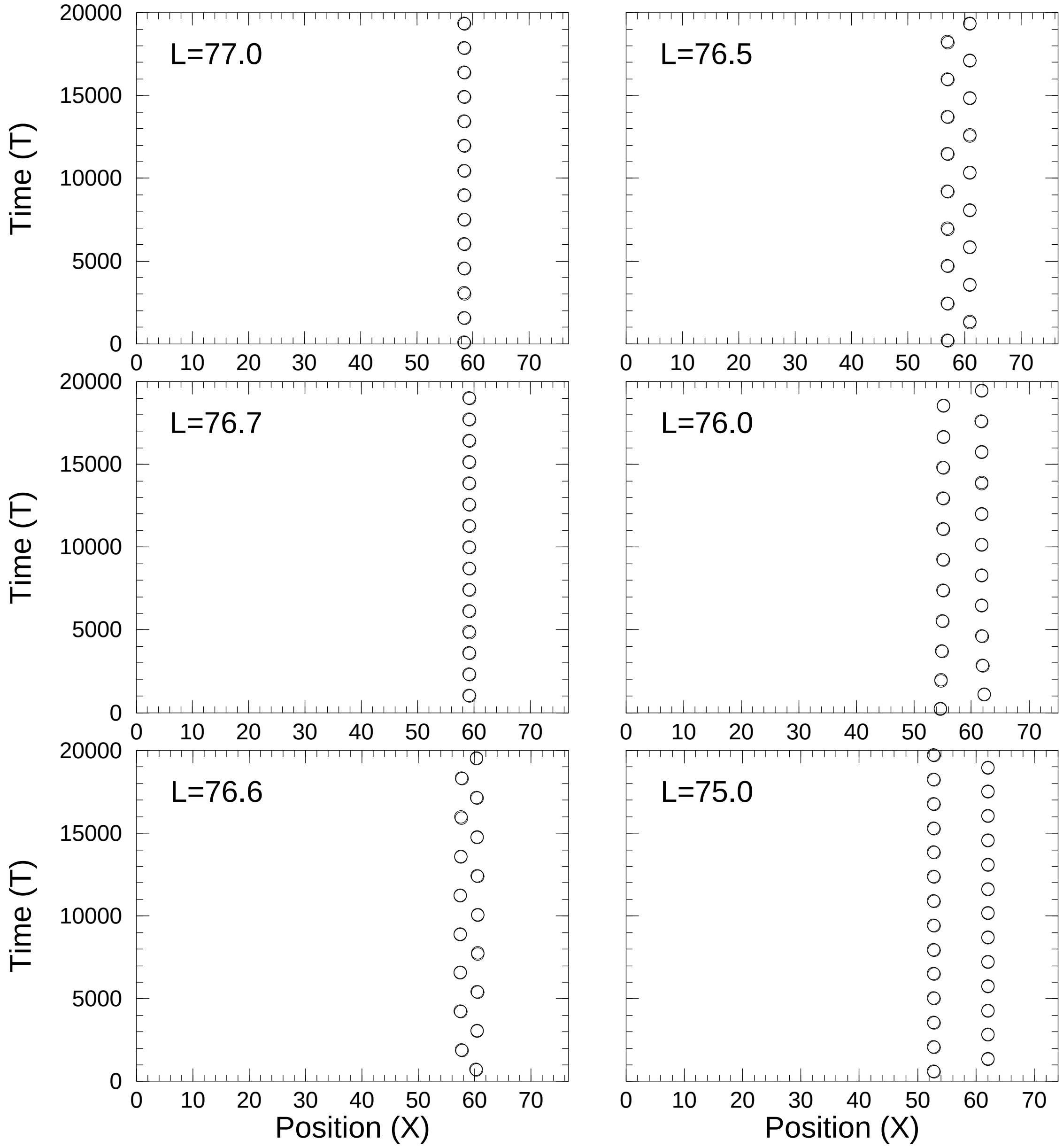

Figure 5.8: Location of double phase slips for $b = 0.81$ and various system sizes; period doubling bifurcation occurs at $L \approx 76.7$.

$b = 0.81$. Increasing the wavenumber further results in even more complicated periodic (or quasiperiodic) states such as those shown in Figure 5.9 where a wave of double phase slips propagate through the system. A *quasi*periodic traveling wave solution would be one where the period of time required for the wave of double phase slips to propagate through the system is not a rational multiple of the period at which double phase slips occur within the wave. The exact form of the more complicated periodic solutions may depend on the value of b but the trend of simple periodic solutions losing stability to more complicated periodic solutions was observed for all investigated values of b that exhibit periodic solutions.

5.3 Complex Solutions

Figure 5.10 shows a complex solution where the double phase slips occur irregularly in space and time. The complex solutions occur for even larger wavenumbers (for a given value of b) than the periodic solutions. If the average wave number of the initial condition is too large however, a single phase slip occurs, which reduces the wavenumber. The phase slip need not take the solution all the way into the stable band. Instead the solution can remain in the domain of periodic or even complex dynamics.

5.4 Remarks About (Q,b) Space

Figure 5.1 gave example values of the wavenumber Q and forcing amplitude b where each of the three solution types discussed in this chapter were found. No attempt was made to carefully delineate the regions in (Q, b) space where each type solution occurs. However, some general remarks can be made based on all of the simulations done for this investigation.

No double phase slips were seen in any simulation with $b < 0.45$. As b is decreased the time between the phase slips within a double phase slip increases and appears to diverge as shown in Figure 5.11. The data for this figure was obtained

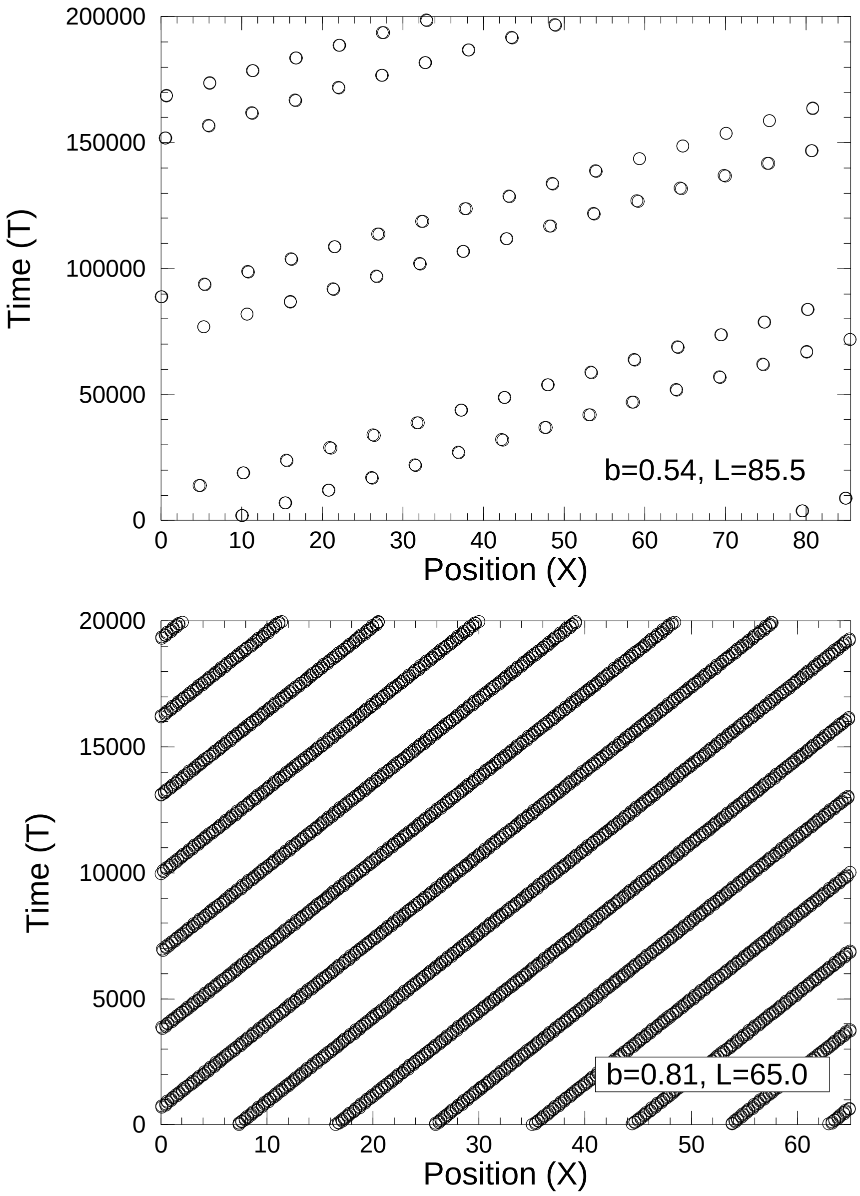

Figure 5.9: Location of double phase slips for solutions where a wave of double phase slips propagates through the system. a) $b = 0.54$, $Q = 5(2\pi)/L = 0.3674$; b) $b = 0.81$, $Q = 5(2\pi)/L = 0.4833$.

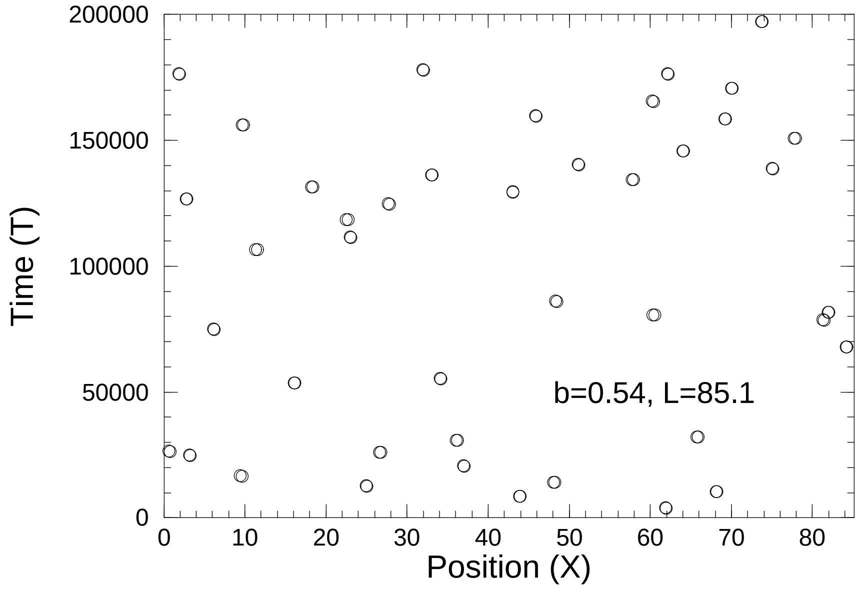

Figure 5.10: A complex solution where the double phase slips occur irregularly in space and time ($b = 0.54$, $Q = 5(2\pi)/L = .3692$).

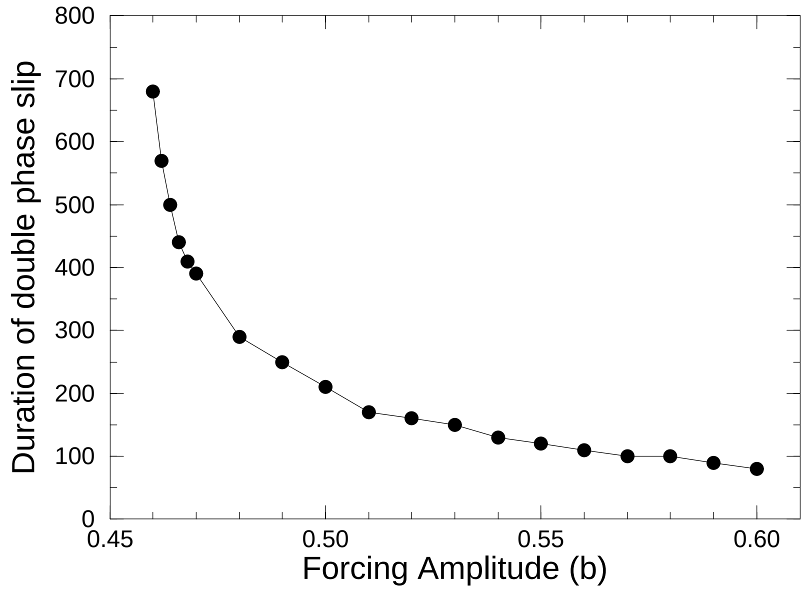

Figure 5.11: Divergence of the time between the two phase slips which make up a double phase slip as the forcing amplitude is decreased.

by varying the length of the system as well as the forcing amplitude b so that the the initial condition for each value of b had an average wavenumber Q which was approximately the same distance from the Eckhaus curve. For $b \geq 0.54$ this resulted in periodic solutions. For $0.46 \leq b \leq 0.53$ there were transients involving double phase slips. In each case only the time between the phase slips in the first double phase slip was measured. For $b \leq 0.458$ there was a single phase slip.

A number of simulations were made with large values of $b > 0.86$ to see if there was a transition from solutions with double phase slips to solutions with single phase slips. No such transition was found although for large values of b the time between double phase slips at a given location can become similar to the time between the phase slips within a double phase slip.

A few simulations were made with initial conditions on the left side of the Eckhaus stable region in Figure 3.1 to see if double phase slips would occur in the opposite order. In all of these simulations there was always only a single phase slip which increased the wavenumber into the stable region. No double phase slips were found but this was not investigated thoroughly.

A final observation is that in general the dynamics of the system are faster for larger values of b as can be seen by comparing the time scales of Figures 5.7 and 5.8, and the two parts of figure 5.9.

Chapter 6

Dynamics of a Large System

This chapter presents solutions for larger domains than the solutions discussed in the previous chapter. For the particular solutions discussed, approximately 50 wavelengths with a wavenumber near the Eckhaus curve fit in the domain whereas in the previous chapter only 5 did. The focus is on complex solutions where the double phase slips occur irregularly in space and time. The irregular appearance of these solutions suggests they are chaotic. Autocorrelation functions calculated using the location of the double phase slips show that these locations are not correlated for large distances and times, confirming the chaotic nature of the solutions in both space and time. Two different solution types are discussed: 1) Extended spatio-temporal chaos where the double phase slips occur irregularly across the entire domain, and 2) Localized spatio-temporal chaos where the irregular occurrence of double phase slips is restricted to only part of the spatial domain.

6.1 Extended Spatio-Temporal Chaos

Figure 6.1a shows a space-time diagram similar to Figure 5.10 for an extended chaotic solution in a large system, with each double phase slip represented by a single dot. The extended chaotic states exist over a range of wavenumbers with the space-time density of double phase slips increasing with wavenumber as seen in Figure 6.1b. Beyond a certain wavenumber the chaotic state loses stability, however. A solution with such a large initial wavenumber is represented in Figure 6.1c where at $t \approx 13000$ and $x \approx 265$ a *single* phase slip occurs, which reduces the local

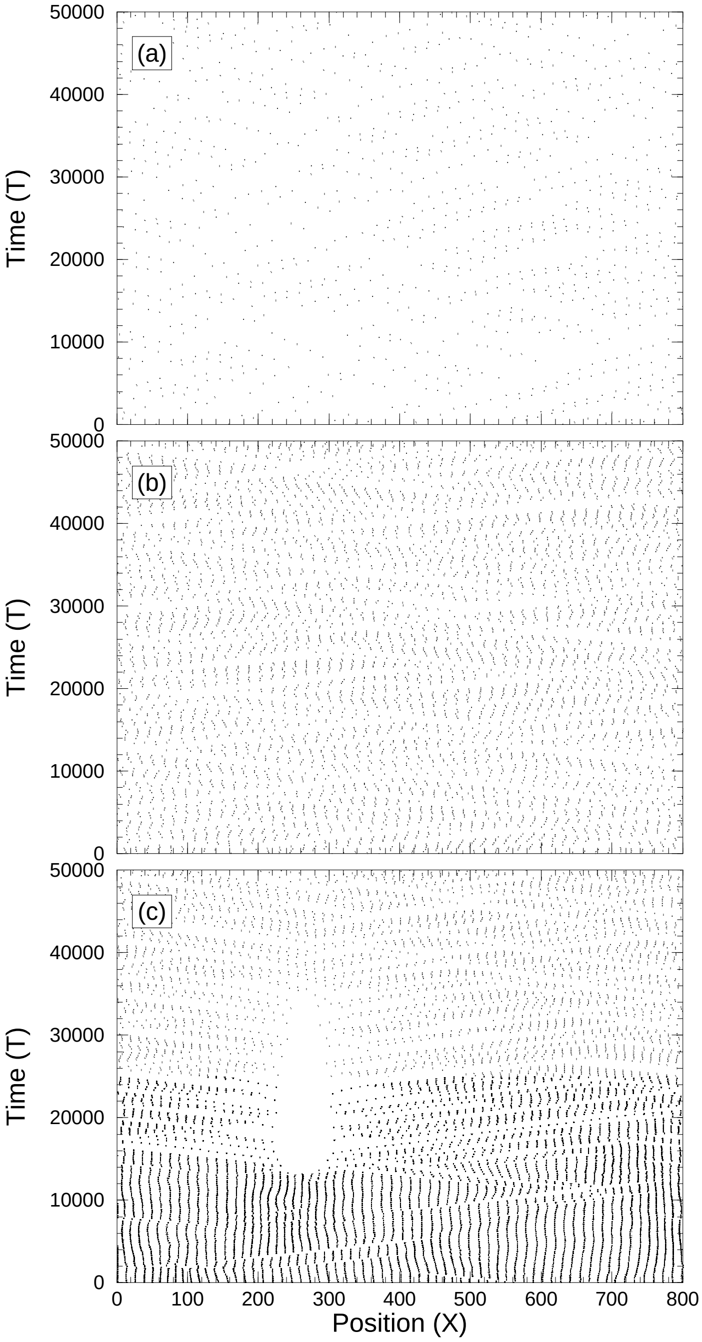

Figure 6.1: Extended spatio-temporal chaos in a large system ($b = 0.6$, $L = 800$): (a) $Q = 50(2\pi)/L = 0.3927$, (b) $Q = 51(2\pi)/L = 0.4006$, (c) Initial wavenumber $Q_0 = 52(2\pi)/L = 0.4084$, after a single phase slip at $t \approx 13000$ the wavenumber is $Q = 0.4006$.

wavenumber. Subsequently there are no phase slips in this area until the higher wavenumber in the regions on either side diffuses in. Eventually the wavenumber and the density of double phase slips in Figure 6.1c become homogeneous again and their final values are the same as those in Figure 6.1b. The transition appears to be related to the fact that with the large wavenumber (that is, before the single phase slip in Figure 6.1c) the time between the occurrence of double phase slips at a given location in space is similar to the duration of each double phase slip, i.e. the time between the two phase slips within a double phase slip. This is due to both the high density of double phase slips and their tendency to reoccur at the same location in space.

6.2 Localized Spatio-Temporal Chaos

Perhaps the most interesting solutions arising in the one-dimensional simulations are those featuring localized spatio-temporal chaos. An example is shown in Figure 6.2. As in Figure 6.1, each double phase slip is represented by a single dot. The simulation starts with an initial condition with a maximum in the local wavenumber that triggers an initial double phase slip. This initial double phase slip triggers additional double phase slips in the vicinity of the first. Originally the size of the region in which the double phase slips occur grows with time. However, for later time, the size of the region ceases to grow and the chaos is seen to be localized. Outside of the region in which the double phase slips occur, the solution is the time-independent solution which corresponds to regular standing waves in the underlying system.

Figure 6.3 shows the width of the chaotic region as a function of time for different initial widths bracketing the final width of the state shown in Figure 6.2. For both initial conditions the width converges to the same final value indicating that in the final state the spatio-temporal chaos is indeed localized. Here the width of the chaotic region was measured by taking the difference in the locations of the rightmost and leftmost double phase slip within a period of time $\tau = 100,000$. The

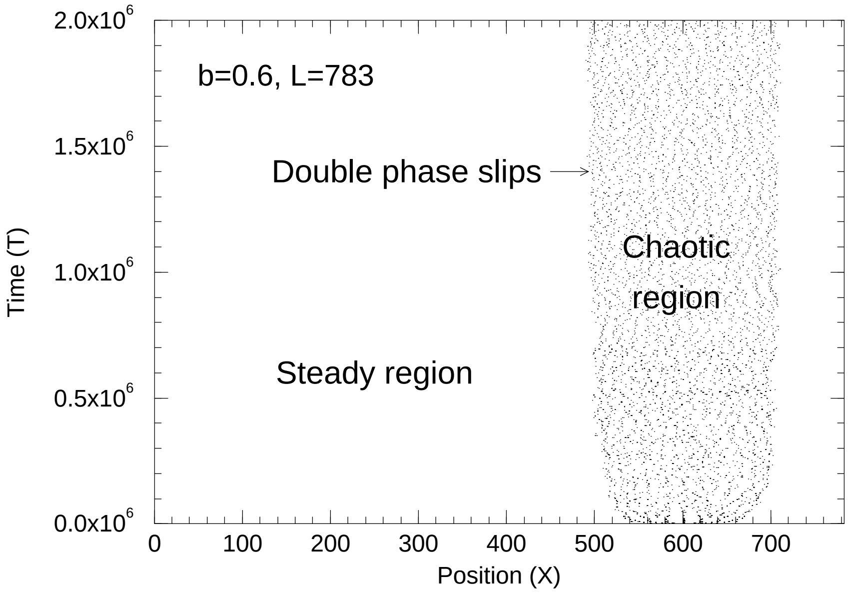

Figure 6.2: Localized spatio-temporal chaos in a large domain. Each dot represents a double phase slip ($b = 0.6$, $L = 783$, $Q = 47(2\pi)/L = 0.377$).

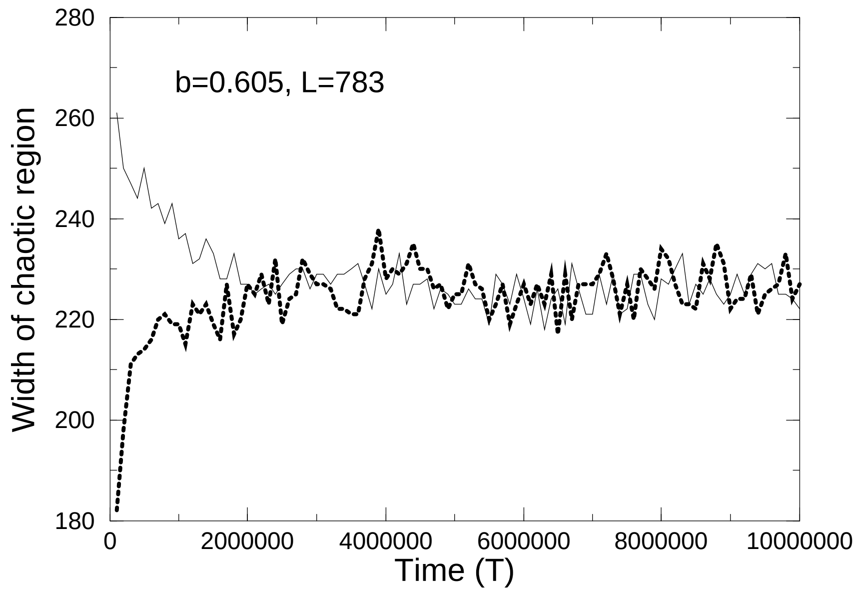

Figure 6.3: Temporal evolution of the width of the localized region exhibiting spatio-temporal chaos for two different initial conditions ($b = 0.605$, $Q = 47(2\pi)/L = 0.377$).

initial condition with a larger chaotic region was taken from a long time solution with a smaller value of $b = 0.600$.

6.3 Effective Phase Equation

That (2.1,2.2) would have solutions with persistent localized domains is somewhat surprising since the term involving ∂_x^2 tends to diffuse away inhomogeneities (as in, for example, the heat equation $\partial_t T = \partial_x^2 T$) and there is nothing in the equations that distinguishes any region from another. The localization mechanism for the steady and chaotic regions in Figure 6.2 can be understood using an effective phase diffusion equation. This analysis is presented in this section. The analysis uses the phase of $A(X,T)$ but an analysis based on $B(X,T)$ would yield the same results.

From the investigation of solutions with extended chaos it is natural to expect the chaotic region to have a larger local wavenumber than the region where the solution is time independent (see Figure 5.1). Figure 6.4 shows the local wavenumber of the time average of the solution $A(X,T)$ (averaged from $t = 2,000,000$ to $t = 2,010,000$) for the state represented in Figure 6.2 and confirms this; the local wavenumber in the chaotic region is larger than the local wave number in the quiescent region. The local wavenumber for $B(X,T)$ is similar. So the steady and chaotic regions in Figure 6.2 can be viewed as domains with differing wavenumber.

Somewhat similar stationary states consisting of domains of differing wavenumber have been observed experimentally in convection in narrow channels [30], as well as in Taylor vortex flow [2] and in two-dimensional optical patterns [66]. The convection states can be described by the phase diffusion equation [1] [6, 68, 62, 63]

$$\partial_T \phi(X,T) = D(Q)\partial_X^2 \phi(X,T) + h.o.t., \tag{6.1}$$

which is nonlinear due to the dependence of D on $Q \equiv \partial_X \phi$. The higher order terms

[1] Certain phenomena such as the locking of adjacent domain walls into each other are not captured by the phase equation (6.1). For small amplitudes of the pattern the locking can be described by suitable Ginzburg-Landau equations [62, 63].

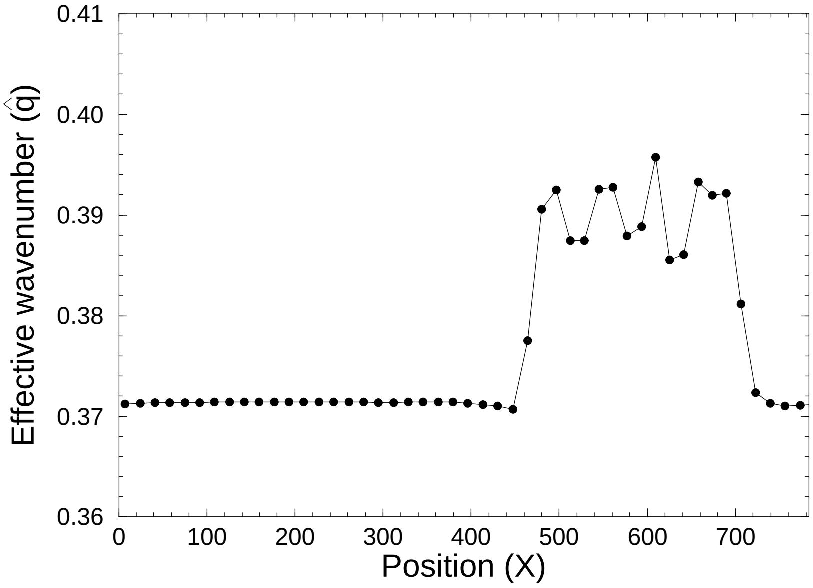

Figure 6.4: Local wavenumber of the time average of $A(X,T)$ for a localized chaotic solution. The local wavenumber in the chaotic region is larger than in the quiescent region. ($b = 0.6$, $L = 783$, $Q = 47(2\pi)/L = 0.377$).

include higher derivative terms (e.g. $G\partial_X^4\phi(X,T)$) which are important when D is small or negative, or when these higher derivatives are large. Stable solutions of (6.1) that consist of domains of differing wavenumber can occur if the diffusion coefficient $D(Q)$ is negative only over a small range of wavenumbers. In this situation, initial conditions with a uniform wavenumber in this unstable range will evolve to a structure consisting of domains in which the local wavenumber lies in either of the two adjacent ranges of stable wavenumbers. At the interface between these domains, the higher-order terms in (6.1) are important and there is an internal transition layer (similar to a boundary layer). These transition layers can be studied using matched asymptotic expansions as has been done for the Cahn-Hilliard equation and other related equations similar to (6.1) [85].

Equation (6.1) is only valid as long as the gradients in the wavenumber are small. During phase slips this is not the case. In fact, the phase ϕ is not even defined at one instant during the phase slip process. The solution shown in Figure 6.2 includes phase slips and thus cannot be described by (6.1). However, because each phase slip in the solution in Figure 6.2 is immediately followed by a second phase slip which restores the phase to its value before the first phase slip, on a long time scale the effective total phase $\Delta\hat{\phi} = \int_0^L \hat{Q}dX$ of the system is conserved. Here the effective wavenumber $\hat{Q}$ is defined to be $\partial_X\hat{\phi}$ where $\hat{\phi}$ is the phase of a running time average of $A(X,T)$:

$$\hat{A}(X,T) = \frac{1}{\Delta T}\int_{T-\Delta T}^{T} A(X,\check{T})d\check{T} \equiv \hat{R}e^{i\hat{\phi}}. \tag{6.2}$$

The time interval ΔT is chosen so that (6.2) averages over many double phase slips. An equivalent analysis could also be based on the phase of a running time average of $B(X,T)$ instead of $A(X,T)$. The $A(X,T)$ portion of the solution to (2.1,2.2) can be written as

$$A(X,T) = \hat{A}(X,T) + F_A(X,T) \tag{6.3}$$

where $F_A(X,T) \equiv A(X,T) - \hat{A}(X,T)$ contains the rapid fluctuations due to the phase slips and has small magnitude except in the neighborhood of a phase slip. $\hat{A}(X,T)$ contains variations on slower time and space scales and it is assumed that

$\hat{R} = \hat{R}(\hat{Q})$ (this is similar to (2.6)). Due to the translation symmetry in time and translation and reflection symmetries in space of (2.4,2.5), the long-wave evolution equation for the effective phase $\hat{\phi}(X,T)$ is expected to be a diffusion equation similar to (6.1)

$$\partial_T \hat{\phi}(X,T) = \hat{D}(\hat{Q})\partial_X^2 \hat{\phi}(X,T) + h.o.t.. \tag{6.4}$$

In order to test this explicitly, measurement of the effective phase diffusion coefficient $\hat{D}$ is made by measuring the response of the effective phase of the chaotic state to a localized time-periodic forcing. This approach to measuring the effective diffusion coefficient of a chaotic state is similar to that used in experiments on turbulent Taylor vortex flow wherein an endcap was moved sinusoidally [86]. Perhaps it should be emphasised that, while the motivation to measure the effective diffusion coefficient is to understand the localized chaotic states (as shown in Figure 6.2), the actual measurements described in this section are done on extended chaotic states (as shown in Figure 6.1). Localized forcing of the effective phase in the simulations is accomplished by including a spatially local, time-periodic advection term in (2.1,2.2) giving:

$$\begin{aligned}
\partial_T A + (v+s)\partial_X A &= d\partial_X^2 A + aA + bB + cA(|A|^2+|B|^2) + gA|B|^2 && (6.5)\\
\partial_T B + (v-s)\partial_X B &= d^*\partial_X^2 B + a^*B + bA + c^*B(|A|^2+|B|^2) + g^*B|A|^2 && (6.6)\\
\text{with } v &= \begin{cases} v_0 \sin(\omega_0 T) & \text{for } X_1 \le X \le X_2 \\ 0 & \text{otherwise.} \end{cases}
\end{aligned}$$

For small values of v_0 and ω_0, the localized advection term causes formerly stationary solutions to drift within the region $X_1 \le X \le X_2$, periodically reversing their direction according to the sign of v. For the regions $X < X_1$, and $X > X_2$ the situation resembles an imposed boundary condition at $X = X_1$, and $X = X_2$ at which the phase of the solution varies sinusoidally.

The solution to (6.4) for $X > X_2$, which satisfies the boundary condition $\hat{\phi}(X_2,T) = \epsilon \sin(\omega_0 T)$, is

$$\hat{\phi}(X,T) = \hat{Q}_0(X - X_2) + \epsilon e^{-\alpha(X-X_2)} \sin(\omega_0 T - \beta(X - X_2)) \tag{6.7}$$

$$\text{where } \alpha = \beta = \sqrt{\frac{\omega_0}{2\hat{D}}}. \tag{6.8}$$

If the effective phase of the solution $A(X,T)$ in the region $X > X_2$ obeys this relationship then

$$\hat{A}(X,T) = \hat{R}e^{i\hat{\phi}(X,T)} = \hat{R}e^{i(\hat{Q}_0(X-X_2)+\tilde{\phi})} \tag{6.9}$$

$$\text{where } \tilde{\phi} = \epsilon e^{-\alpha(X-X_2)}\sin(\omega_0 T - \beta(X-X_2)) \tag{6.10}$$

$$\text{and } \hat{R} = \hat{R}(\partial_X\hat{\phi}(X,T)) = \hat{R}(\hat{Q}_0 + \partial_X\tilde{\phi}). \tag{6.11}$$

If v_0 and ω_0 are small then the magnitude of the periodic variations in the effective phase $\tilde{\phi}$ will also be small. Taylor expanding $\hat{R}(\hat{Q}_0 + \partial_X\tilde{\phi})$ and $e^{i\tilde{\phi}}$ gives

$$\hat{A}(X,T) \sim (\hat{R}(\hat{Q}_0) + \hat{R}'(\hat{Q}_0)\partial_X\tilde{\phi} + \ldots)e^{i\hat{Q}_0(X-X_2)}(1 + i\tilde{\phi} + \ldots). \tag{6.12}$$

Taking the Fourier transform of $A(X,T)$ in time,

$$\mathcal{A}(X,\Omega) = \frac{1}{\tau}\int_0^\tau e^{i\Omega T}A(X,T)dT = \frac{1}{\tau}\int_0^\tau e^{i\Omega T}\hat{A}(X,T)dT + \frac{1}{\tau}\int_0^\tau e^{i\Omega T}F_A(X,T)dT, \tag{6.13}$$

and assuming that the fast variations $F_A(X,T)$ give only negligible contributions to the Fourier components at low frequencies yields

$$\mathcal{A}(X,-\omega_0) \approx \frac{\epsilon}{2}\left[(\hat{R}(\hat{Q}_0) - \beta\hat{R}'(\hat{Q}_0)) + i\alpha\hat{R}'(\hat{Q}_0)\right]e^{-\alpha(X-X_2)+i(\hat{Q}_0-\beta)(X-X_2)} \tag{6.14}$$

$$\mathcal{A}(X,\omega_0) \approx \frac{\epsilon}{2}\left[(-\hat{R}(\hat{Q}_0) - \beta\hat{R}'(\hat{Q}_0)) - i\alpha\hat{R}'(\hat{Q}_0)\right]e^{-\alpha(X-X_2)+i(\hat{Q}_0+\beta)(X-X_2)}. \tag{6.15}$$

Thus, the magnitude of the Fourier modes $\mathcal{A}(X,-\omega_0)$ and $\mathcal{A}(X,\omega_0)$ (corresponding to the frequency ω_0 in the localized advection term) will decay exponentially in space as $X - X_2$ increases if the phase behaves diffusively. Figure 6.5 shows that this exponential behavior is realized in the simulations. It gives the absolute value of the Fourier mode $\mathcal{A}(X,\omega_0)$ versus space for two different values of the frequency ω_0. According to (6.8) the decay rate α is proportional to $\omega_0^{1/2}$ for diffusive behavior. The ratio of the slopes of the curves in Figure 6.5 are consistent with this diffusive scaling. Note that for larger frequencies, and therefore larger gradients of $\hat{\phi}$, higher

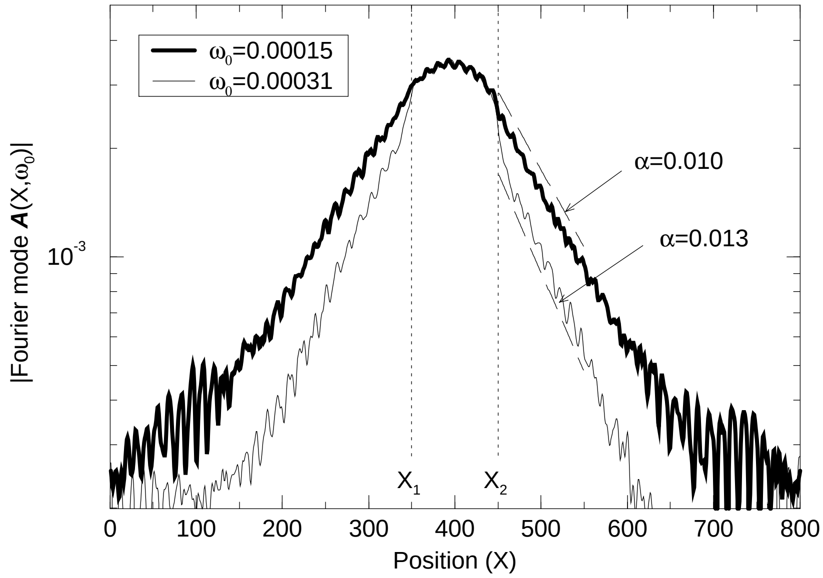

Figure 6.5: Decay of the magnitude of the coefficient of the time Fourier transform of A corresponding to the frequency ω_0 in the localized advection term v in equations (6.5,6.6), for two different values of ω_0 ($b = 0.61$, $L = 800$, $Q = 51(2\pi)/L = 0.4006$, $v_0 = 1.630\omega_0$).

order terms (like $-\hat{G}\partial_X^4\hat{\phi}$, etc.) have to be kept in the diffusion equation which affect the dependence on ω. For $\hat{G} > 0$, α is expected to go to zero slower than $\omega^{1/2}$:

$$\frac{\alpha(\omega_1)}{\alpha(\omega_2)} = \left(\frac{\omega_1}{\omega_2}\right)^{1/2}[1 + \frac{\hat{G}}{2\hat{D}^2}(\omega_2 - \omega_1) + O(\omega_1\omega_2)]. \tag{6.16}$$

Analogous behavior was found in the nonchaotic regime where numerical simulations were able to reproduce the analytical value of the diffusion coefficient.

The phase slips introduce short-scale deviations from the exponential behavior which can be seen in Figure 6.5. In order to reduce the effect of this noise and extract a reliable decay rate α, the Fourier integral (6.13) has been extended over many periods ($\tau = 88 \times 2\pi/\omega_0$) of the function $v(X,T)$ in the advection term in (6.5,6.6).

From the decay rate α the diffusion coefficient $\hat{D}$ can be calculated using (6.8). The diffusion coefficient $\hat{D}$ can also be calculated using β which is obtained from the ratio of the Fourier coefficients $\mathcal{A}(X,\omega_0)$ and $\mathcal{A}(X,-\omega_0)$ given by (6.14,6.15):

$$\log\left(\frac{\mathcal{A}(X,\omega_0)}{\mathcal{A}(X,-\omega_0)}\right) = \log\left(\frac{(-\hat{R}(\hat{Q}_0) - \beta\hat{R}'(\hat{Q}_0)) - i\alpha\hat{R}'(\hat{Q}_0)}{(\hat{R}(\hat{Q}_0) - \beta\hat{R}'(\hat{Q}_0)) + i\alpha\hat{R}'(\hat{Q}_0)}\right) + i2\beta X. \tag{6.17}$$

A plot of the imaginary part of this quantity versus X will be linear with slope 2β if the effective phase is behaving diffusively. Figure 6.6 shows this plot for the same simulations as presented in Figure 6.5 and exhibits the expected linear behavior near X_1 and X_2.

The diffusion equation (6.4) yields $\alpha = \beta$ (cf. (6.8)) so the slopes indicated on Figure 6.6 should be twice those indicated on Figure 6.5. Although the small discrepancies could be due to higher order terms in (6.4) they are within the margin of error in the measurement which is mainly due to the short-scale chaotic dynamics.

The conclusion drawn from the results in Figures 6.5 and 6.6 is that the dynamics of the effective phase are indeed diffusive. Figure 6.7 shows the wavenumber dependence of the effective phase diffusion coefficient $\hat{D}(\hat{Q})$ along with the analytical phase diffusion coefficient for the stationary solution [68]. The solid curve shows

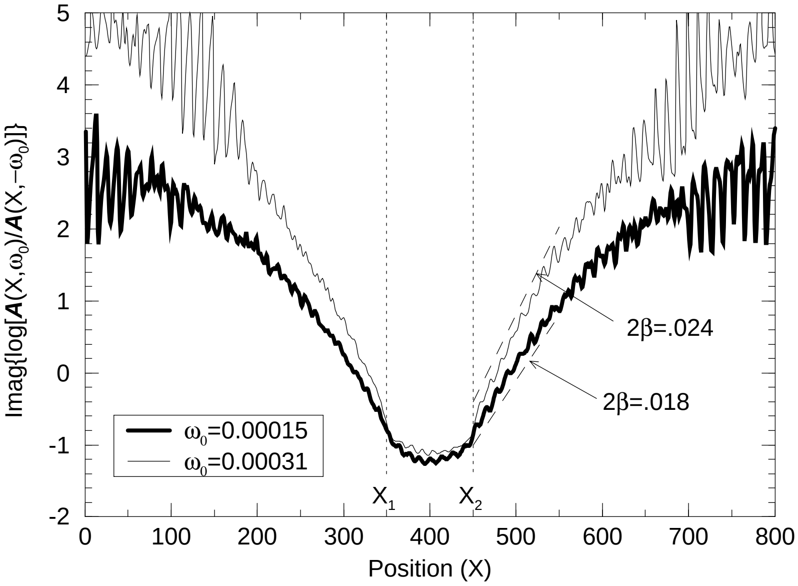

Figure 6.6: Imaginary part of the ratio of the coefficients of the time Fourier transform of A corresponding to the frequencies $\pm\omega_0$ in the localized advection term v in equations (6.5,6.6), for two different values of ω_0 ($b = 0.61$, $L = 800$, $Q = 51(2\pi)/L = 0.4006$, $v_0 = 1.630\omega_0$).

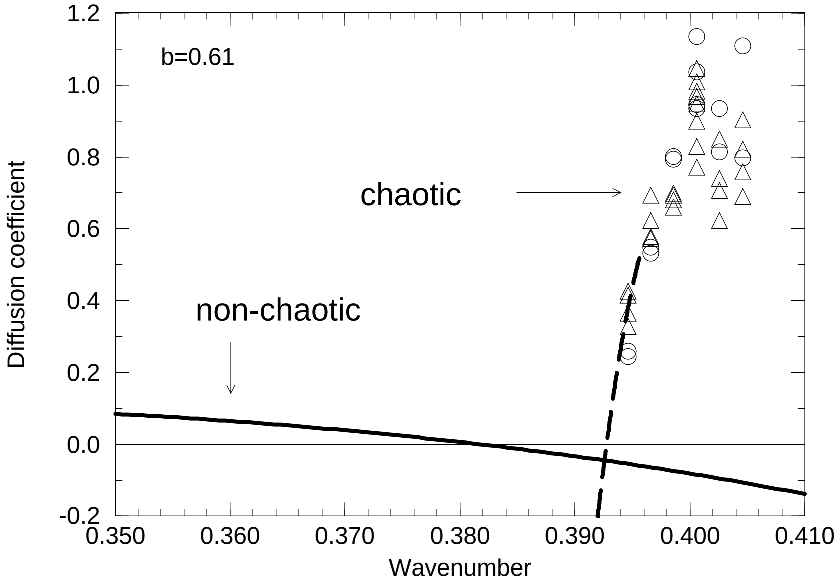

Figure 6.7: Analytical phase diffusion coefficient D for the stationary solution (solid line) and effective diffusion coefficient $\hat{D}$ for the chaotic solution; Triangles and circles represent numerical results as obtained from α and β (cf. Figures 6.5 and 6.6), the dashed line is the presumed extension of these results ($b = 0.61$).

the analytical phase diffusion coefficient D for the stationary solution. The triangles give the effective phase diffusion coefficient $\hat{D}$ for the chaotic solutions as measured by using the decay rate α, while the circles show $\hat{D}$ as measured using β. For each simulation four triangles can be drawn corresponding to the decay rates for the $+\omega$ and $-\omega$ Fourier modes to the right and to the left of the localized forcing. Two circles can be drawn: one for the left side, one for the right. Despite the scatter in the data it is clear that $\hat{D}(\hat{Q})$ decreases with decreasing $\hat{Q}$ and presumably goes to zero at a wavenumber for which the diffusion coefficient of the nonchaotic state is still negative as shown by the dashed line. Thus the phase of the system is diffusively unstable over a finite range of wavenumbers. This, along with the conservation of the total phase (here the conservation of the total *effective* phase), is known to lead to stable domains of differing wave numbers, and explains the localization of the chaotic region in Figure 6.2.

For the wavenumbers at which the measurement of the effective diffusion coefficient was made, the effective phase of the solution remains almost stationary in the absence of any localized forcing. For larger wavenumbers, however, the effective phase drifts significantly on the time scale over which the attempt was made to make the diffusion coefficient measurements. This is illustrated in figure 6.8. Because of this drift, attempts to measure the effective diffusion coefficient for larger wavenumbers than those included in Figure 6.7 were unsuccessful.

Figure 6.7 suggests that the chaotic activity should not disappear homogeneously if the average wavenumber is decreased towards the stable regime. Instead, the homogeneously chaotic state should become unstable to long-wave modulations and eventually split up into chaotic and stationary domains in which the local wavenumber is in the respective stable regimes ($D > 0$ and $\hat{D} > 0$). A similar breaking up of the homogeneous state is expected as the forcing amplitude b is increased. Numerical simulations confirm this as shown in Figure 6.9.

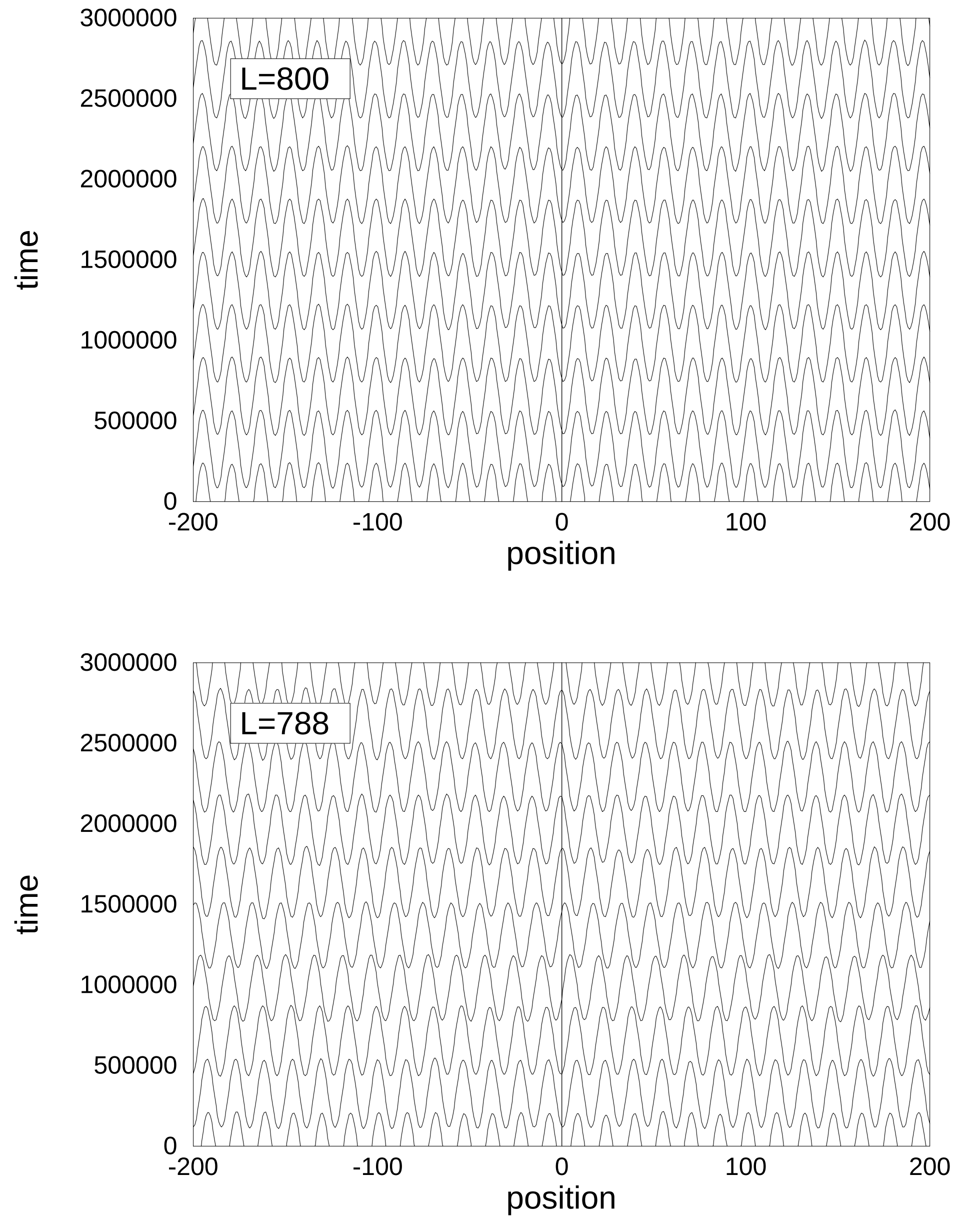

Figure 6.8: Space-time diagram shows the real part of a time average of A ($b = 0.61$). a) Effective phase remains almost stationary ($Q = 51(2\pi)/L = 0.4006$). b) Effective phase drifts significantly ($Q = 51(2\pi)/L = 0.4067$).

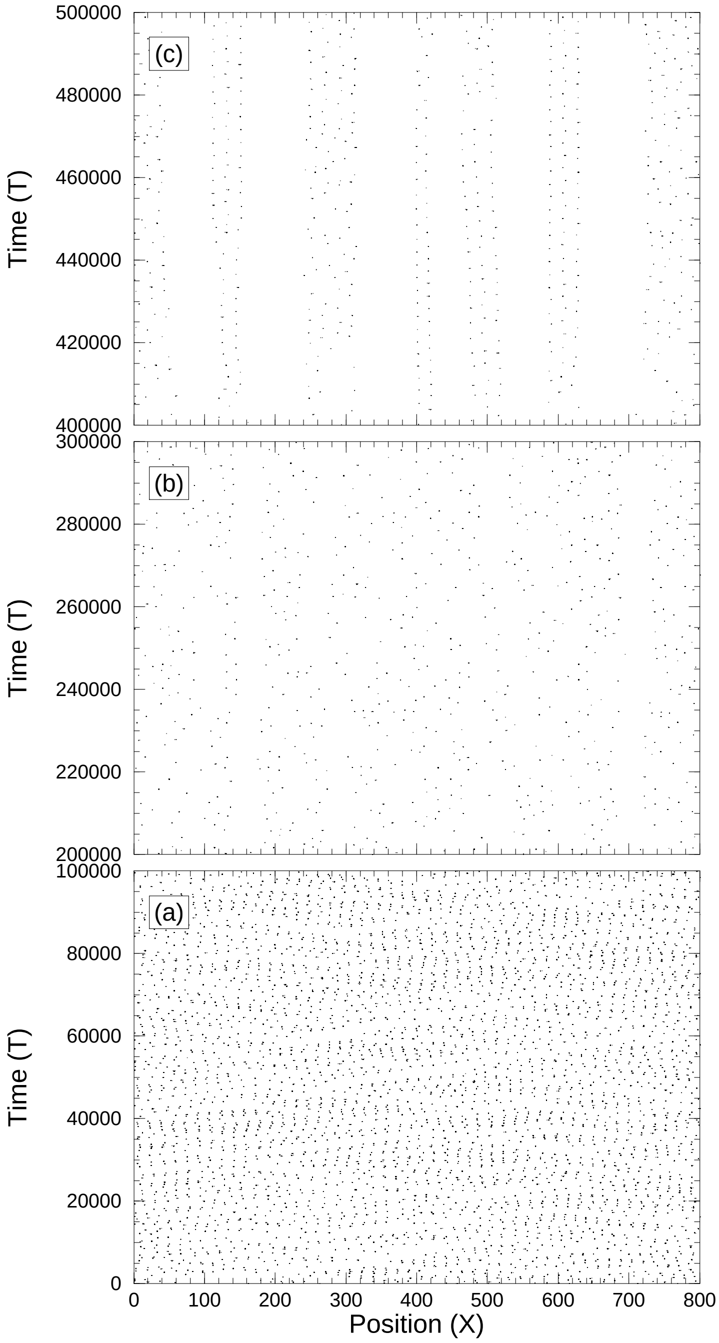

Figure 6.9: A set of solutions obtained by incrementally increasing the forcing amplitude b. The extended spatio-temporal chaos breaks up into localized regions before the Eckhaus stability limit is reached ($L = 800$, $Q = 51(2\pi)/L = .4006$). (a) $b = 0.62$, (b) $b = 0.64$, (c) $b = 0.66$.

Chapter 7

Dynamics of a Very Small System

In this final chapter on the one-dimensional system, dynamics in a very small domain will be briefly presented. One reason for studying the very small system is that it might provide insights towards developing a model that displays double phase slips which could be analyzed without relying on numerical simulations. The simulations reported in this chapter use only eight collocation points (that is, only Fourier modes with wavenumbers $k = n2\pi/L$ for $n = -4$ to 4 are included). The fact that double phase slips are still seen in these simulations indicates that this basic feature does not require more than 32 degrees of freedom. Although it was not investigated extensively, double phase slips were not seen in simulations with only four collocation points. The solutions of interest are similar to the simple periodic solutions discussed in chapter 5 but arise in a supercritical Hopf bifurcation from a mixed mode state. Double phase slips move the system between a configuration where the total phase of the system is zero and one where the total phase of the system is 2π. This is to be contrasted with the simple periodic solutions in chapter 5 where the system oscillated between states with total phase $4(2\pi)$ and $5(2\pi)$ and the apparent mixed mode enclosed by the periodic orbit was never seen to be stable.

The initial condition for the simulations presented here was a perturbed wave with only one wavelength in the domain. For a domain size $L = 8$ the solution goes to the uniform stationary solution given by (2.4-2.9) with $Q = 0$. For slightly larger domains (and hence initial conditions with slightly smaller wavenumbers) the solution goes to a stationary solution where the Fourier modes corresponding to zero and one wavelength in the domain both have nonzero amplitudes. Figure 7.1a shows a phase plane representation (the amplitude of Fourier mode one plotted versus the amplitude of Fourier mode zero amplitude) for such a simulation. The final state for this solution and its Fourier spectrum are shown in Figure 7.2.

Increasing the domain size further results in periodic solutions such as the one whose phase plane representation is shown in Figure 7.1b. The numerical simulations indicate that the periodic solutions bifurcate supercritically from the mixed mode solution. As L is increased further the amplitude of the periodic oscillations grow. At the bifurcation point the periodic oscillations do not actually represent double phase slips since the magnitude of the mixed mode solution is nonzero everywhere in space. To clarify this point the mixed mode solution near the bifurcation point has been plotted in the complex plane in Figure 7.3. Since the solution is bounded away from the origin, the small oscillations arising from the supercritical bifurcation cannot cause the solution to pass through the origin as required for a phase slip. But, for domain sizes greater than $L \approx 11.3$ the periodic variations are large enough to cause double phase slips in the solution. When L is slightly larger than 12 the initial condition becomes attracted to the stationary solution given by (2.4-2.9) with $Q = 1$.

Figures 7.4 and 7.5 show phase plane representations over the entire range of domain sizes L discussed above. Note that these plots include a transient which leads to the final state of the system. The initial condition is towards the upper left hand corner of each graph. For the periodic solutions the periodic trajectory is shown by what appears to be a solid closed curve. The figures were made by plotting a point at each time step ($\Delta t = 0.25$) in a simulation.

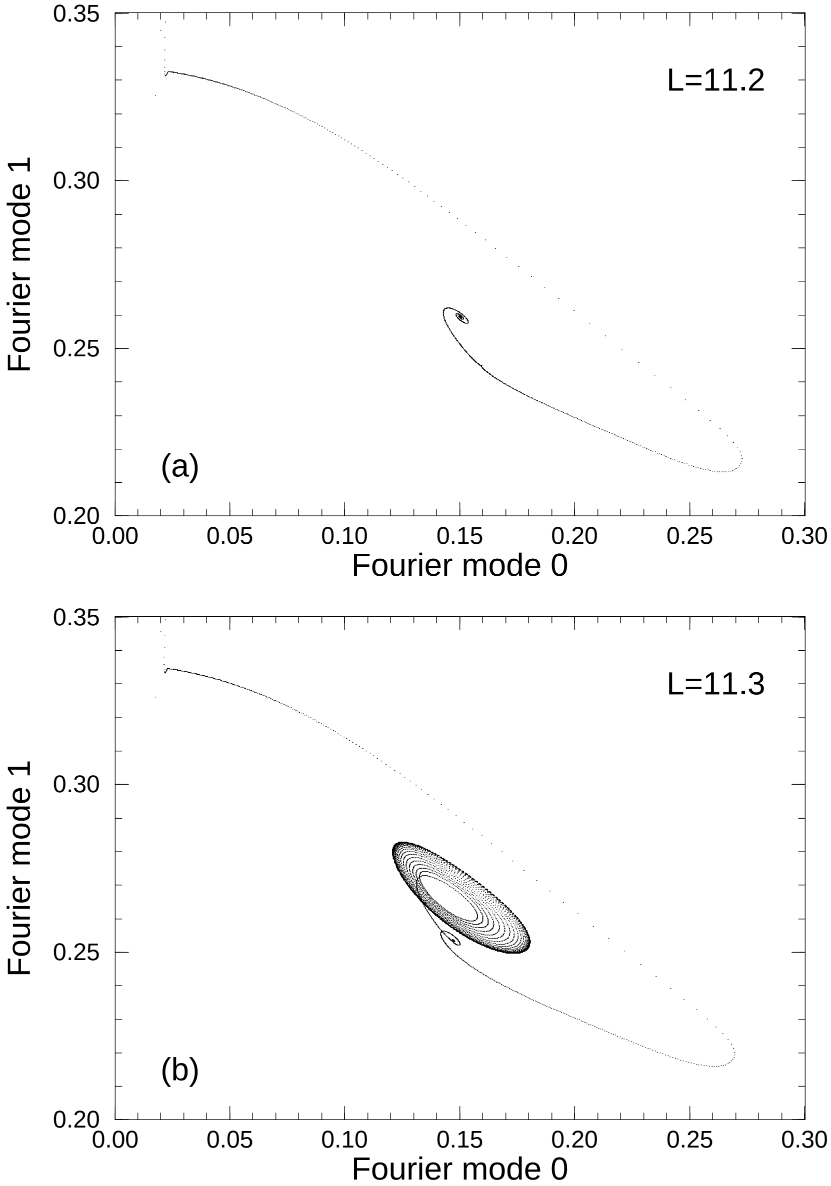

Figure 7.1: Phase plane representation including a transient for two types of solutions in a very small system (a) L=11.2, final state is a stationary mixed mode solution; (b) L=11.3, final state is periodic in time. ($a = -0.05$, $b = 1.0$, $c = -1 + 4i$, $d = 1 + 0.5i$, $s = 0.2$, $g = -1 - 12i$)

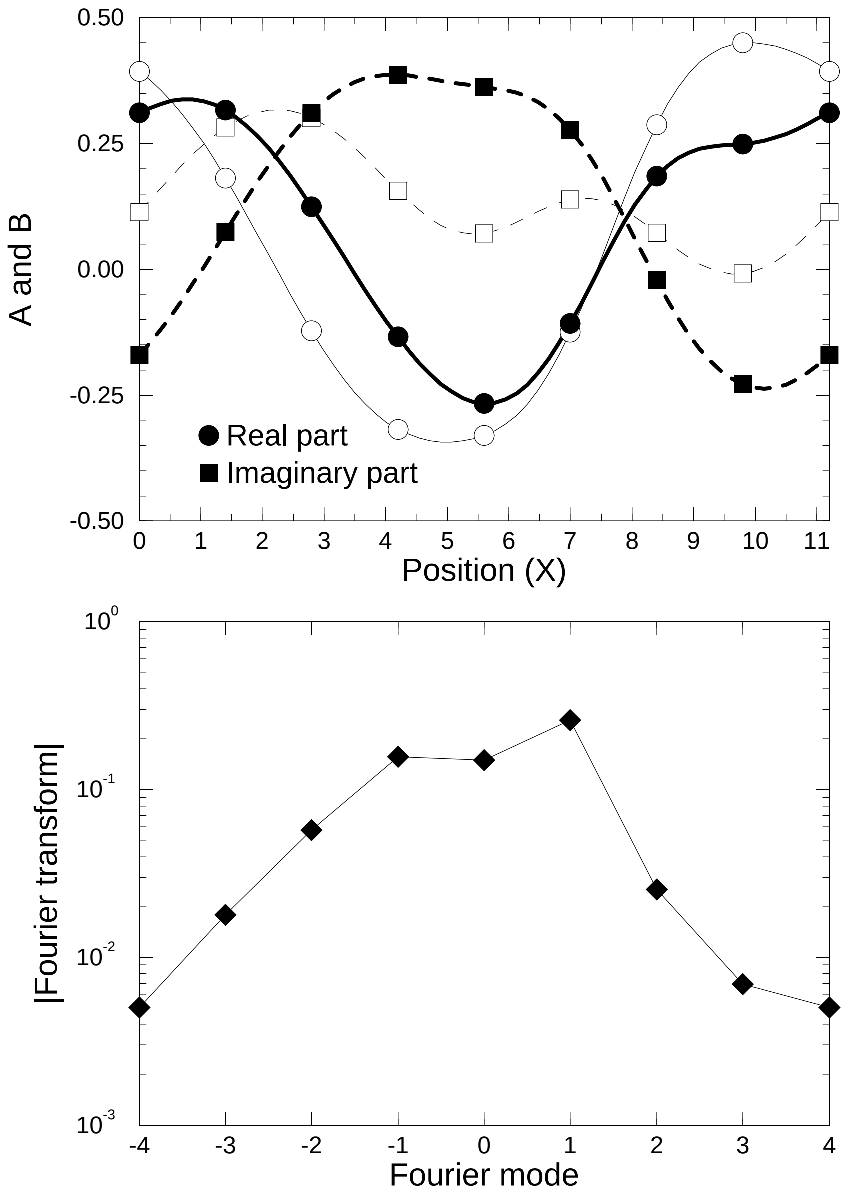

Figure 7.2: Final state for the mixed mode solution whose phase plane representation is shown in figure 7.1a ($L = 11.2$). a) Real and imaginary parts of $A(X)$ (solid symbols) and $B(X)$ (open symbols). b) Magnitude of the Fourier coefficients for either A or B (the magnitudes are equal).

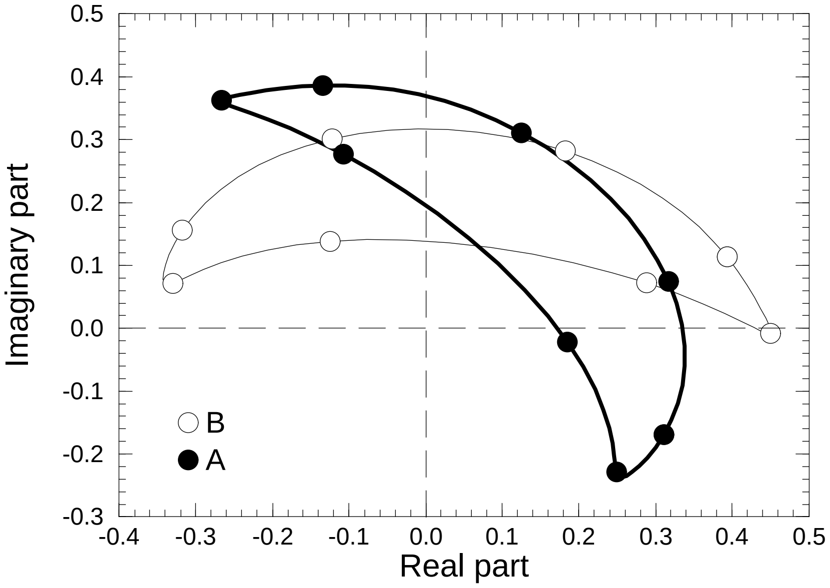

Figure 7.3: Mixed mode solution for $L = 11.2$ plotted in the complex plane.

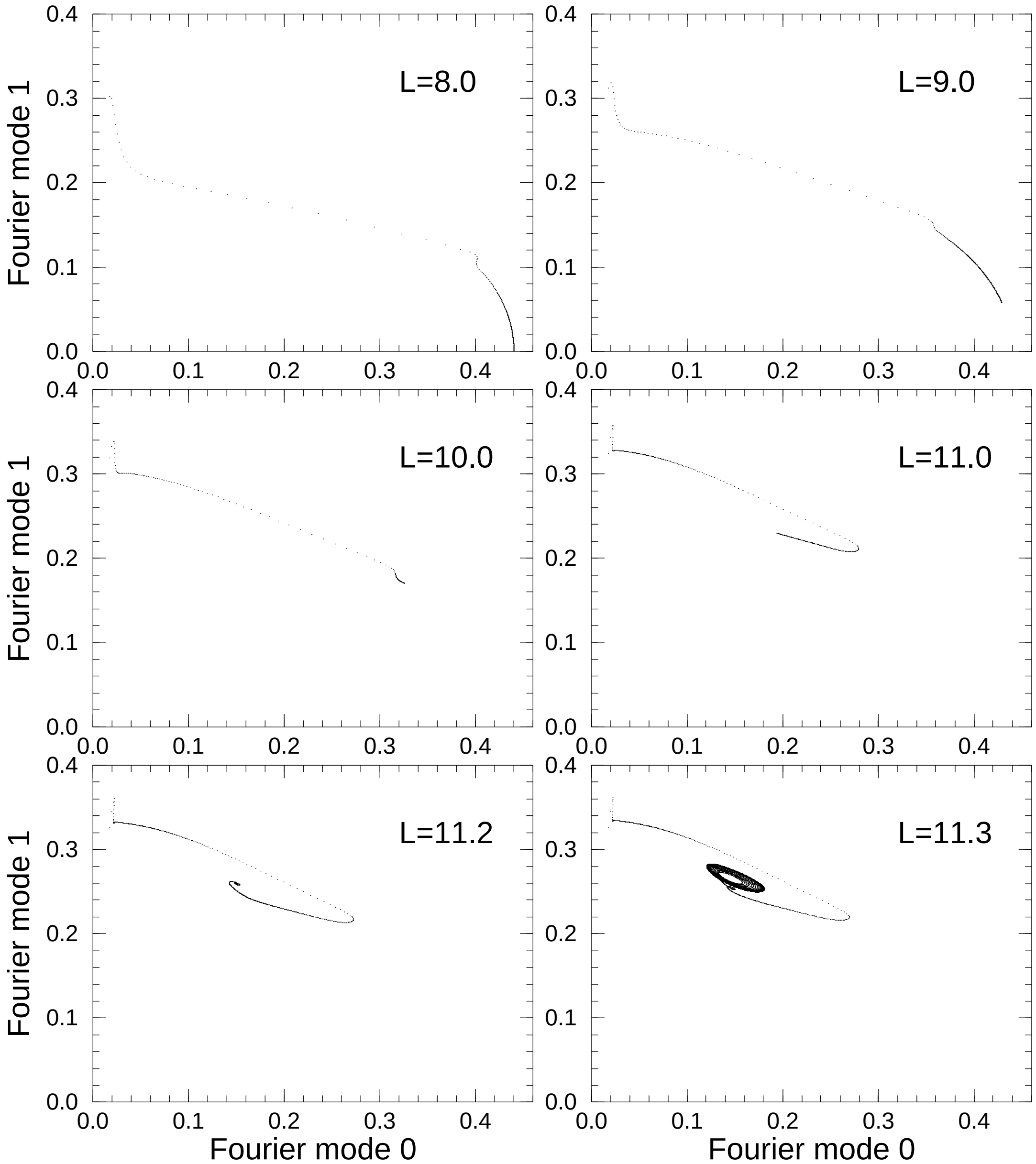

Figure 7.4: Phase plane representations of solutions for $L = 8.0$ to $L = 11.3$.

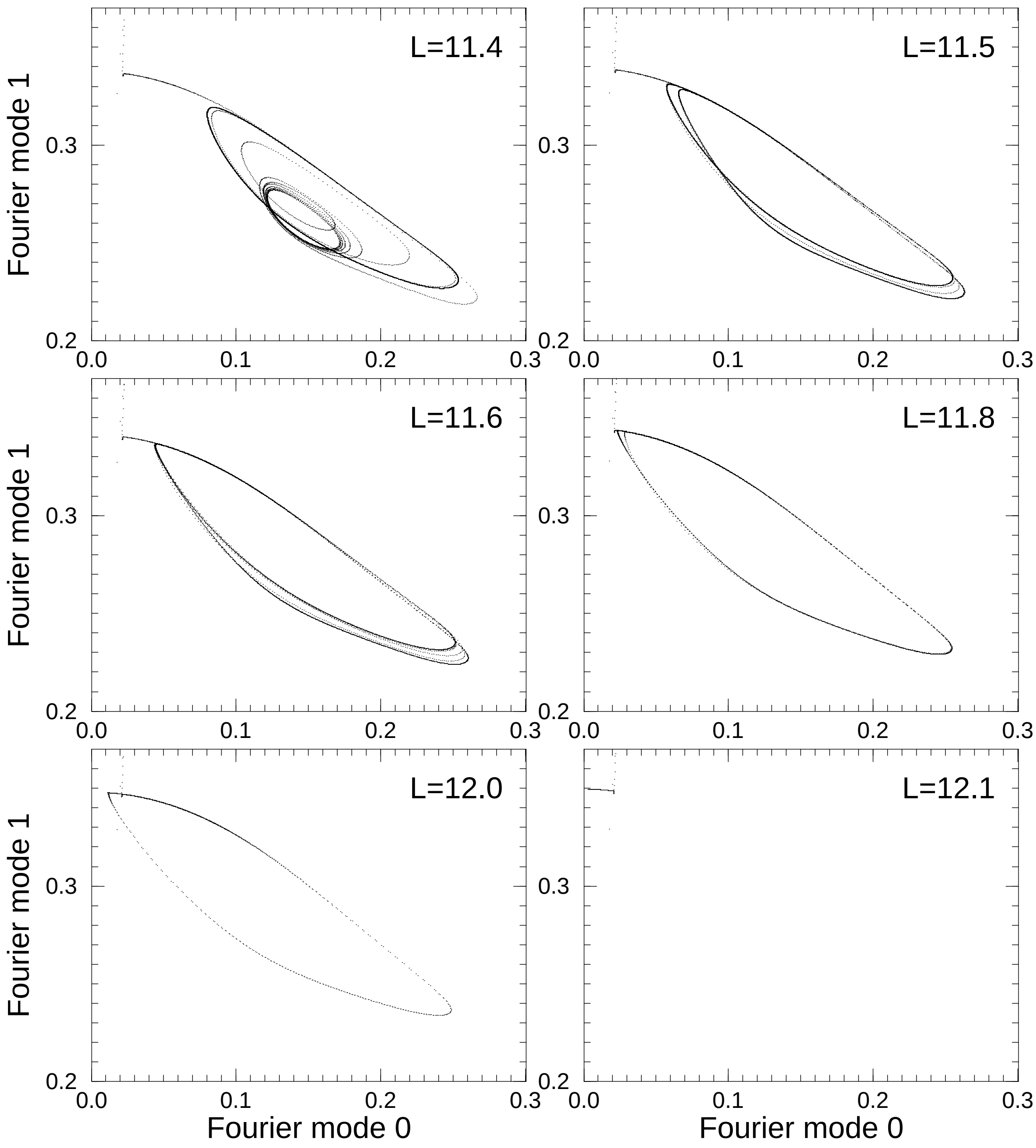

Figure 7.5: Phase plane representations of solutions for $L = 11.4$ to $L = 12.1$. Note that the scales have changed from the previous figure.

Part II

Two-Dimensional System

Chapter 8

The Model

Part two of the dissertation considers the dynamics of parametrically excited waves within the framework of coupled *two-dimensional* Ginzburg-Landau equations very similar to (2.1,2.2). Recall from chapter 2 that these describe the temporal evolution of the complex amplitudes A and B of oppositely traveling waves that are coupled due to a parametric forcing at a frequency ω_e, which is close to twice the frequency of the traveling waves. The traveling waves are assumed to arise in a supercritical Hopf bifurcation. In terms of the amplitudes A and B, physical quantities u like the vertical fluid velocity in the mid-plane of a convection system are given by

$$u(x,y,t) = \epsilon A(X,Y,T)e^{i(q_c x - \frac{\omega_e}{2}t)} + \epsilon B(X,Y,T)e^{i(q_c x + \frac{\omega_e}{2}t)} + c.c. + o(\epsilon). \qquad (8.1)$$

The amplitudes A and B vary on the slow time and space scales, $T = \epsilon^2 t$, $X = \epsilon x$, $Y = \epsilon y$ with $\epsilon \ll 1$.

The ansatz (8.1) introduces an anisotropy into the system since the slowly varying coordinates X and Y do not capture large variations in the orientation of the waves. Thus, use of this ansatz in an isotropic system requires restriction to situations where the orientation of the wavevector varies only slightly. This leads to coupled Newell-Whitehead-Segel equations (which include spatial derivatives $(\partial_x - i\partial_y^2)^2$, cf. (1.1)) for the amplitudes A and B (e.g. [13]).

The anisotropy inherent in (8.1) is appropriate if the physical system has an axial anisotropy and the waves travel essentially along a preferred direction. This is the case, for instance, in electro-convection in nematic liquid crystals [1] [65,64,18].

[1]The anisotropy in electroconvection in nematic liquid crystals is due to a preferred direction

In such an anisotropic system, if the waves arise in a supercritical bifurcation, they can be described by coupled Ginzburg-Landau equations of the form [69, 83]

$$\partial_T A + s\partial_X A = d\partial_X^2 A + d_2\partial_Y^2 A + aA + bB + cA(|A|^2 + |B|^2) + gA|B|^2 \qquad (8.2)$$

$$\partial_T B - s\partial_X B = d^*\partial_X^2 B + d_2^*\partial_Y^2 B + a^*B + bA + c^*B(|A|^2 + |B|^2) + g^*B|A|^2. \quad (8.3)$$

These equations are the same as the one-dimensional system (2.1,2.2) except for the additional term involving d_2, which describes the dissipation in the Y direction. As in the one-dimensional case, (8.2,8.3) possess three types of simple solutions: $|A| = |B| = const$, $|A| \neq |B|$ (both constant), and $|A| = |B|$ (both time-periodic) [69], in addition to the trivial solution $A = B = 0$. Again our interest is focused on solutions of the first type, which correspond in the physical system to standing waves that are phase-locked to the parametric forcing. These solutions are given by

$$A = Re^{i(QX+PY+\phi_A)} \qquad (8.4)$$

$$B = Re^{i(QX+PY+\phi_B)} \qquad (8.5)$$

where:

$$R^2 = \frac{-(\hat{a}_r n_r + \hat{a}_i n_i) \pm \sqrt{(\hat{a}_r n_r + \hat{a}_i n_i)^2 - (n_r^2 + n_i^2)(\hat{a}_r^2 + \hat{a}_i^2 - b^2)}}{(n_r^2 + n_i^2)} \qquad (8.6)$$

$$\phi_B - \phi_A = \arctan\frac{\hat{a}_i + n_i R^2}{\hat{a}_r + n_r R^2} \qquad (8.7)$$

and:

$$\hat{a} \equiv \hat{a}_r + i\hat{a}_i = a - isQ - dQ^2 - d_2P^2 \qquad (8.8)$$

$$n \equiv n_r + in_i = 2c + g. \qquad (8.9)$$

With $P = 0$ equations (8.4-8.9) are the same as (2.4-2.9). Solutions with $P \neq 0$ correspond to waves oblique to the x direction.

of the rod-like molecules. Parametrically excited waves have been observed in both the normal roll regime [64], in which the waves are perpendicular to the preferred direction of the molecules, and in the oblique roll regime [17], in which the waves are at an oblique angle to the preferred direction. The normal rolls are described by (8.2,8.3) while the oblique rolls are described by *four* coupled amplitude equations [75].

Chapter 9

Linear Stability Analysis

The linear stability analysis of the solutions of the two-dimensional problem (8.2,8.3) is very similar to the one-dimensional linear stability analysis presented in chapter 3 but must consider perturbations with wave vectors in all directions. Analyzing the stability of the trivial solution $A = B = 0$ gives the neutral surface

$$b^2 = (a_i - sQ - d_i Q^2 - d_{2,i}^2)^2 + (a_r - d_r Q^2 - d_{2,r} P^2)^2. \tag{9.1}$$

The linear stability analysis of the solutions of (8.2,8.3) given by (8.4-8.9) uses a perturbation of the form

$$\begin{aligned} \tilde{A} &= A_1 e^{\sigma T + i((Q+k_x)X + (P+k_y)Y)} + A_2 e^{\sigma^* T + i((Q-k_x)X + (P-k_y)Y)} & (9.2) \\ \tilde{B} &= B_1 e^{\sigma T + i((Q+k_x)X + (P+k_y)Y)} + B_2 e^{\sigma^* T + i((Q-k_x)X + (P-k_y)Y)} & (9.3) \end{aligned}$$

where $|A_1|, |A_2|, |B_1|, |B_2| \ll 1$ and results in the eigenvalue problem $M\mathbf{x} = \sigma\mathbf{x}$ where

$$M = \begin{bmatrix} m_{11} & cR^2 e^{i2\phi_A} & b + \hat{g}R^2 e^{i(\phi_A - \phi_B)} & \hat{g}R^2 e^{i(\phi_A + \phi_B)} \\ c^* R^2 e^{-i2\phi_A} & m_{22} & \hat{g}^* R^2 e^{-i(\phi_A + \phi_B)} & b + \hat{g}^* R^2 e^{i(\phi_B - \phi_A)} \\ b + \hat{g}^* R^2 e^{i(\phi_B - \phi_A)} & \hat{g}^* R^2 e^{i(\phi_A + \phi_B)} & m_{11}^* & c^* R^2 e^{i2\phi_B} \\ \hat{g}R^2 e^{-i(\phi_A + \phi_B)} & b + \hat{g}R^2 e^{i(\phi_A - \phi_B)} & cR^2 e^{-i2\phi_B} & m_{22}^* \end{bmatrix} \tag{9.4}$$

$$\text{and} \quad \mathbf{x} = \begin{bmatrix} A_1 \\ A_2^* \\ B_1 \\ B_2^* \end{bmatrix}. \tag{9.5}$$

Here

$$\hat{g} = c + g \tag{9.6}$$

and

$$\begin{aligned} m_{11} &= a - is(Q + k_x) - d(Q + k_x)^2 - d_2(P + k_y)^2 + (2c + \hat{g})R^2 & (9.7) \\ m_{22} &= a^* + is(Q - k_x) - d^*(Q - k_x)^2 - d_2^*(P - k_y)^2 + (2c^* + \hat{g}^*)R^2. & (9.8) \end{aligned}$$

The only difference from the one-dimensional problem being the definitions of m_{11} and m_{22} which are now dependent on the parameter d_2 and the Y direction wavenumbers P and k_y.

For given values of the parameters a, b, c, d, d_2, g, s, the solution wavenumbers Q and P, and the perturbation wavenumbers k_x and k_y, the eigenvalues of this matrix can be found numerically [76]. The real part of these eigenvalues can be represented by surfaces in (k_x, k_y) space. The curves in Figure 3.2 discussed in the one-dimensional stability analysis are cross sections of such surfaces.

Not all of the solutions which are stable in the one-dimensional system considered in part one are stable in the two-dimensional system (with $d_2 = d$). Some of the solutions are unstable to a long wavelength perturbation in the Y direction. This zig-zag instability reduces the band of stable wavenumbers from that found in the one-dimensional problem as shown in figure 9.1.

The instability is known as a zig-zag instability because it often results in patterns such as that shown in figure 9.2.

As seen in figure 9.1 there remains a band of stable wavenumbers for X direction waves, that is for $P = 0$. There are also stable waves oblique to the X direction, $P \neq 0$. Figure 9.3 gives a three dimensional representation of the volume enclosing stable wavenumbers in (Q, P, b) space. The regions of stable wavevectors for $b = 0.1$ to $b = 0.85$ which were used to generate Figure 9.3 are shown in Figure 9.4.

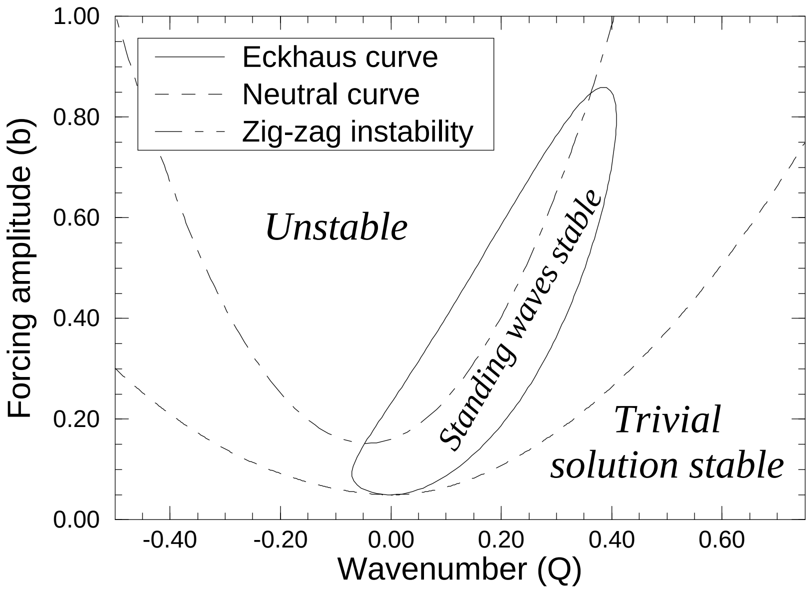

Figure 9.1: Linear Stability diagram for X direction waves for parameter values $a = -0.05$, $c = -1 + 4i$, $d = d_2 = 1 + 0.5i$, $s = 0.2$, $g = -1 - 12i$. The zig-zag instability reduces the band of stable wavenumbers for $b > 0.15$.

Figure 9.2: Transitory state which results from an initial condition which is zigzag unstable. Shown is a snapshot of the real part of A. White regions represent high values ($A \approx 0.3$), black regions represent low values ($A \approx -0.3$). The initial condition was vertical rolls perturbed with a small amount of random noise ($b = 0.5$, $Q = 5(2\pi)/L = .2$).

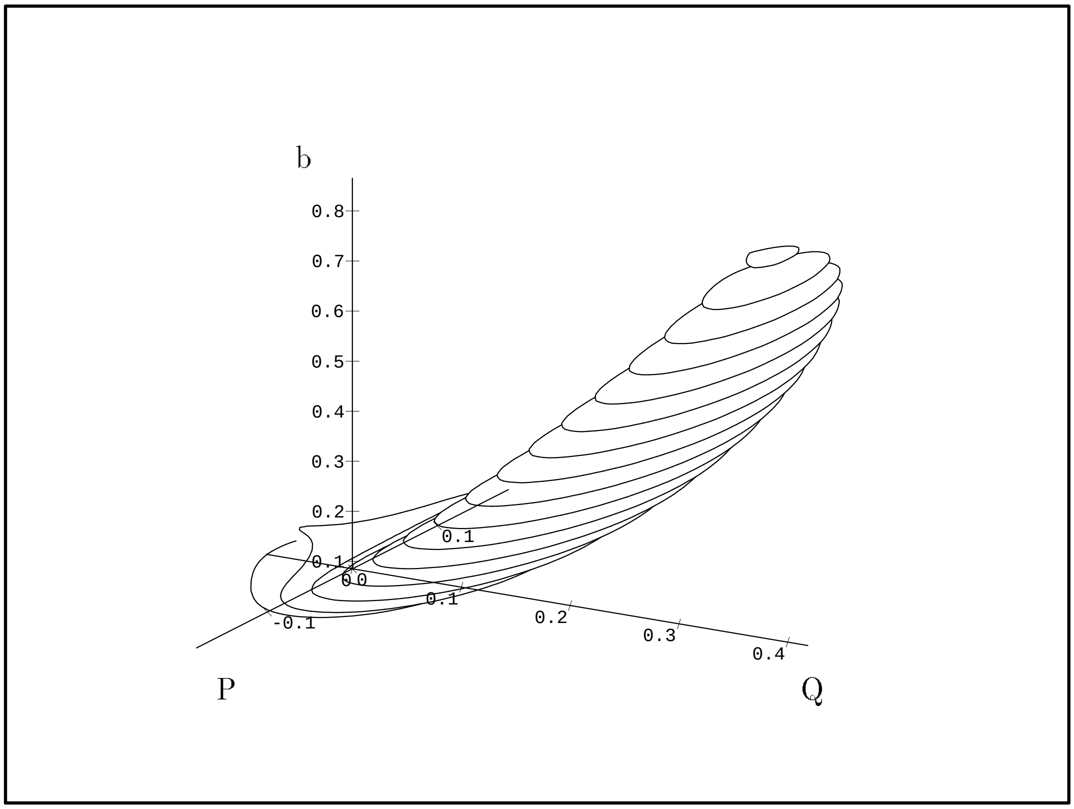

Figure 9.3: Linearly stable wavevectors for the two-dimensional system. The stable region indicated in Figure 9.1 is a cross section of this volume in the Q, b plane.

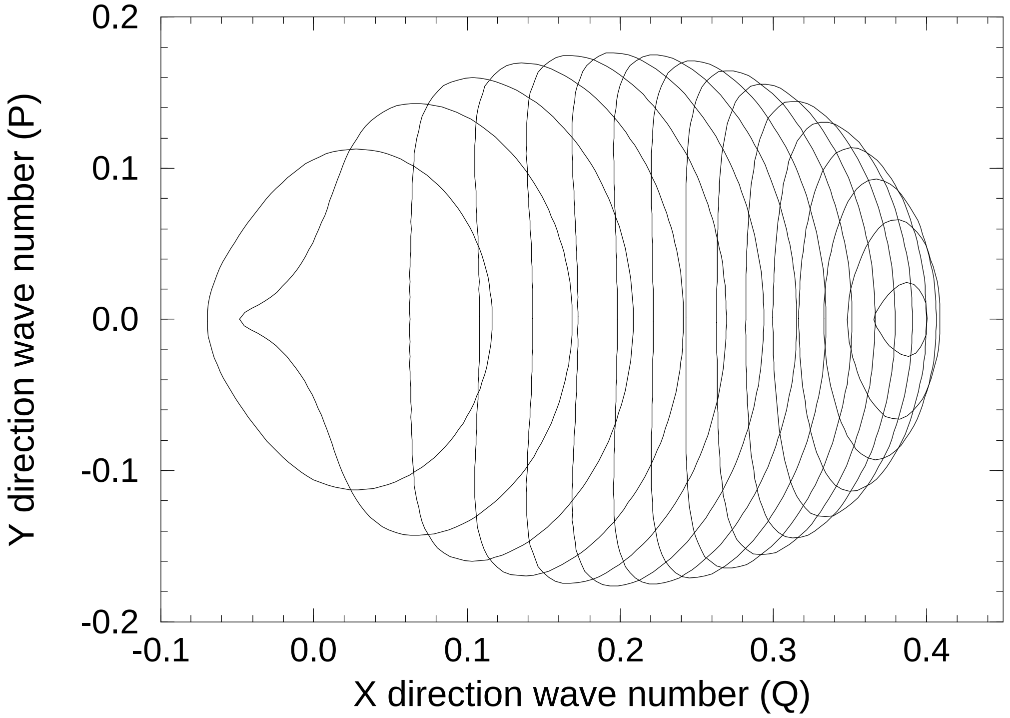

Figure 9.4: Linearly stable wavevectors for standing waves in the two-dimensional system for $b = 0.10, 0.15, 0.20, \ldots, 0.80, 0.85$. The leftmost curve is $b = 0.10$, the smallest closed curve (located near the right end of the figure) is $b = 0.85$.

Chapter 10

Defect Pairs and Bound Defect Pairs

As in the one-dimensional case (8.2,8.3) can be reduced to a single Ginzburg-Landau equation with real coefficients near onset. Therefore the solutions for small b are similar to those of a single real Ginzburg-Landau equation and the solution with an initial condition slightly outside the Eckhaus stability limit undergoes a transition which reduces the wavenumber. In two dimensions the transition from an Eckhaus unstable wave number to a stable wave number involves the creation of defect pairs which are created together and then move apart as shown in Figure 10.1.

There, part of the spatial domain of the problem at eight sequential times is represented by the eight squares. Within each square the solid curves represent locations where the real part of the solution is zero, and the dashed curves represent locations where the imaginary part of the solution is zero. Locations where a solid curve crosses a dashed curve are the "defects" where the amplitude of the solution is zero. These defects are indicated by circles in Figure 10.1. The defects, which form as a pair (at some $500 < t < 600$ in Figure 10.1), move apart leaving one less wave in the domain after they have moved far apart ($t = 2500$). This is analogous to a phase slip in one dimension.

For larger values of b the solutions to (8.2,8.3) also involve the creation of defect pairs. However, the defects often do not move far apart but stop after separating some finite distance, turn around and annihilate each other. This can be

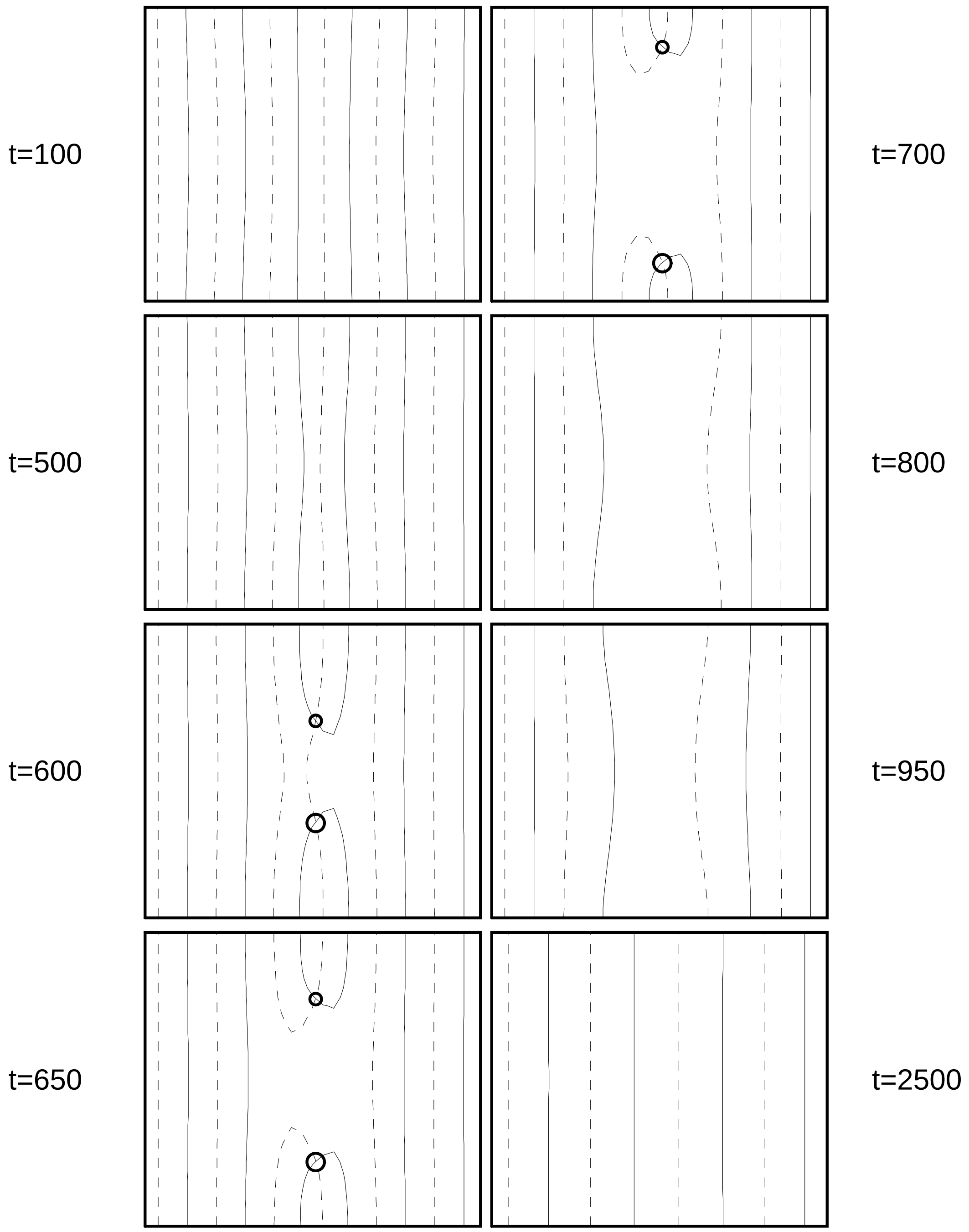

Figure 10.1: Standard wavenumber reducing transition in two dimensions. Solid curves represent locations where the real part of the solution is zero. Dashed curves represent locations where the imaginary part of the solution is zero. A *bound defect pair* can be visualized by considering the left column only, progressing from the top to the bottom then returning to the top.

visualized by considering only the left column of Figure 10.1. The solution begins with the downward sequence of squares from the top as sequential in time (as in the standard Eckhaus transition). However, on reaching the bottom of the column ($t = 650$) the time sequence reverses and leads back to the top of the column where the wavenumber resumes its original value. Such a *bound defect pair* is analogous to a *double* phase slip in one dimension. Solutions in the two-dimensional simulations have not consisted of only a single bound defect pair or the simple periodic solutions that are suggested by this visualization. But there are solutions where many of the defects which are created together as pairs annihilate each other. Figure 10.2 is a space-time diagram of such a solution for $b = 1.2$. The spatial aspect of Figure 10.2 is a projection; the y coordinate is not represented. Each circle represents the x-coordinate of the position of a defect and the time it was at this location. Small and large circles denote defects of opposite polarity (as they do in Figure 10.1). Focusing on the "loop" formed by the pair of defects created at $x \approx 29$ and $t \approx 2680$ one sees that the defects in this pair indeed move apart for a short time before they reverse their directions, ultimately annihilating each other at $x \approx 30$ and $t \approx 2710$. There are many such loops on the diagram as well as more complex events such as loops involving two or three defect pairs. While for this value of b most defects are "bound" in such a loop, there are also a few isolated "unbound" defects which travel large distances before annihilation.

Figures 10.1 and 10.2 are based on $A(X, Y, T)$. Similar to the phase slips in the one-dimensional problem, in the two-dimensional simulations a defect in A is always accompanied by a defect in B at a nearby location. The distance between a defect in A and the corresponding defect in B is discussed in [13].

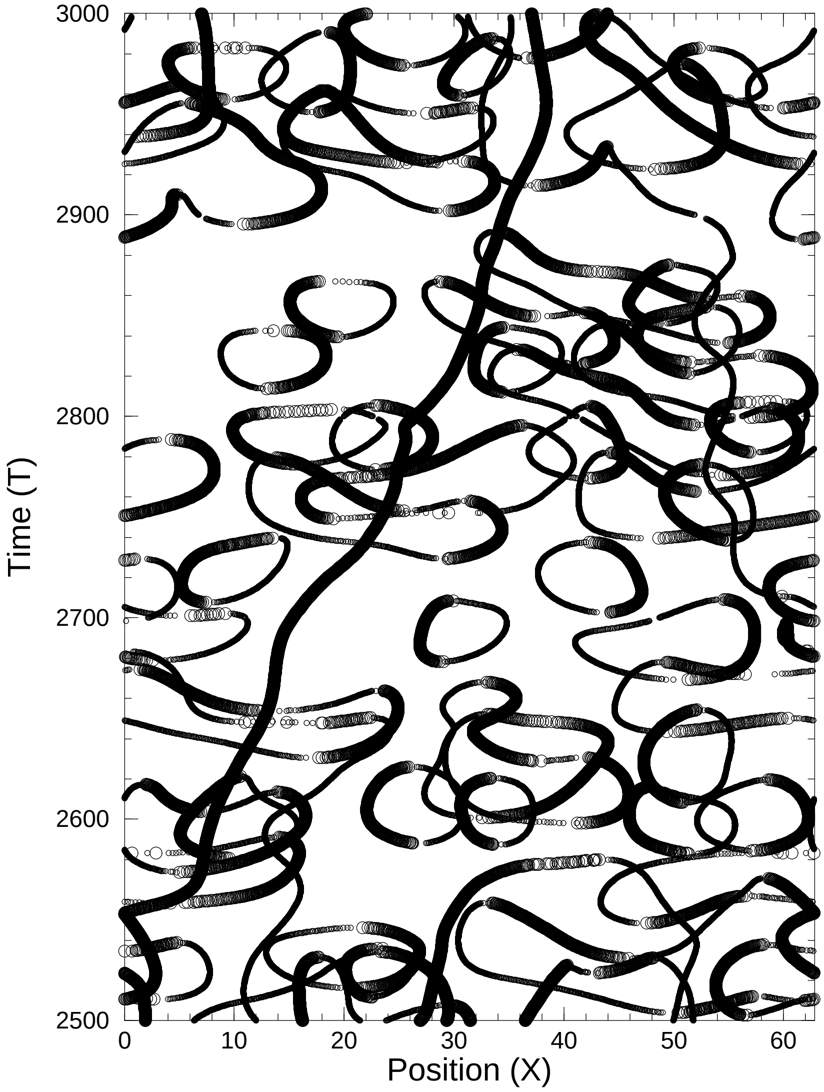

Figure 10.2: Space-time diagram showing the projection of the location of defects on the x-axis for a simulation of the two-dimensional system. The *loops*, for example the one starting at $x \approx 29$ and $t \approx 2680$, represent bound defect pairs ($b = 1.2$, $L = 62.832$).

Chapter 11

Ordered and Disordered Defect Chaos

In the previous chapter certain defect pairs were characterized as 'bound' meaning that each defect in the pair does not escape the influence of the other. This appears to be true for most of the defect pairs represented in Figure 10.2 as indicated by the many simple 'loops' in that figure. The question to be addressed in this chapter concerns the possibility of an 'unbinding' of the defect pairs and as a consequence a transition from a more ordered to a less ordered chaotic state. To investigate this, the behavior of the defects for a regime where the system exhibits a strongly ordered stripe pattern such as that shown in Figure 11.3 is compared with the behavior of the defects for a regime where the system exhibits a more disordered pattern such as that shown in Figure 11.4. The computations show that the drastic decrease in the order of the chaotic state is connected with the disappearance of a typical lifetime of the defects and other signatures in the defect statistics.

The time step size used for the simulations in this chapter is $dt = 0.25$ and the highest Fourier mode is $N = 64$ for a system length $L = 136$. During these simulations the motion of the defects is traced in detail yielding their life-times, annihilation partners, and distances traveled.

For the simulations presented here, the value of the real part of the parameter a has been chosen positive. This corresponds to a point beyond the Hopf bifurcation point so that traveling waves exist and are stable without any periodic forcing, i.e. $b = 0$. In addition to the Eckhaus instability discussed previously for $a_r < 0$, there is a parity-breaking instability at which the phase-locked standing waves become unstable to the traveling waves. Figure 11.1 shows the stability limits relevant for the present chapter. The neutral curve, above which the trivial state is unstable to standing waves, is given by the short-dashed line. Their Eckhaus instability is denoted by a solid line and their parity-breaking instability by a dashed-dotted line. For $Q > 0.37$ the parity-breaking instability is preempted by a mode that arises first at finite modulation wavenumber (bold line and open squares). To illustrate this finite wavenumber instability the real part of the eigenvalues from the linear stability analysis are shown in Figure 11.2 (cf. Figure 3.2). This instability (labeled "finite-k" in Figure 11.1) emerges from the parity-breaking instability. The standing waves are stable only inside the small region bounded by the Eckhaus instability above (solid line) and the finite-wavenumber instability below (bold line and open squares). For completeness it should be noted that to the left of the minimum of the neutral curve the bifurcation to standing waves becomes subcritical; the saddle-node line is shown as a thin long-dashed line. As seen from the top part of Figure 11.1 a minimum of the neutral curve exists for negative Q, but the only stable regime of the standing waves is for positive Q, which is zoomed in on in the bottom part of the figure. Traveling waves exist below the parity-breaking instability and to the left of the neutral curve indicated by the dotted line at $Q = 0.5$. As in the case studied so far in this dissertation, where $a_r < 0$ and no traveling waves arise, the region of stable standing waves is closed in Figure 11.1 ($a_r = 0.25$) with the standing waves becoming Eckhaus-unstable for large forcing. The stability diagram in Figure 11.1 is for a one-dimensional system; in the two dimensional simulations there is evidence of a zig-zag instability (mentioned below) which is not shown.

The decision to choose $a_r > 0$ was motivated by results in one dimension. As discussed in part one, in one dimension the unstable standing waves exhibit chaotic solutions featuring double phase slips. In the complex Ginzburg-Landau equation describing unforced traveling waves, however, no regime with double phase slips seems to exist. One may therefore expect an interesting transition from chaotic dynamics characterized by double phase slips to one dominated by single phase

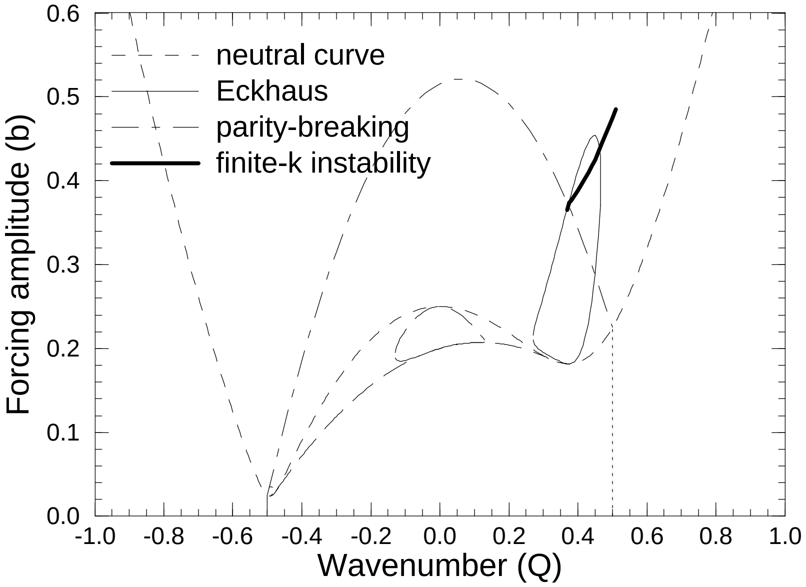

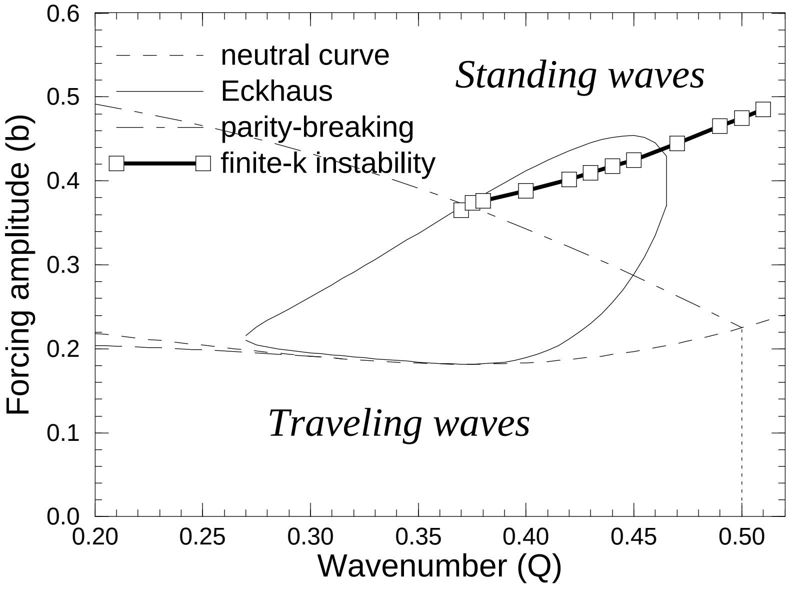

Figure 11.1: Linear stability diagram for $a = 0.25$, $c = -1 + 4i$, $d = 1 + 0.5i$, $s = 0.2$, $g = -1 - 12i$. For details see text.

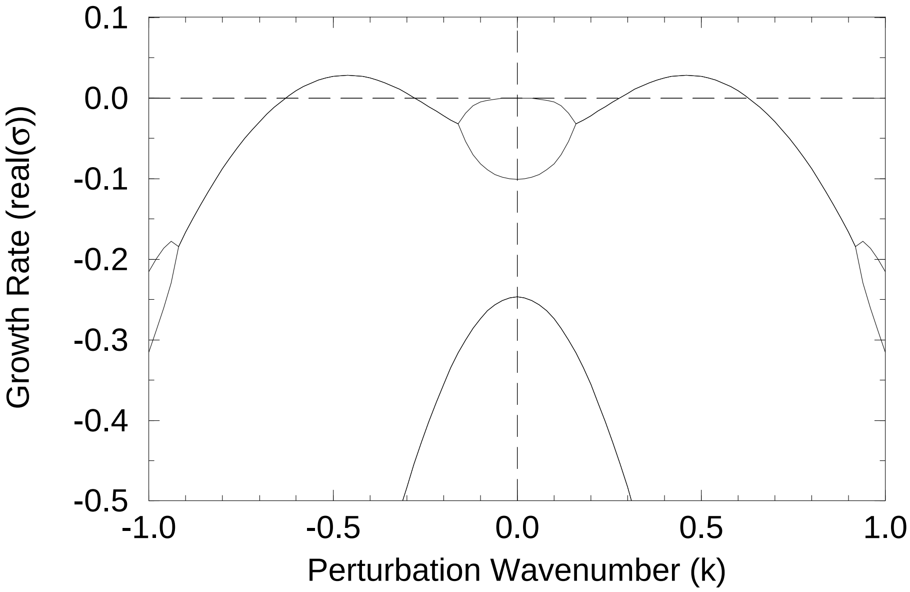

Figure 11.2: The real part of the eigenvalues of the matrix M given by equation (3.13) for $a = 0.25$, $b = 0.4$, $c = -1 + 4i$, $d = 1 + 0.5i$, $s = 0.2$, $g = -1 - 12i$, and (unstable) solution wavenumber $Q = 0.45$. Positive growth rates occur for a band of perturbation wavenumbers which is bounded away from zero.

slips when b is decreased towards the parity-breaking instability. Associating bound defect pairs with the double phase slips and unbound defect pairs with single phase slips leads to anticipation of a transition from bound defects to unbound defects with decreasing b.

Here results are presented for $b = 1$, i.e. far away from the parity-breaking instability, and for $b = 0.5$, which is much closer to that instability (the other parameters are chosen as in Figure 11.1). A typical snapshot of the waves is shown in Figure 11.3 for $b = 1$ and in Figure 11.4 for $b = 0.5$.

For $b = 1$ the wave pattern consists of a quite ordered array of stripes with a number of defects. The correlation function in Figure 11.5, which is an average over $\Delta T = 20000$ shows that in this regime the correlation function decays only very little over the whole system. In analogy to the one-dimensional chaotic state that is driven by double phase slips, it is expected that the large-scale dynamics of this stripe pattern can be described by a diffusion equation with noise. No true long-range order is expected in such a stripe pattern. However, the system size investigated in this study ($L = 136$), is too small to address this question. Since the pattern has a quite well-defined wavenumber the dynamics depend somewhat sensitively on the length, which discretizes the possible wavenumbers. When the effective wavenumber is decreased (by increasing the length of the system) the pattern develops into a zig-zag pattern (cf. Figure 9.2), very similar to what is observed in non-chaotic systems. To avoid this complication the length was adjusted such that no zig-zags were apparent.

For $b = 0.5$ the wave pattern is quite disordered. The correlation function in Figure 11.6 (averaged over $\Delta T = 10000$) shows that the pattern becomes statistically almost isotropic in this case (despite the small anisotropy due to the group velocity $s = 0.2$). The decay of the correlation function appears to be exponential. The relatively high correlation at $X = \pm L/2$ is apparently a vestige of the initial condition which was created by tiling a solution with half the system size and thus was highly correlated at this length.

In order to investigate the possibility that an unbinding of defects is as-

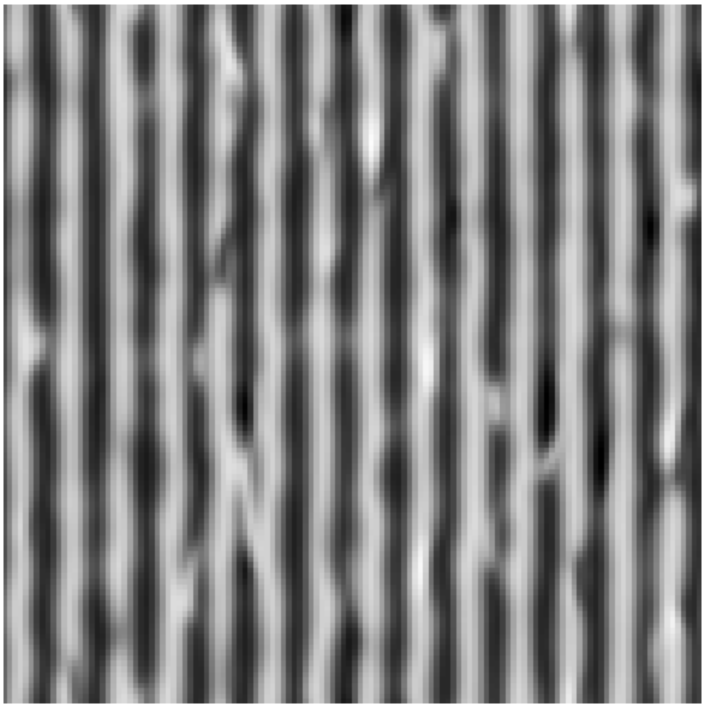

Figure 11.3: Snapshot of the real part of the wave pattern for $b = 1$ (other parameters as in Figure 11.1).

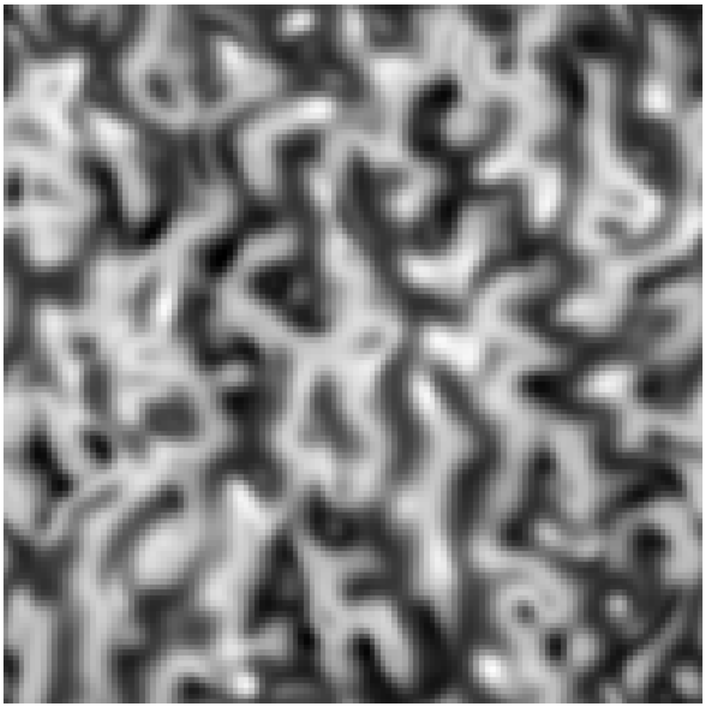

Figure 11.4: Snapshot of the real part of the wave pattern for $b = 0.5$ (other parameters as in Figure 11.1).

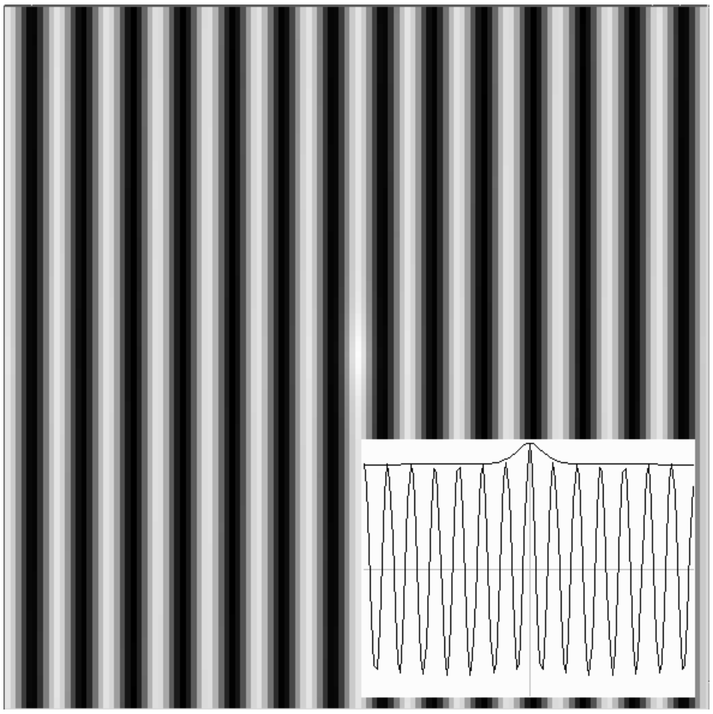

Figure 11.5: Time-averaged correlation function of the wave pattern for $b = 1$. The inset shows one-dimensional cuts in the X-direction and Y-direction on a linear scale. The other parameters are as in Figure 11.1.

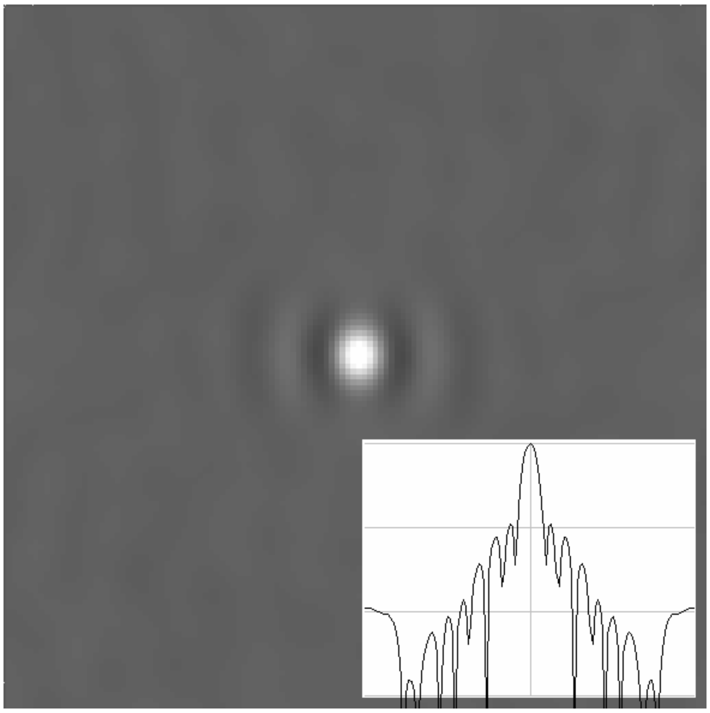

Figure 11.6: Time-averaged correlation function of the wave pattern for $b = 0.5$. The inset shows a one-dimensional cut in the X-direction of the absolute value of the correlation function on a linear-logarithmic scale. The other parameters are as in Figure 11.1.

sociated with the reduced structure in Figure 11.4 as compared with Figure 11.3 the dynamics of the defects were tracked throughout simulations with $b = 0.5$ and $b = 1$. The computer algorithm used to do this involves first detecting defects by looking for locations where the contour lines representing real(A) cross the contour lines representing imaginary(A) (cf. Figure 10.1). The polarity of each defect, that is whether the phase of the solution increases or decreases when encircling the defect in a clockwise manner, is also determined. After all of the defects at a given time step are located they are compared to the defects which had been found at the previous time step to determine which of the defects correspond to defects that already existed at the previous time step, and which defects are new defect pairs which have just been created. For defects which existed at the previous time step but no nearby defect of the same polarity is found at the current time step, a nearby defect of opposite polarity which could be responsible for its annihilation is looked for at the previous time step. For each of these situations: continuation of a defect, creation of a defect pair, and annihilation of a defect pair, the distance between the two defects involved must be less than a prescribed criterion to be considered valid. Error counters tally the exceptions.

In order to address the question whether there are 'bound' defect pairs each defect pair is labeled and it is noted which defect is annihilated by which other defect. In space-time the defects trace out loops as described in chapter 10. If a defect is annihilated by the same defect with which it was created such a loop consists only of this defect pair and is opened when they are created and closed when they annihilate each other. In general, the loops can consist of any number of defect pairs. In Figure 11.7 the probability distribution function for the number of defect pairs making up a loop is shown for $b = 1$ and $b = 0.5$. In both cases most loops contain only a single defect pair. At first glance this might suggest that the defects are bound to each other in both cases. This is, however, not the case as the other diagnostics indicate. In fact, even in simulations of the single Ginzburg-Landau equation, in which no double phase slips occur in one dimension and for which no bound defects are expected, most loops contain only a single defect pair.

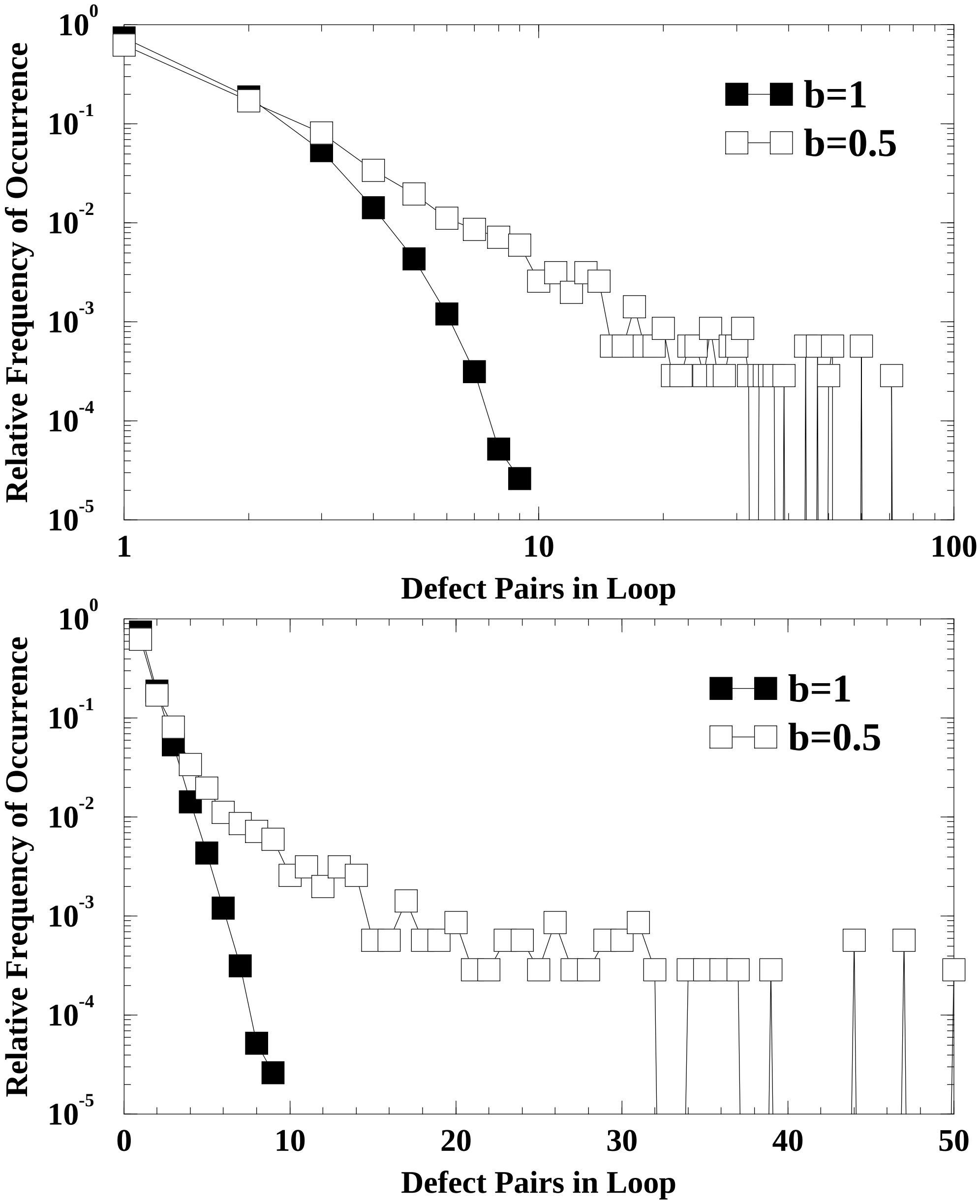

Figure 11.7: Relative frequency of defect loops in space-time containing n defect pairs for $b = 1$ (solid squares) and $b = 0.5$ (open squares). The other parameters are as in Figure 11.1. a) log-log plot, b) linear-log plot.

A strong difference between the two regimes arises, however, in the probability of multi-loops: loops containing many defects are much more likely for $b = 0.5$ than for $b = 1$. Significantly, the data in Figure 11.7 suggests that the probability might decay exponentially for $b = 0.5$, but algebraically for $b = 1$.

Another striking difference in the two regimes is noticed in the distribution of the life-times of each defect. As seen in Figure 11.8 the distribution has a clear peak for $b = 1$ indicating a typical life-time of the individual defects while for $b = 0.5$ the distribution is exponential over the whole range. The latter indicates that during each time interval a defect has a certain probability to be annihilated; correlations between defects appear not to be important.

Because the idea of a bound defect pair implies that the motion of the defects is restricted an interesting quantity is the 'size' of the loops, i.e. the distance in the X- and in the Y-direction that is covered by a loop during its life. To determine this size it has to be taken into account that, due to the periodic boundary conditions, loops can 'wrap around' the system and can, in principle, become larger than the system size. The results are shown in Figure 11.9. Again, there is a strong difference between the two parameter regimes. While for $b = 0.5$ there is a substantial number of loops that cover a large part of the system in the Y- as well as the X-direction, the loops remain very restricted in the X-direction in the ordered regime, $b = 1$. Thus, for $b = 1$ the defects exhibit essentially only climb motion while for $b = 0.5$ they travel in all directions. The latter changes the orientation of the pattern and is responsible for the near isotropy in the correlation function. Note that for $b = 0.5$ some of the loops cover the whole length of the system ($L = 136$ in both simulations).

The probability distribution for the number of defect pairs n in the system for $b = 1$ and $b = 0.5$ is shown in Figure 11.10. The mean $< n >$ and variance σ^2 for these distributions is shown in table 11.1. In reference [26] it is shown that a stochastic model with a constant rate of creation of defect pairs and a rate of annihilation of defect pairs proportional to the square of the number of defects in the system predicts $< n >= 2\sigma^2$. Surprisingly the statistics for the more ordered

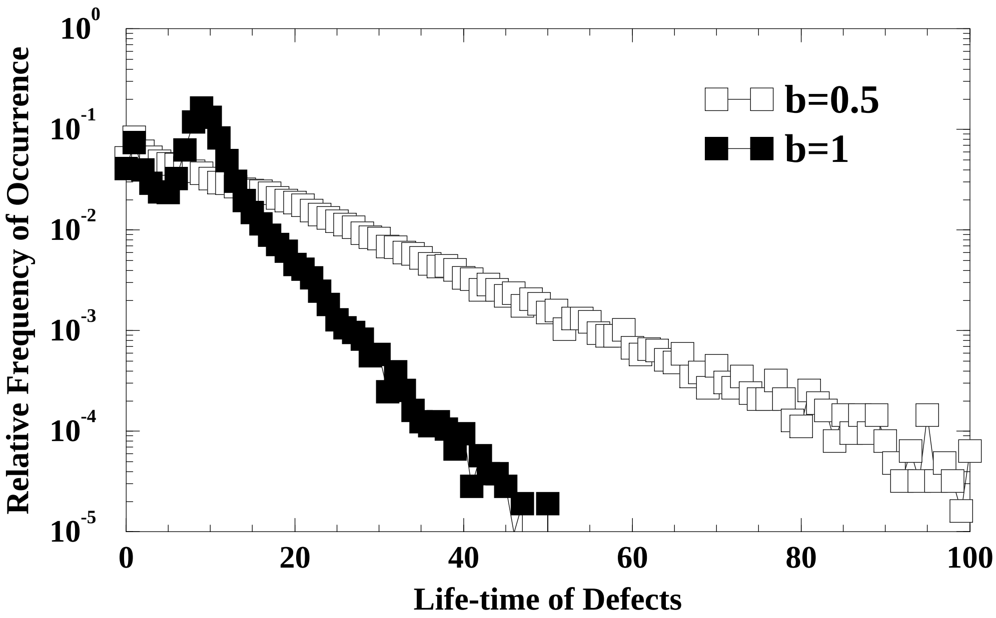

Figure 11.8: Relative frequency of defect loops in space-time with life-time τ for $b = 1$ (solid squares) and $b = 0.5$ (open squares). The other parameters are as in Figure 11.1.

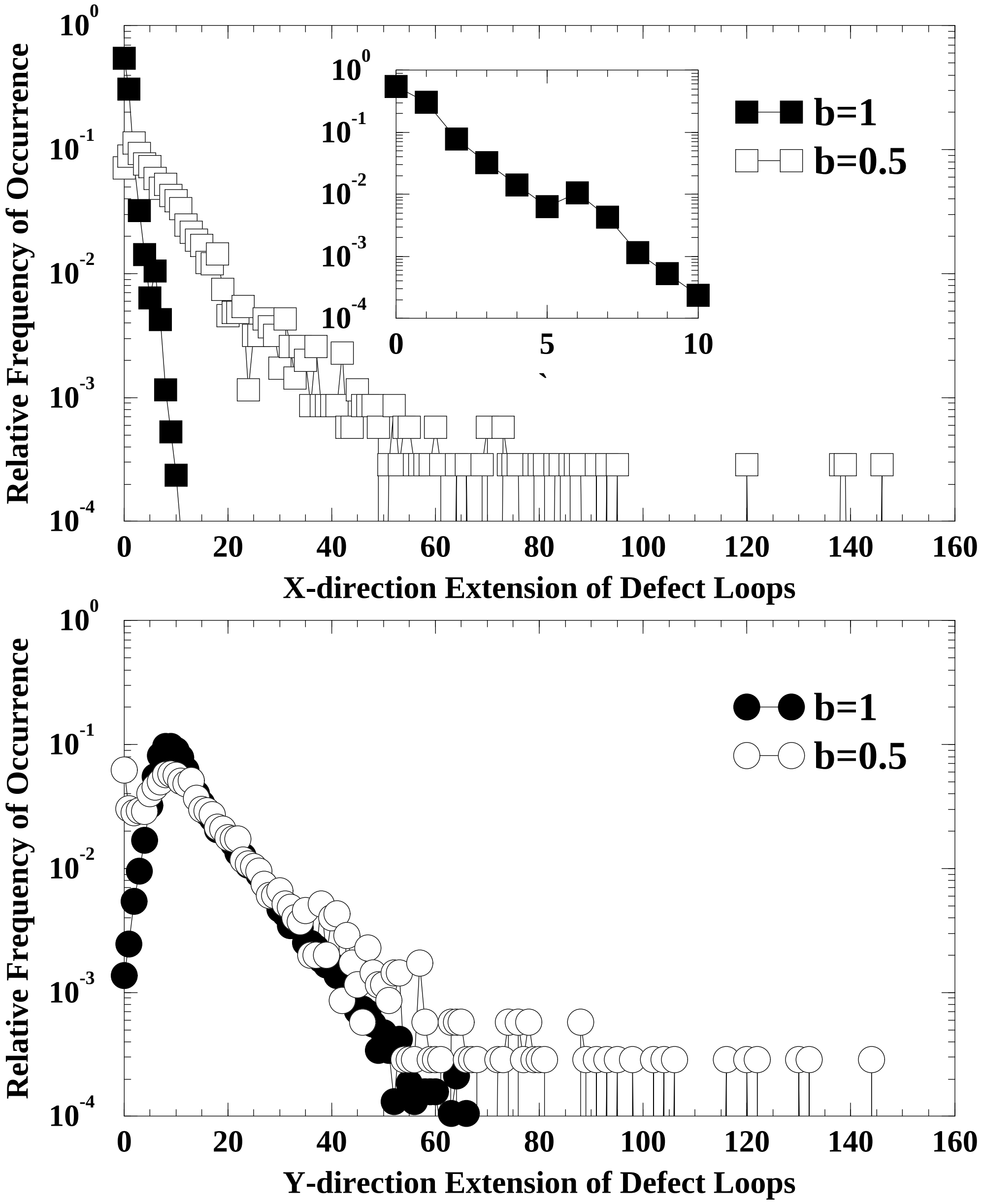

Figure 11.9: Relative frequency of defect loops in space-time with extension d_x in the x-direction (top figure) and d_y in the y-direction (bottom figure) for $b = 1$ (solid symbols) and $b = 0.5$ (open symbols). The other parameters are as in Figure 11.1. The inset in the top figure shows there is a local minimum in the the distribution for $b = 1$ corresponding to half the wavelength of the underlying stripe pattern.

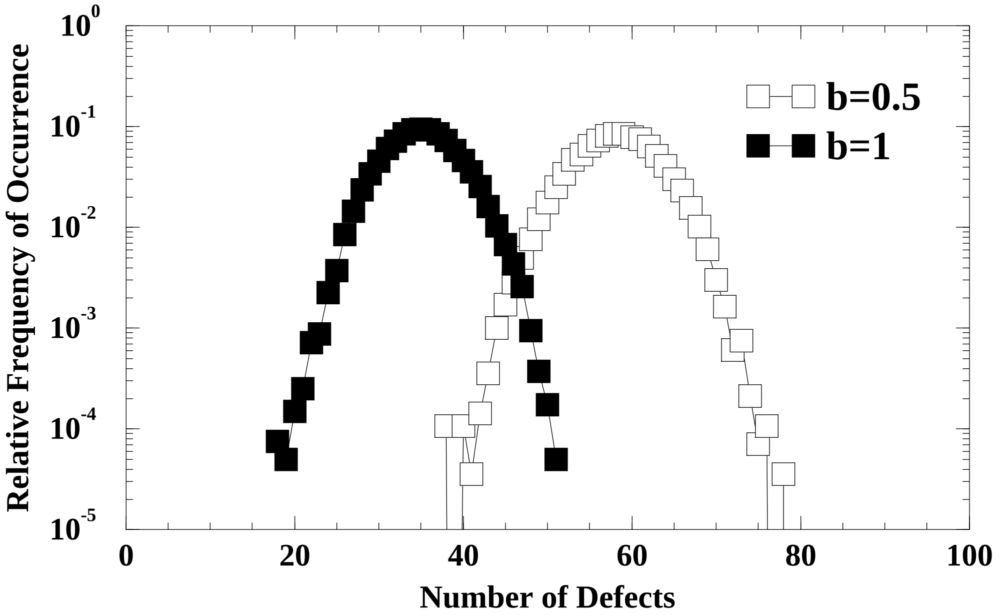

Figure 11.10: Relative frequency of the number of defects pairs in the system for $b = 1$ (solid symbols) and $b = 0.5$ (open symbols). The other parameters are as in Figure 11.1.

chaotic state ($b = 1$) are in closer agreement with this model than the less ordered chaotic state ($b = 0.5$). The premise that the defects in the less ordered state are unbound and thus more random in their motion leads one to expect the opposite.

b	$< n >$	σ^2
1.0	34.9	18.4
0.5	58.3	21.9

Table 11.1: Mean and variance for the probability distributions of the number of defect pairs in the system for $b = 1$ and $b = 0.5$ shown in Figure 11.10

.

Chapter 12

Conclusions and Discussion

This dissertation describes the dynamics of a pair of coupled Ginzburg-Landau equations that are amplitude equations for parametrically excited waves. The dynamics are studied using numerical simulations. Emphasis is on the ensuing dynamics when solutions of the equations corresponding to standing waves which are phase locked to the external forcing are perturbed. The usual transition from an Eckhaus-unstable state to a stable state is found near onset but not for larger forcing amplitudes. It is solutions at these larger forcings that are studied here. The one-dimensional solutions are characterized by a new feature heretofore unreported in any pattern forming system. In two dimensions a new method based on statistics of defect motion is introduced to characterize chaotic solutions seen in the simulations.

The new feature found in one-dimensional simulations is a *double phase slip*. Double phase slips allow periodic dynamics with an average wavenumber that is Eckhaus unstable even for parameters for which there is a range of stable wavenumbers. Solutions with an average wave number that is stable can also exhibit transient and periodic solutions that include double phase slips. In this regime the system can be excitable.

Also found in one dimension are solutions where the dynamics are chaotic and characterized by the irregular occurrence of double phase slips in both space and time. Particularly striking are solutions in which the chaos is confined to only a part of the homogeneous system. As mentioned in the introduction a similar phenomenon has been observed in Taylor vortex flow where domains with large turbulent vortices can exist with domains of smaller regular vortices on each side

[2]. These experimental results resemble the localized states found in our numerical simulations in that there are two distinct states with differing underlying wavenumber, one of which is regular, the other irregular. However, the irregular state in the experimental system, which consists of Taylor vortices with a turbulent secondary flow, appears to be quite different from the spatio-temporal chaos in the numerical simulations of parametrically excited waves, which is characterized by the occurrence of double phase slips. The occurence of double phase slips would imply that pairs of vortex rolls would disappear then reappear. This was not reported in the experiment.

In the localized chaotic states which have been reported in Rayleigh-Bénard experiments [11] the underlying state on which there are localized chaotic perturbations is much less regular than in the Taylor vortex system. There is no obvious difference in the wavenumber between the nonchaotic and chaotic domains, so the connection with the current results seems more remote.

The localized spatio-temporal chaos recently found in Faraday experiments [41,42] has strongly disordered fluctuating domains existing simultaneously with a stripe pattern. This is qualitatively what could be expected from the one-dimensional simulations presented in section 6.2. However, as in the Taylor vortex system the disordered domains in the Faraday experiment appear to be qualitatively different from the spatio-temporal chaos generated by the model in this investigation. In particular, the underlying wave structure assumed in the model and present in the disordered domains in section 6.2 is not apparent in the disordered domains in the Faraday experiment. The experimenters point out that the location at which the spatio-temporal chaos occurs is determined by the local curvature of the stripes and not the local wavenumber as would be expected if the situation was modeled by the analysis in section 6.3.

An effective phase diffusion equation utilizing the long-term phase conservation of the solution explains the localization of the spatio-temporal chaos in the model equations. It is quite possible that this approach could also explain the localization in the Taylor vortex experiments. An effective diffusion coefficient has been measured for the turbulent vortices which compose the chaotic domains in these experiments [86]. However, no attempt to investigate whether this coefficient becomes negative at a smaller wavenumber than the one at which the regular vortices become stable has been reported. This is the scenario expected in order for the situation to be analogous to the results presented here (cf. Figure 6.7).

The use of an effective phase diffusion equation for the large scale behavior of the chaotic state is similar to studies using the Kardar-Parisi-Zhang equation [34]

$$\partial_t \phi + \frac{1}{2}(\nabla\phi)^2 = \nu\nabla^2\phi + \eta(x,t) \tag{12.1}$$

to model chaotic solutions of the Kuramoto-Sivashinsky equation (1.3) [87, 88, 33]. Equation (12.1) is Burgers' equation ($\partial_t \phi + \frac{1}{2}(\nabla\phi)^2 = \nu\nabla^2\phi$) [7] with a Gaussian forcing term $\eta(x,t)$ added. Studies which relate the Kuramoto-Sivashinski equation (1.3) to the Kardar-Parisi-Zhang equation (12.1) claim to show similar behavior at large scales. The key point is that an equation with a negative diffusion coefficient ((1.3) with $c_1 c_3 > 1$) is modeled on large scales by an equation with a positive diffusion coefficient and a stochastic forcing term (12.1). Presumably a similar noise term $\eta(X,T)$ could be added to (6.4) to describe the effect of the shortscale chaotic dynamics on the effective phase,

$$\partial_T \hat{\phi} = \hat{D}_0 \partial_X^2 \hat{\phi} + \hat{D}_1 \partial_X \hat{\phi} \partial_X^2 \hat{\phi} + \eta(X,T) + \ldots. \tag{12.2}$$

The form of the nonlinear term, which results from expanding the diffusion coefficient $\hat{D}$ around some wavenumber $\hat{q}_0$, differs from that found in the Kardar-Parisi-Zhang equation since the parametrically driven standing waves have an additional reflection symmetry as compared to the traveling waves described by the Kuramoto-Sivashinsky equation. A particularly interesting feature of (12.2) is that even the effective diffusion coefficient $\hat{D}_0$ can become negative. This is not reported for the Kardar-Parisi-Zhang equation as applied to the Kuramoto-Sivashinsky equation. It suggests that noise may be quite important in the regime in which $\hat{D}$ is small, i.e. near the onset of domain formation.

A double phase slip in one dimension corresponds to a *bound defect pair* in two dimensions. Here, "defect" refers to a location where the amplitude of the solution is zero. This type of defect is also known as a dislocation. A bound defect pair consists of two dislocations which are formed together, move apart, then move back together and annihilate each other. These bound defect pairs are prominent in the two-dimensional simulations.

An interesting theoretical question arises with regard to the bound defect pairs in two dimensions. In thermodynamic equilibrium the unbinding transition of defect pairs has been studied in great detail in the context of two-dimensional melting [57, 39]. This approach has been used, for example, to explain unusual scaling properties in quantities such as the specific heat and structure factor near the transition to superfluidity in thin films. It has been conjectured that such a transition should also be possible in nonequilibrium systems [84, 15]. Indeed this has been asserted for experiments in Bénard-Marangoni convection, nematic shear flow [59], and magnetic bubbles [73]. However, the existence of an unbinding transition in nonequilibrium systems analogous to the Kosterlitz-Thouless transition in equilibrium systems has not been established.

In this investigation two types of behavior were found in numerical simulations of a model for parametrically driven waves in a two-dimensional anisotropic system: in a regime in which in one dimension all phase slips occur in sequential pairs the two-dimensional waves form an ordered stripe pattern with a very slowly decaying correlation function; for smaller forcing, i.e. closer to the parity-breaking instability, the waves form a very disordered pattern with a rapidly decaying correlation function which is almost isotropic. An analysis of various statistics of the motion of the defects involved in the dynamics shows that in the ordered regime they have a typical life-time whereas in the disordered regime the distribution function is purely exponential. The number of defect pairs in the space-time loops traced out by the defects increases strongly in the disordered regime. Another signature of the disordered state is the extension of the loops. In the disordered regime they extend over large portions of the system in the X and the Y direction, while in the ordered regime their extension in the X direction is strongly restricted.

At present it is not clear whether there is a true transition separating the two regimes or whether the change from one to the other is smooth. This needs to be investigated. The extension in the X direction should be a good diagnostic tool for this question.

It also remains unclear whether there is any connection between the disappearance of spatial order in this spatio-temporally chaotic system and two-dimensional melting [56] and the Kosterlitz-Thouless transition [39] in equilibrium systems.

The "ordered" and "disordered" chaotic regimes and possible defect unbinding transition were presented for $a_r > 0$. Here, the solution became less ordered as the parity-breaking instability was approached by decreasing b. For $a_r < 0$ a similar decrease of order in the solution is seen with increasing b. Some short simulations were made which showed an increase in the number of defects, the appearance of loops with many defects, and a trend towards an exponential distribution of defect lifetimes as b was increased from 2 to 10. These results are similar to those found when approaching the parity-breaking instability. A detailed study and comparison has not been made.

Statistics of defects motion could also be studied in other systems including the complex Ginzburg-Landau equation (1.2). A preliminary simulation of (1.2) showed that many of the defect pairs were annihilated by the defect they were created with.

So far no particular physical system has been identified which exhibits the behavior described here. It is natural to suspect that the closing of the Eckhaus curve is related to the occurrence of double phase slips. If that should be the case, parametric driving of waves which are Benjamin-Feir unstable in the absence of any forcing should be a good candidate for this behavior. Within the framework of the coupled Ginzburg-Landau equations (2.1,2.2) these waves become unstable near the band center when forced sufficiently strongly [67]. Depending on the sign of certain nonlinear coefficients this indicates instability at all wavenumbers and a closing of the Eckhaus curve. Further work is needed to investigate the origin of the double phase slips and determine the range of parameter values for which the dynamics seen in our study can be observed. Of particular interest is whether double phase slips might occur in a Faraday experiment or in electroconvection in liquid crystals.

References

[1] I. Aranson, L. Kramer, and A. Weber. Core instability and spatiotemporal intermittency of spiral waves in oscillatory media. *Phys. Rev. Lett.*, 72:2316, 1994.

[2] B.W. Baxter and C.D. Andereck. Formation of dynamical domains in a circular Couette system. *Phys. Rev. Lett.*, 57:3046, 1986.

[3] T.B. Benjamin and J.E. Feir. The disintegration of wave trains on deep water. *J. Fluid Mech.*, 27:417, 1967.

[4] T.B. Benjamin and F. Ursell. The stability of the plane free surface of a fluid in vertical periodic motion. *Proc. R. Soc. Lond. A*, 225:505, 1954.

[5] W.E. Boyce and R.C. DiPrima. *Elementary differential equations.* John Wiley & Sons, New York, 1997.

[6] H.R. Brand and R.J. Deissler. Confined states in phase dynamics. *Phys. Rev. Lett.*, 63:508, 1989.

[7] J.M. Burgers. *The nonlinear diffusion equation.* Riedel, Boston, 1974.

[8] C. Canuto, M.Y. Hussaini, A. Quarteroni, and T.A. Zang. *Spectral methods in fluid dynamics.* Springer-Verlag, Berlin, 1988.

[9] E. Cerda and E. Tirapegui. Faraday's instability for viscous fluids. *Phys. Rev. Lett.*, 78:859, 1997.

[10] H. Chaté and P. Manneville. Phase diagram of the two-dimensional complex Ginzburg-Landau equation. *Physica A*, 224:348, 1996.

[11] S. Ciliberto and M.A. Rubio. Local oscillations, traveling waves, and chaos in Rayleigh-Bénard convection. *Phys. Rev. Lett.*, 58:2652, 1987.

[12] P. Coullet and K. Emilsson. Strong resonances of spatially distributed oscillators: a laboratory to study patterns and defects. *Physica D*, 61:119, 1992.

[13] P. Coullet, K. Emilsson, and D. Walgraef. Phase instability and defect behavior in modulated wave patterns. *Physica D*, 61:132, 1992.

[14] P. Coullet and J. Lega. Defect-mediated turbulence in wave patterns. *Europhys. Lett.*, 7:511, 1988.

[15] M.C. Cross and P.C. Hohenberg. Pattern formation outside of equilibrium. *Rev. Mod. Phys.*, 65:851, 1993.

[16] J.G. Dash. *Films on solid surfaces.* Academic Press, New York, 1975.

[17] M. de la Torre-Juarez and I. Rehberg. Four-wave resonance in electrohydrodynamic convection. *Phys. Rev. A*, 42:2096–2100, 1990.

[18] M. Dennin, M. Treiber, L. Kramer, G. Ahlers, and D.S. Cannell. Origin of traveling rolls in electroconvection of nematic liquid-crystals. *Phys. Rev. Lett.*, 76:319, 1996.

[19] W. Eckhaus. *Studies in nonlinear stability theory.* Springer, New York, 1965.

[20] J.P. Eckmann, Th. Gallay, and C.E. Wayne. Phase slips and the Eckhaus instability. *Nonlinearity*, 8:943, 1995.

[21] W.S. Edwards and S. Fauve. Patterns and quasi-patterns in the Faraday experiment. *J. Fluid Mech.*, 278:123, 1994.

[22] D.A. Egolf and H.S. Greenside. Characterization of the transition from defect to phase turbulence. *Phys. Rev. Lett.*, 74:1751–1754, 1995.

[23] F.J. Elmer. Pattern-formation due to spin-wave instabilities: squares, hexagons, and quasi-periodic patterns. *Phys. Rev. Lett.*, 70:2028, 1993.

[24] A.B. Ezerskiĭ, M.I. Rabinovich, V.P. Reutov, and I.M. Starobinets. Spatiotemporal Chaos in the Parametric Excitation of a Capillary Ripple. *Sov. Phys. JETP*, 64:1228, 1986.

[25] M. Faraday. On the forms and states assumed by fluids in contact with vibrating elastic surfaces. *Phil. Trans. R. Soc. Lond*, 319, 1831.

[26] L. Gil, J. Lega, and J.L. Meunier. Statistical properties of defect-mediated turbulence. *Phys. Rev. A*, 41:1138–1141, 1990.

[27] P. Glendinning. *Stability, instability and chaos: an introduction to the theory of nonlinear differential equations.* Cambridge University Press, Cambridge, 1994.

[28] M. Golubitsky, I. Stewart, and D.G. Schaeffer. *Singularities and Groups in Bifurcation Theory.* Applied Mathematical Sciences 69. Springer, New York, 1988.

[29] R. Haberman. *Elementary applied partial differential equations with Fourier series and boundary value problems.* Prentice-Hall, Englewood Cliffs, 1987.

[30] J. Hegseth, J.M. Vince, M. Dubois, and P. Bergé. Pattern domains in Rayleigh-Bénard slot convection. *Europhys. Lett.*, 17:413, 1992.

[31] F.B. Hildebrand. *Advanced calculus for applications.* Prentice-Hall, Englewood Cliffs, 1976.

[32] J.M. Hyman, B. Nicolaenko, and S. Zaleski. Order and complexity in the Kuramoto-Sivashinsky model of weakly turbulent interfaces. *Physica D*, 23:265, 1986.

[33] C. Jayaprakash, F. Hayot, and R. Pandit. Universal properties of the two-dimensional Kuramoto-Sivashinsky equation. *Phys. Rev. Lett.*, 71:12, 1993.

[34] M. Kardar, G. Parisi, and Y. Zhang. Dynamic scaling of growing interfaces. *Phys. Rev. Lett.*, 56:889, 1986.

[35] I.G. Kevrekidis, B. Nicolaenko, and J.C. Scovel. Back in the saddle again: a computer assisted study of the Kuramoto-Sivashinsky Equation. *SIAM J. Appl. Math.*, 50:760, 1990.

[36] S.V. Kiyashko, L.N. Korzinov, M.I. Rabinovich, and L.S. Tsimring. Rotating spirals in a Faraday experiment. *Phys. Rev. E*, 54:5037, 1996.

[37] E. Knobloch. Nonlocal amplitude equations. In S. Kai, editor, *Pattern Formation in Complex Dissipative Systems*. World Scientific, 1992.

[38] E. Knobloch and J. De Luca. Amplitude equations for travelling wave convection. *Nonlinearity*, 3:975, 1990.

[39] J.M. Kosterlitz and D.J. Thouless. Ordering, metastability and phase transitions in two-dimensional systems. *J. Phys. C*, 6:1181, 1973.

[40] L. Kramer and W. Zimmermann. On the Eckhaus instability for spatially periodic patterns. *Physica D*, 16:221, 1985.

[41] A. Kudrolli and J.P. Gollub. Localized spatiotemporal chaos in surface waves. *Phys. Rev. E*, 54:1052, 1996.

[42] A. Kudrolli and J.P. Gollub. Patterns and spatiotemporal chaos in parametrically forced surface waves: a systematic survey at large aspect ratio. *Physica D*, 97:133, 1996.

[43] K. Kumar and L.S. Tuckermann. Parametric instability of the interface between two fluids. *J. Fluid Mech.*, 279:49, 1994.

[44] K. Kumar. Linear theory of Faraday instability in viscous liquids. *Proc. R. Soc. Lond. A*, 452:1113, 1996.

[45] Y. Kuramoto. Diffusion-induced chaos in reaction systems. *Prog. Theor. Phys. Suppl.*, 64:346, 1978.

[46] Y. Kuramoto and T. Tsuzuki. Persistent propagation of concentration waves in dissipative media far from thermal equilibrium. *Prog. Theo. Phys.*, 55:356, 1976.

[47] H. Lamb. *Hydrodynamics.* Cambridge University Press, Cambridge, 1932.

[48] E. N. Lorenz. Deterministic nonperiodic flow. *J. Atmosp. Sci*, 20:130, 1963.

[49] P. Manneville. *Dissipative Structures and Weak Turbulence.* Academic Press, Boston, 1990.

[50] P. Manneville and H. Chaté. Phase turbulence in the two-dimensional complex Ginzburg-Landau equation. *Physica D*, 96:30, 1996.

[51] B.J. Matkowsky and V. Volpert. Coupled nonlocal complex Ginzburg-Landau equations in gasless combustion. *Physica D*, 54:203, 1992.

[52] F. Melo and P.B. Umbanhowar and H.L. Swinney. Hexagons, kinks, and disorder in oscillated granular layers. *Phys. Rev. Lett.*, 75:3838, 1995.

[53] F. Melo and P. Umbanhowar and H.L. Swinney. Transition to parametric wave patterns in a vertically oscillated granular layer. *Phys. Rev. Lett.*, 72:172, 1994.

[54] J. Miles and D. Henderson. Parametrically Forced Surface-Waves. *Annu. Rev. Fluid Mech.*, 22:143, 1990.

[55] S.T. Milner. Square Patterns and Secondary Instabilities in Driven Capillary Waves. *J. Fluid Mech.*, 225:81, 1991.

[56] D.R. Nelson. *Defect-mediated phase transitions*, volume 7 of *Phase Transitions and Critical Phenomena*, chapter 1. Academic, New York, 1983.

[57] D.R. Nelson and B.I. Halperin. Dislocation-mediated melting in two dimensions. *Phys. Rev. B*, 19:2457, 1979.

[58] A.C. Newell and J.A. Whitehead. Finite bandwidth finite amplitude convection. *J. Fluid Mech.*, 38:279, 1969.

[59] R. Occelli, E. Guazzelli, and J. Pantaloni. Order in convective structures. *J. Phys. Lett.*, 44:567, 1983.

[60] R.D. Pierce and E. Knobloch. On the modulational stability of traveling and standing water waves. *Phys. Fluids*, 6:1177, 1994.

[61] W.H. Press, B.P. Flannery, S.A. Teukolsky, and W.T. Vetterling. *Numerical recipes in FORTRAN: the art of scientific programming*. Cambridge University Press, Cambridge, 1992.

[62] D. Raitt and H. Riecke. Domain structures in fourth-order phase and Ginzburg-Landau equations. *Physica D*, 82:79–94, 1995.

[63] D. Raitt and H. Riecke. Parametric forcing of waves with a nonmonotonic dispersion relation: domain structures in ferrofluids. *Phys. Rev. E*, 55:5448, 1997.

[64] I. Rehberg, S. Rasenat, J. Fineberg, M. de la Torre-Juarez, and V. Steinberg. Temporal modulation of traveling waves. *Phys. Rev. Lett.*, 61:2449, 1988.

[65] I. Rehberg, S. Rasenat, and V. Steinberg. Traveling waves and defect-initiated turbulence in electroconvecting nematics. *Phys. Rev. Lett.*, 62:756, 1989.

[66] S. Residori, P.L. Ramazza, E. Pampaloni, S. Boccaletti, and F.T. Arecchi. Domain coexistence in 2-dimensional optical-patterns. *Phys. Rev. Lett.*, 76:1063, 1996.

[67] H. Riecke. On the stability of parametrically excited standing waves. In F.H. Busse and L. Kramer, editors, *Nonlinear Evolution of Spatio-Temporal Structures in Dissipative Continuous Systems*, pages 437–444. Plenum Press, New York, 1990.

[68] H. Riecke. Stable wave-number kinks in parametrically excited standing waves. *Europhys. Lett.*, 11:213, 1990.

[69] H. Riecke, J.D. Crawford, and E. Knobloch. Time-modulated oscillatory convection. *Phys. Rev. Lett.*, 61:1942, 1988.

[70] H. Riecke, J.D. Crawford, and E. Knobloch. Temporal modulation of a subcritical bifurcation to travelling waves. In P. Coullet and P. Huerre, editors, *The Geometry of Nonequilibrium*, pages 61–64. Plenum Press, 1991.

[71] B.W. Roberts, E. Bodenschatz, and J.P. Sethna. A bound on the decay of defect–defect correlation functions in two-dimensional complex order parameter equations. *Physica D*, 99:252, 1996.

[72] L.A. Segel. Slow amplitude modulation of cellular convection. *J. Fluid Mech.*, 38:203, 1969.

[73] R. Seshadri and R.M. Westervelt. Hexatic-to-liquid melting transition in two-dimensional magnetic-bubble lattices. *Phys. Rev. Lett.*, 66:2774, 1991.

[74] B.I. Shraiman, A. Pumir, W. van Saarloos, P.C. Hohenberg, H. Chaté, and M. Hofen. Spatiotemporal chaos in the one-dimensional complex Ginzburg-Landau equation. *Physica D*, 57:241, 1992.

[75] M. Silber, H. Riecke, and L. Kramer. Symmetry-breaking Hopf bifurcation in anisotropic systems. *Physica D*, 61:260–278, 1992.

[76] B.T. Smith, J.M.Boyle, J.J. Dongarra, B.S. Garbow, Y. Ikebe, V.C. Klema, and C.B. Moler. *Matrix Eigensystems routines - EISPACK Guide*. Springer-Verlag, Berlin, 1976.

[77] H. Suhl. The theory of ferromagnetic resonance at high signal powers. *J. Phys. Chem. Solids*, 1:209, 1957.

[78] S.G.K. Tennakoon, C.D. Andereck, J.J. Hegseth, and H. Riecke. Temporal modulation of traveling waves in the flow between rotating cylinders with broken azimuthal symmetry. *Phys. Rev. E*, 54:5053, 1996.

[79] L. Tuckerman and D. Barkley. Bifurcation analysis of the Eckhaus instability. *Physica D*, 46:57, 1990.

[80] N.B. Tufillaro, R. Ramshankar, and J.P. Gollub. Order-disorder transition in capillary ripples. *Phys. Rev. Lett.*, 62:422, 1989.

[81] P.B. Umbanhowar and F. Melo and H.L. Swinney. Localized excitations in a vertically vibrated granular layer. *Nature*, 382:793, 1996.

[82] J.M. Vega. On the amplitude equations arising at the onset of the oscillatory instability in pattern-formation. *SIAM J. Math. Anal.*, 24:603, 1993.

[83] D. Walgraef. External forcing of spatio-temporal patterns. *Europhys. Lett.*, 7:485, 1988.

[84] D. Walgraef, G. Dewel, and P. Borckmans. Melting of 2d nonequilibrium structures at low and high constraints. *Z. Phys. B*, 48:167, 1982.

[85] T.P. Witelski. The structure of internal layers for unstable nonlinear diffusion equations. *preprint*, 1996.

[86] M. Wu, C.D. Andereck, and H.R. Brand. The phase dynamics of turbulent Taylor vortex flow. *Europhys. Lett.*, 19:587, 1992.

[87] V. Yakhot. Large-scale properties of unstable systems governed by the Kuramoto-Sivashinski equation. *Phys. Rev. A*, 24:642, 1981.

[88] S. Zaleski. A stochastic model for the large scale dynamics of some fluctuating interfaces. *Physica D*, 34:427–438, 1989.

[89] W. Zhang and J. Viñals. Pattern formation in weakly damped parametric surface waves. *J. Fluid Mech.*, submitted, 1996.

Appendix A

Amplitude Equations from Symmetries

To derive the amplitude equations

$$\begin{aligned}\partial_T A + s\partial_X A &= d\partial_X^2 A + aA + bB + cA(|A|^2 + |B|^2) + gA|B|^2 \quad &(A.1)\\ \partial_T B - s^*\partial_X B &= d^*\partial_X^2 B + a^*B + b^*A + c^*B(|A|^2 + |B|^2) + g^*B|A|^2 \quad &(A.2)\end{aligned}$$

we begin by considering a system which is invariant under translation and reflection in space and under translation in time, undergoing a Hopf bifurcation. Assuming the critical mode has frequency ω and nonzero wave number q we obtain the traveling wave ansatz

$$u(x,t) = A(X,T)e^{i(qx-\omega t)} + B(X,T)e^{i(qx+\omega t)} + c.c. + \dots \quad (A.3)$$

where *c.c.* stands for the complex conjugate. We now look for the partial differential equations that govern the slowly varying amplitudes A and B

$$\begin{aligned}\partial_T A &= \sum a_j \partial_T^\gamma \partial_X^\delta A^\alpha B^\beta (A^*)^{\hat{\alpha}} (B^*)^{\hat{\beta}} \quad &(A.4)\\ \partial_T B &= \sum b_j \partial_T^\gamma \partial_X^\delta A^\alpha B^\beta (A^*)^{\hat{\alpha}} (B^*)^{\hat{\beta}}. \quad &(A.5)\end{aligned}$$

These equations must be equivariant under the symmetries of the system. The effects of translation and reflection in space and translation in time are

$$\begin{array}{lrclrcl}\Gamma_{\Delta x} u: & A & \to & Ae^{iq\Delta x}, & B & \to & Be^{iq\Delta x}\\ \Gamma_\kappa u: & A(-X,T) & \to & B^*(X,T), & B(-X,T) & \to & A^*(X,T)\\ \Gamma_{\Delta t} u: & A & \to & Ae^{-i\omega\Delta t}, & B & \to & Be^{i\omega\Delta t}\end{array}$$

Spatial translation ($\Gamma_{\Delta x} u$) results in the following operation on each of the terms in equations (A.4,A.5)

$$\partial_T^\gamma \partial_X^\delta A^\alpha B^\beta (A^*)^{\hat{\alpha}} (B^*)^{\hat{\beta}} \to \partial_T^\gamma \partial_X^\delta A^\alpha B^\beta (A^*)^{\hat{\alpha}} (B^*)^{\hat{\beta}} e^{iq(\alpha-\hat{\alpha}+\beta-\hat{\beta})\Delta x}. \tag{A.6}$$

In order for equations (A.4,A.5) to be equivariant under spatial translation requires $\alpha - \hat{\alpha} + \beta - \hat{\beta} = C_1$ (where C_1 is a constant) for all terms in each equation. The left hand side of each equation (where $\alpha = 1$, $\hat{\alpha} = \beta = \hat{\beta} = 0$ in (A.4), and $\beta = 1$, $\alpha = \hat{\alpha} = \hat{\beta} = 0$ in (A.5)) specifies $C_1 = 1$.

Similarly, translation in time ($\Gamma_{\Delta t} u$) results in

$$\partial_T^\gamma \partial_X^\delta A^\alpha B^\beta (A^*)^{\hat{\alpha}} (B^*)^{\hat{\beta}} \to \partial_T^\gamma \partial_X^\delta A^\alpha B^\beta (A^*)^{\hat{\alpha}} (B^*)^{\hat{\beta}} e^{iq(\hat{\alpha}-\alpha+\beta-\hat{\beta})\Delta t}. \tag{A.7}$$

Equivariance requires $\hat{\alpha} - \alpha + \beta - \hat{\beta} = -1$ in equation (A.4) and $\hat{\alpha} - \alpha + \beta - \hat{\beta} = 1$ in equation (A.5).

Taken together, the translation symmetries in space and time require that $\beta = \hat{\beta}$ and $\alpha - \hat{\alpha} = 1$ in each term in equation (A.4), while $\alpha = \hat{\alpha}$ and $\beta - \hat{\beta} = 1$ in each term in equation (A.5). These considerations result in the following equations

$$\partial_T A = a_1 \partial_X A + a_2 \partial_X^2 A + a_3 A + a_4 |A|^2 A + a_5 |B|^2 A + \ldots \tag{A.8}$$

$$\partial_T B = b_1 \partial_X B + b_2 \partial_X^2 B + b_3 B + b_4 |B|^2 B + b_5 |A|^2 B + \ldots. \tag{A.9}$$

Equivariance under reflection in space (Γ_κ) requires

$$b_1 = -a_1^* \tag{A.10}$$

$$b_j = a_j^* \quad \text{for} \quad 2 \le j \le 5. \tag{A.11}$$

Parametric forcing breaks the time translation symmetry ($\Gamma_{\Delta t} u$) which allows terms

$$\partial_T A = \ldots + a_6 B + a_7 \partial_X B + a_8 \partial_X^2 B + a_9 |A|^2 B + a_{10} |B|^2 B + \ldots \tag{A.12}$$

$$\partial_T B = \ldots + a_6^* A - a_7^* \partial_X A + a_8^* \partial_X^2 A + a_9^* |B|^2 A + a_{10}^* |A|^2 A + \ldots. \tag{A.13}$$

Since A and B are small and X is a slow scale, the terms with coefficients a_j with $j > 6$ are higher order than the a_6 term. Setting $s = -a_1$, $d = a_2$, $a = a_3$, $b = a_6$, $c = a_4$, and $g = a_5 - a_4$ results in equations (A.1,A.2).

The parameter b in (A.1,A.2) can be taken as real by an appropriate rotation of A and B in the complex plane:

$$\begin{aligned} \text{if} \quad b &= |b|e^{i\theta}, && \text{(A.14)} \\ \text{let} \quad A &= \tilde{A}e^{i\frac{\theta}{2}} && \text{(A.15)} \\ \text{and} \quad B &= \tilde{B}e^{-i\frac{\theta}{2}}. && \text{(A.16)} \end{aligned}$$

Substituting (A.14,A.15,A.16) into (A.1,A.1) and multiplying by $e^{\mp i\frac{\theta}{2}}$ one obtains equivalent equations for $\tilde{A}$ and $\tilde{B}$ with b replaced by $|b|$.

Appendix B

Numerical Technique

B.1 Pseudospectral Methods

Pseudospectral (or "collocation") methods (e.g. [8]) are schemes for numerically approximating the solutions of partial differential equations based on the expansion of the solution in terms of orthogonal polynomials that are solutions of a Sturm-Liouville eigenvalue problem (e.g. [29, 31]). The particular set of orthogonal polynomials used are chosen based on the boundary conditions in the problem to be solved. The functions e^{ikx} and e^{-ikx} are solutions to the Sturm-Liouville problem $\frac{d^2u}{dx^2} + k^2u = 0$ with periodic periodic boundary conditions on the domain $[0, 2\pi]$, and are thus often used for problems with periodic boundary conditions. This results in writing the solution as a standard Fourier series after rescaling the problem onto the domain $[0, 2\pi]$.

To illustrate the numerical techniques discussed in this appendix, the following simple partial differential equation is considered:

$$\partial_t u = d\partial_x^2 u + f(u). \tag{B.1}$$

Here $f(u)$ represents a nonlinear term (or terms) such as u^2. For more complicated equations (or systems of equations) the methods discussed for this simple equation can be generalized. All linear terms can be treated like the term $d\partial_x^2 u$ in equation B.1, any nonlinear terms can be included in $f(u)$. Expanding the solution $u(x, t)$ and the nonlinear term $f(u(x, t))$ in (truncated) Fourier series

$$u(x, t) = \sum_{k=-N}^{N} \hat{u}_k(t) e^{ikx} \tag{B.2}$$

$$f(u(x,t)) = \sum_{k=-N}^{N} \hat{f}_k(t)e^{ikx} \tag{B.3}$$

and substituting into equation B.1 gives

$$\sum_{k=-N}^{N} \frac{d}{dt}\left[\hat{u}_k(t)\right]e^{ikx} = -d\sum_{k=-N}^{N} k^2\hat{u}_k(t)e^{ikx} + \sum_{k=-N}^{N} \hat{f}_k(t)e^{ikx}. \tag{B.4}$$

Applying orthogonality results in ordinary differential equations for each of the Fourier coefficients

$$\frac{d\hat{u}_k}{dt} = -dk^2\hat{u}_k + \hat{f}_k. \tag{B.5}$$

The equations are coupled through the term $\hat{f}_k$ which appears due to the non-linear terms in equation B.1. In a *true* spectral method, $\hat{f}_k$ would be evaluated by analytically considering the Fourier transform of $f(u(x,t^{(n)}))$, generally resulting in convolution integrals, which become multiple sums in equation B.4. In the *pseudo*spectral method described here, the nonlinear term $f(u)$ is always evaluated in real space, then the (discrete) Fourier transform is taken giving the $\hat{f}_k$'s. Thus the pseudospectral method requires many transformations to and from Fourier space as the solution evolves in time. A fast Fourier transform routine (e.g. [61]) is used to efficiently perform these transformations .

B.2 Runge-Kutta Method

One way to calculate an approximate solution of an ordinary differential equation (or system of ordinary differential equations) is to use Runge-Kutta methods (e.g. [5, 31]). The approximate solution to the equation $\frac{du}{dt} = g(t,u)$ using the popular fourth order Runge-Kutta method is calculated by applying the formula:

$$u(t+\Delta t) = u(t) + \frac{\Delta t}{6}(K_1 + 2K_2 + 2K_3 + K_4) \tag{B.6}$$

$$\text{where} \quad K_1 = g(t,u) \tag{B.7}$$

$$K_2 = g\left(t + \frac{\Delta t}{2}, u(t) + K_1\frac{\Delta t}{2}\right) \tag{B.8}$$

$$K_3 = g\left(t + \frac{\Delta t}{2}, u(t) + K_2\frac{\Delta t}{2}\right) \tag{B.9}$$

$$K_4 = g\left(t + \Delta t, u(t) + K_3 \Delta t\right). \tag{B.10}$$

Using this method to approximate the solution of the system of equations represented by equation B.5 gives:

$$\hat{u}_k(t + \Delta t) = \hat{u}_k(t) + \frac{\Delta t}{6}(K_{1,k} + 2K_{2,k} + 2K_{3,k} + K_{4,k}) \tag{B.11}$$

where:

$$K_{1,k} = -dk^2 \hat{u}_k(t) + \hat{f}_k\Big|_{u=u(t)} \tag{B.12}$$

$$K_{2,k} = -dk^2 \left(\hat{u}_k(t) + K_{1,k}\frac{\Delta t}{2}\right) + \hat{f}_k\Big|_{u=\sum_{j=-N}^{N}\left(\hat{u}_j(t)+K_{1,j}\frac{\Delta t}{2}\right)e^{ijx}} \tag{B.13}$$

$$K_{3,k} = -dk^2 \left(\hat{u}_k(t) + K_{2,k}\frac{\Delta t}{2}\right) + \hat{f}_k\Big|_{u=\sum_{j=-N}^{N}\left(\hat{u}_j(t)+K_{2,j}\frac{\Delta t}{2}\right)e^{ijx}} \tag{B.14}$$

$$K_{4,k} = -dk^2 \left(\hat{u}_k(t) + K_{3,k}\Delta t\right) + \hat{f}_k\Big|_{u=\sum_{j=-N}^{N}\left(\hat{u}_j(t)+K_{3,j}\Delta t\right)e^{ijx}}. \tag{B.15}$$

To evaluate the term $\hat{f}_k\Big|_{u=\sum_{j=-N}^{N}\left(\hat{u}_j(t)+K_{1,j}\frac{\Delta t}{2}\right)e^{ijx}}$ in equation B.13 the following steps would be taken:

1) Calculate temporary values of each $\hat{u}_j$ by adding $K_{1,j}\frac{\Delta t}{2}$ to $\hat{u}_j(t)$.
2) Calculate a temporary value of $u(x)$ by taking the inverse (discrete) Fourier transform of these temporary values of $\hat{u}_j$ (this is the sum in equation B.13).
3) Evaluate the nonlinear terms $f(u)$ in equation B.1 using the temporary $u(x)$.
4) Take the (discrete) Fourier transform giving the $\hat{f}_k$'s.

Similar steps would be used for equations B.14 and B.15.

B.3 Integrating Factor

When applied to the equation $\frac{d\hat{u}_k}{dt} = -dk^2\hat{u}_k$ the Runge-Kutta method described above (as well as many other numerical schemes) has a stability criterion of the form $\Delta t < \frac{\alpha}{dk^2}$ ($\alpha \approx 2.79$ for the fourth order Runge-Kutta scheme if d is real [8] which has been assumed here for simplicity of presentation). Therefore, when applied to equation B.5 a very small time step Δt is typically required in order that the high wavenumber modes (large k) be stable. To allow larger time steps an integrating factor is used. To do this a new variable $\hat{v}_k$ defined by

$$\hat{u}_k(t) = \hat{v}_k(t)e^{-dk^2t} \tag{B.16}$$

is introduced. Differentiating this expression with respect to time and substituting into equation B.5 gives

$$\frac{d\hat{v}_k}{dt} = \hat{f}_k e^{dk^2t}. \tag{B.17}$$

Using the fourth order Runge-Kutta method to approximate the solution of the system of equations represented by equation B.17 gives:

$$\begin{aligned}
\hat{v}_k(t+\Delta t) &= \hat{v}_k(t) + \frac{\Delta t}{6}(K_{1,k} + 2K_{2,k} + 2K_{3,k} + K_{4,k}) && \text{(B.18)}\\
\text{where}\quad K_{1,k} &= e^{dk^2t}\,\hat{f}_k\Big|_{u=u(t)} && \text{(B.19)}\\
K_{2,k} &= e^{dk^2\left(t+\frac{\Delta t}{2}\right)}\,\hat{f}_k\Big|_{u=\sum_{j=-N}^{N}\left(\hat{v}_j(t)+K_{1,j}\frac{\Delta t}{2}\right)e^{-dj^2\left(t+\frac{\Delta t}{2}\right)}e^{ijx}} && \text{(B.20)}\\
K_{3,k} &= e^{dk^2\left(t+\frac{\Delta t}{2}\right)}\,\hat{f}_k\Big|_{u=\sum_{j=-N}^{N}\left(\hat{v}_j(t)+K_{2,j}\frac{\Delta t}{2}\right)e^{-dj^2\left(t+\frac{\Delta t}{2}\right)}e^{ijx}} && \text{(B.21)}\\
K_{4,k} &= e^{dk^2(t+\Delta t)}\,\hat{f}_k\Big|_{u=\sum_{j=-N}^{N}(\hat{v}_j(t)+K_{3,j}\Delta t)e^{-dj^2(t+\Delta t)}e^{ijx}}. && \text{(B.22)}
\end{aligned}$$

Directly implementing this scheme on a computer one will encounter an overflow problem at some time t due to the growth of the e^{dk^2t} factor. To avoid this the quantities $K^\star_{1,k} \equiv K_{1,k}e^{-dk^2t}$, $K^\star_{2,k} \equiv K_{2,k}e^{-dk^2\left(t+\frac{\Delta t}{2}\right)}$, $K^\star_{3,k} \equiv K_{3,k}e^{-dk^2\left(t+\frac{\Delta t}{2}\right)}$, and $K^\star_{4,k} \equiv K_{4,k}e^{-dk^2(t+\Delta t)}$ are calculated instead of $K_{1,k}$, $K_{2,k}$, $K_{3,k}$, and $K_{4,k}$. Note that these quantities are just $\hat{f}_k$ evaluated at appropriate temporary values of u. Using these quantities, the updated values of the Fourier coefficients $\hat{u}_k$ are

$$\begin{aligned}
\hat{u}_k(t+\Delta t) &= \hat{v}_k(t+\Delta t)e^{-dk^2(t+\Delta t)}\\
&= \left[\hat{v}_k(t) + \frac{\Delta t}{6}(K_{1,k} + 2K_{2,k} + 2K_{3,k} + K_{4,k})\right]e^{-dk^2(t+\Delta t)}\\
&= \left[\hat{u}_k(t)e^{dk^2t} + \frac{\Delta t}{6}\left(K^\star_{1,k}e^{dk^2t} + 2K^\star_{2,k}e^{dk^2\left(t+\frac{\Delta t}{2}\right)}\right.\right.\\
&\qquad\left.\left. + 2K^\star_{3,k}e^{dk^2\left(t+\frac{\Delta t}{2}\right)} + K^\star_{4,k}e^{dk^2(t+\Delta t)}\right)\right]e^{-dk^2(t+\Delta t)}\\
&= \hat{u}_k(t)e^{-dk^2\Delta t} + \frac{\Delta t}{6}\left(K^\star_{1,k}e^{-dk^2\Delta t} + 2K^\star_{2,k}e^{-dk^2\left(\frac{\Delta t}{2}\right)}\right.
\end{aligned}$$

$$+2K^{\star}_{3,k}e^{-dk^2\left(\frac{\Delta t}{2}\right)} + K^{\star}_{4,k}\Big) \quad \text{(B.23)}$$

Note that only negative exponentials appear in the final line of the above equation. The $K^{\star}$'s can also be evaluated without using positive exponentials (as shown below) so overflow due to exponentially large coefficients in the solution technique is no longer a problem.

From equation B.19 and the definition of $K^{\star}_{1,k}$, it is seen that $K^{\star}_{1,k} = \hat{f}_k\big|_{u=u(t)}$. From equation B.20 and the definition of $K^{\star}_{2,k}$,

$$K^{\star}_{2,k} = \hat{f}_k\Big|_{u=\sum_{j=-N}^{N}\left(\hat{v}_j(t)+K_{1,j}\frac{\Delta t}{2}\right)e^{-dj^2\left(t+\frac{\Delta t}{2}\right)}e^{ijx}}. \quad \text{(B.24)}$$

The following algebraic identity (which follows from the definitions of $\hat{v}_k$ and $K^{\star}_{1,j}$) is used to evaluate $K^{\star}_{2,k}$ using $\hat{u}_j(t)$ and $K^{\star}_{1,j}$ instead of $\hat{v}_j(t)$ and $K_{1,j}$:

$$\sum_{j=-N}^{N}\left(\hat{v}_j(t)+K_{1,j}\frac{\Delta t}{2}\right)e^{-dj^2\left(t+\frac{\Delta t}{2}\right)}e^{ijx} = \sum_{j=-N}^{N}\left(\hat{u}_j(t)+K^{\star}_{1,j}\frac{\Delta t}{2}\right)e^{-dj^2\frac{\Delta t}{2}}e^{ijx}. \quad \text{(B.25)}$$

Similarly for $K^{\star}_{3,k} = \hat{f}_k\Big|_{u=\sum_{j=-N}^{N}\left(\hat{v}_j(t)+K_{2,j}\frac{\Delta t}{2}\right)e^{-dj^2\left(t+\frac{\Delta t}{2}\right)}e^{ijx}}$ one has

$$\sum_{j=-N}^{N}\left(\hat{v}_j(t)+K_{2,j}\frac{\Delta t}{2}\right)e^{-dj^2\left(t+\frac{\Delta t}{2}\right)}e^{ijx} = \sum_{j=-N}^{N}\left(\hat{u}_j(t)e^{-dj^2\frac{\Delta t}{2}}+K^{\star}_{2,j}\frac{\Delta t}{2}\right)e^{ijx}. \quad \text{(B.26)}$$

Finally for $K^{\star}_{4,k} = \hat{f}_k\Big|_{u=\sum_{j=-N}^{N}(\hat{v}_j(t)+K_{3,j}\Delta t)e^{-dj^2(t+\Delta t)}e^{ijx}}$

$$\sum_{j=-N}^{N}\left(\hat{v}_j(t)+K_{3,j}\Delta t\right)e^{-dj^2(t+\Delta t)}e^{ijx} = \sum_{j=-N}^{N}\left(\hat{u}_j(t)e^{-dj^2\Delta t}+K^{\star}_{3,j}\Delta t e^{-dj^2\frac{\Delta t}{2}}\right)e^{ijx}. \quad \text{(B.27)}$$

B.4 Implementation

To implement the Runge-Kutta/integrating-factor pseudospectral scheme given by equation B.23 the following steps are taken:

1) The initial condition for the problem is calculated and (fast) Fourier transformed

giving initial values for all $\hat{u}_k(t)$.

2) The nonlinear term $f(u)$ in equation 5 is evaluated and (fast) Fourier transformed giving values for $K^\star_{1,k} = \hat{f}_k$.

3) $K^\star_{2,k}$, $K^\star_{3,k}$, and $K^\star_{4,k}$ are successively calculated by taking (fast) Fourier transforms of the temporary values of u calculated using the right hand sides of equations B.25, B.26, and B.27. (The sum in each of these equations is actually evaluated using a Fast Fourier Transform routine.)

4) $\hat{u}_k$ is updated using equation B.23. (The change in $\hat{u}_k$ can be accumulated as the $K^\star$'s are calculated to avoid having to store all the $K^\star$'s.)

5) The updated $\hat{u}_k$'s are inverse (fast) Fourier transformed to give $u(t + \Delta t, x)$.

6) Steps 2 through 5 are repeated to progress in time.

Note that all of the exponential coefficients ($e^{-dk^2 \frac{\Delta t}{2}}$ and $e^{-dk^2 \Delta t}$) can be calculated in an initialization routine before the time loop is begun. Also note that although the scheme was derived using $\hat{v}_k$ and K, they do not explicitly appear in the implementation; only $\hat{u}_k$ and $K^\star$.

Appendix C

2-D Parametrically Excited Wave Program (parallel version)

This is a parallel version of the program which calculates numerical approximations to the solutions of (8.2,8.3). It was written to run on the IBM SP at the Cornell Theory Center. Subroutine *pdcft2* is a parallel library routine to calculate fast Fourier transforms. The function subprogram *ran0* is a random number generator from [61]. It was modified to return double precision values by changing the *real* declaration statement to *real*8*. The relationship between variable names in the program and those used in the text are given in the table below:

program	text
u(i,j,1)	$A(x,y)$
u(i,j,2)	$B^*(x,y)$
c1	s
c2	a
c3	d
c4	d_2
c5	$-c$
c6	$-(c+g)$
c7	b

```
c ---------------------------------------------------------------------
c   Description:  2-D Parametrically Excited Wave model
c        Author:  Glen Granzow
c          Date:  April 18, 1997
c       Version:  Run 9; b=0.5, areal=.25, dt=.25, L=136, n=128.
c                 Writes defects and movie files.
```

```
c -----------------------------------------------------------------------
      program main
      implicit none
      integer  m1, m2
      parameter ( m1 = 128, m2 = 2 )
      complex*16 u(m1,m1,m2), v(m1,m1,m2), dv(m1,m1,m2),
     *           e0(m1,m1,m2), e1(m1,m1,m2), e2(m1,m1,m2)
      integer    nx, ny, neqs, presetids(4), allnodes, i
      real*8     timef, time, times(0:255), sum1, sum2, mint, maxt,
     *           startclock, epsilon
      character  filename*32

      real*8          Lx, Ly
      complex*16      c1, c2, c3, c4, c5, c6, c7
      common /params/ c1, c2, c3, c4, c5, c6, c7, Lx, Ly

      real*8        t, dt, dtover2, dtover3, dtover6
      common /time/ t, dt, dtover2, dtover3, dtover6

      integer       nsteps, nascii, nmovie
      common /step/ nsteps, nascii, nmovie

      real*8           amplitude(2), wavenumber(2), phase(2), noise(2)
      integer          ictype, iseed
      common /icparam/ amplitude, wavenumber, phase, noise,
     *                 ictype, iseed

      integer           node, nnodes, icontxt, ip(40)
      common /parallel/ node, nnodes, icontxt, ip

      call blacs_pinfo(node,nnodes)
      if( node .eq. 0 ) write(*,*) 'Running on', nnodes, 'nodes'
      call blacs_get(0,0,icontxt)
      call blacs_gridinit(icontxt,('R'),(1),nnodes)
      call blacs_gridinfo(icontxt,(1),nnodes,(1),node)
      ip(1) = 0
      call mp_task_query( presetids, 4, 3 )
      allnodes = presetids(4)

      neqs  = m2

c *** Model parameters ***
      c1 = ( 0.20d0, 0.0d0)
```

```
      c2 = ( 0.25d0, 0.0d0)
      c3 = ( 1.00d0, 0.5d0)
      c4 = ( 1.00d0, 0.5d0)
      c5 = ( 1.00d0,-4.0d0)
      c6 = ( 2.00d0, 8.0d0)
      c7 = ( 0.50d0, 0.0d0)
      Lx = 136.0d0
      Ly = 136.0d0

c *** Numerical simulation parameters ***
      nx     = 128
      ny     = 128
      dt     = .25d0
      nsteps = 40000

c *** Initial condition parameters ***
      ictype        =  4
      amplitude(1)  =  0.2d0
      amplitude(2)  =  0.2d0
      wavenumber(1) =  5.0d0
      wavenumber(2) = -5.0d0
      phase(1)      =  0.0d0
      phase(2)      =  0.0d0
      noise(1)      =  0.0d0
      noise(2)      =  0.0d0
      iseed         = 10

      epsilon       = -0.4d0

c *** File I/O parameters ***
      nascii = 100000
      nmovie = 1000

      if( node .eq. 0 ) write(*,*) 'CALCULATE INITIAL CONDITION:'
      t = 0.
c       call ic(nx,ny,neqs,u)
c       call eckhaus(nx,ny,neqs,u,epsilon)

      call readascii(nx,ny,neqs,u,t)

      write(filename,'(a27,3i1)') '/tmp/scratch/granzow/movie.',
     *  node/100, mod(node,100)/10, mod(node,10)
      open(1,file=filename,form='unformatted')
```

```
      write(filename,'(a29,3i1)') '/tmp/scratch/granzow/defects.',
     *  node/100, mod(node,100)/10, mod(node,10)
      open(3,file=filename)

      if( node .eq. 0 ) write(*,*) 'RUN:'
      call initializerk(nx,ny,neqs,e0,e1,e2,u,v)
      startclock = timef()
      call timeloop(nx,ny,neqs,u,v,dv,e0,e1,e2)
      time = timef()

      close(1)
      close(3)

      if( node .eq. 0 ) write(*,*) 'FILE OUTPUT:'
      call writeascii(nx,ny,neqs,u,t)

      call mp_gather(time,times,8,0,allnodes)
      if( node .eq. 0 ) then
        write(*,*) 'Raw times: ',(sngl(times(i)),i=0,nnodes-1)
        sum1 = times(0)
        sum2 = times(0)**2
        mint = times(0)
        maxt = times(0)
        do i = 1, nnodes-1
          sum1 = sum1+times(i)
          sum2 = sum2 + times(i)**2
          mint = min(mint,times(i))
          maxt = max(maxt,times(i))
        enddo
        write(*,*) 'Statistics: ', nnodes, sngl(sum1/nnodes),
     *             sqrt(sngl(sum2/nnodes-(sum1/nnodes)**2)),
     *             sngl(mint), sngl(maxt)
      endif

      call blacs_gridexit(icontxt)
      call blacs_exit(0)
      stop
      end
c ------------------------------------------------------------------------
      subroutine ic( nx, ny, neqs, u )
      implicit none
      integer    nx, ny, neqs, i, j, k, jj, ijk
```

```
      complex*16 u(*), u1, u2
      real*8     x, y, ran0, twopi, q, curve

      real*8           amplitude(2), wavenumber(2), phase(2), noise(2)
      integer          ictype, iseed
      common /icparam/ amplitude, wavenumber, phase, noise,
     *                 ictype, iseed

      integer           node, nnodes, icontxt, ip(40)
      common /parallel/ node, nnodes, icontxt, ip

      twopi = 8.d0*datan(1.d0)

      ijk = 1
      do 30 k = 1, neqs
        do 20 j = 1, ny/nnodes
          jj = node*ny/nnodes+j
          y = (jj-1)*twopi/ny
          do 10 i = 1, nx
            x = (i-1)*twopi/nx

            q = wavenumber(k)

            if( ictype .eq. 1 )
     *        u(ijk) = amplitude(k)*exp((0.d0,1.d0)*(q*x+phase(k)))

            if( ictype .eq. 2 )
     *        u(ijk) = amplitude(k)*exp((0.d0,1.d0)*(q*y+phase(k)))

            if( ictype .eq. 3 )
     *        u(ijk) = amplitude(k)*exp((0.d0,1.d0)*(q*(x+y)+phase(k)))

            if( ictype .eq. 4 ) then
              u1 = amplitude(k)*exp((0.d0,1.d0)*(q*x+phase(k)))
              q  = wavenumber(k) + sign(1.d0,wavenumber(k))
              u2 = amplitude(k)*exp((0.d0,1.d0)*(q*x+phase(k)))
              if( jj .gt. ny/2 ) jj = ny+1-jj
              if( jj .le. ny/4 ) then
                u(ijk) = u1
              elseif( jj .le. 3*ny/8 ) then
                u(ijk) = cmplx
     *                  (curve(ny/4,dreal(u1),3*ny/8,dreal(u2),jj),
     *                   curve(ny/4, imag(u1),3*ny/8, imag(u2),jj))
```

```
          else
            u(ijk) = u2
          endif
        endif

        if( noise(k) .ne. 0. ) u(ijk) = u(ijk) + 2.d0*noise(k)*
     *                   cmplx((ran0(iseed)-.5d0),(ran0(iseed)-.5d0))
        ijk = ijk + 1
 10     continue
 20   continue
 30 continue

      return
      end
c ----------------------------------------------------------------------
      function curve( i1, y1, i2, y2, i )
      implicit none
      integer i1, i2, i
      real*8  curve, y1, y2
c      curve = y1 + (i-i1)*(y2-y1)/(i2-i1)
      curve = y1 + (y2-y1)*.5d0*(1.d0-cos((i-i1)*3.141592654d0/(i2-i1)))
      return
      end
c ----------------------------------------------------------------------
      subroutine initializerk( nx, ny, neqs, e0, e1, e2, u, v )
      implicit none
      integer    nx, ny, neqs, i, j, k, q, p, ijk, llk
      real*8     rescale, pi
      complex*16 e0(*), e1(*), e2(*), u(*), v(*), d1, d3, d4, phi

      real*8          Lx, Ly
      complex*16      c1, c2, c3, c4, c5, c6, c7
      common /params/ c1, c2, c3, c4, c5, c6, c7, Lx, Ly

      real*8        t, dt, dtover2, dtover3, dtover6
      common /time/ t, dt, dtover2, dtover3, dtover6

      real*8  n2
      common /nnn/ n2

      integer           node, nnodes, icontxt, ip(40)
      common /parallel/ node, nnodes, icontxt, ip
```

```
      n2 = dble(nx*ny)
      dtover2 = dt / 2.d0
      dtover3 = dt / 3.d0
      dtover6 = dt / 6.d0
      pi      = 4.d0 * datan(1.d0)
      rescale = 2.d0*pi / Lx
      d1 = (0.d0,1.d0)*rescale*c1
      d3 = rescale*rescale*c3
      rescale = 2.d0*pi / Ly
      d4 = rescale*rescale*c4

      ijk = 1
      llk = 1
      do 30 k = 1, neqs
        do 20 j = 1, nx/nnodes
          q = node*nx/nnodes + j - 1
          if( q .gt. nx/2 ) q = q - nx
          do 10 i = 1, ny
            p = i - 1
            if( p .gt. ny/2 ) p = p - ny
            if( q .eq. nx/2 ) then
              phi =  d3*dble(q*q) + d4*dble(p*p)
            elseif( k .eq. 1 ) then
              phi =  d1*dble(q) + d3*dble(q*q) + d4*dble(p*p)
            else
              phi = -d1*dble(q) + d3*dble(q*q) + d4*dble(p*p)
            endif
            e0(ijk) = 1.d0 / n2
            e1(ijk) = exp( - phi * dtover2 ) / n2
            e2(ijk) = exp( - phi * dt      ) / n2
            ijk = ijk + 1
   10     continue
   20   continue
        call pdcft2(u(llk),v(llk),nx,ny,1,(1.d0),icontxt,ip)
        llk = ijk
   30 continue

      return
      end
c -----------------------------------------------------------------------
      subroutine timeloop( nx, ny, neqs, u, v, dv, e0, e1, e2 )
      implicit none
      integer    nx, ny, neqs, i, j, k, timestep, ijk
```

```
      complex*16 u(*), v(*), dv(*), e0(*), e1(*), e2(*)

      real*8          Lx, Ly
      complex*16      c1, c2, c3, c4, c5, c6, c7
      common /params/ c1, c2, c3, c4, c5, c6, c7, Lx, Ly

      real*8        t, dt, dtover2, dtover3, dtover6
      common /time/ t, dt, dtover2, dtover3, dtover6

      integer       nsteps, nascii, nmovie
      common /step/ nsteps, nascii, nmovie

      integer           node, nnodes, icontxt, ip(40)
      common /parallel/ node, nnodes, icontxt, ip

      do 100 timestep = 1, nsteps
        t = t + dt

c       PSEUDOSPECTRAL ( RUNGE KUTTA ) TECHNIQUE:
        ijk = 1
        do 80 k = 1, neqs
          do 70 j = 1, nx/nnodes
            do 60 i = 1, ny
              dv(ijk) = (0.d0,0.d0)
              ijk = ijk+1
   60       continue
   70     continue
   80   continue
        call rkstep(dtover6,e2,e1,e1,dtover2,.false.,u,v,dv,nx,ny,neqs)
        call rkstep(dtover3,e1,e1,e0,dtover2,.false.,u,v,dv,nx,ny,neqs)
        call rkstep(dtover3,e1,e2,e1,dt,     .false.,u,v,dv,nx,ny,neqs)
        call rkstep(dtover6,e0,e2,e0,0.,     .true. ,u,v,dv,nx,ny,neqs)

        call finddefects(nx,ny/nnodes,neqs,u)
        if( mod(timestep,nascii).eq.0 ) call writeascii(nx,ny,neqs,u,t)
        if( mod(timestep,nmovie).eq.0 ) call writemovie(nx,ny,neqs,u,t)

  100 continue

      return
      end
c ---------------------------------------------------------------------
      subroutine rkstep( weight, wfactor, ufactor, kfactor, ttemp, step4
```

```
     *                 , u, v, dv, nx, ny, neqs )
      implicit none
      real*8     weight, ttemp
      complex*16 wfactor(*), ufactor(*), kfactor(*), u(*), v(*), dv(*),
     *           kstar
      logical    step4
      integer    nx, ny, neqs, i, j, k, ijk, llk

      real*8  n2
      common /nnn/ n2

      integer           node, nnodes, icontxt, ip(40)
      common /parallel/ node, nnodes, icontxt, ip

      call loop1(nx,ny,u)

      ijk = 1
      llk = 1
      do 60 k = 1, neqs
        call pdcft2(u(llk),u(llk),nx,ny,1,(1.d0),icontxt,ip)
        do 50 j = 1, nx/nnodes
          do 40 i = 1, ny
            kstar = u(ijk)
            dv(ijk) = dv(ijk) + weight*kstar*wfactor(ijk)
            if( step4 ) then
              u(ijk) = v(ijk)*ufactor(ijk) + dv(ijk)
              v(ijk) = u(ijk)*n2
            else
              u(ijk) = v(ijk)*ufactor(ijk) + kstar*ttemp*kfactor(ijk)
            endif
            ijk = ijk+1
   40     continue
   50   continue
        call pdcft2(u(llk),u(llk),ny,nx,-1,(1.d0),icontxt,ip)
        llk = ijk
   60 continue

      return
      end
c ---------------------------------------------------------------------
      subroutine loop1( nx, ny, u )
      implicit none
      integer nx, ny, i, j, ij1, ij2
```

```
      complex*16 u(*), f1, f2, u1, u2
      integer           node, nnodes, icontxt, ip(40)
      common /parallel/ node, nnodes, icontxt, ip

      ij1 = 1
      ij2 = 1+nx*ny/nnodes
      do 20 j = 1, ny/nnodes
        do 10 i = 1, nx
          u1 = u(ij1)
          u2 = u(ij2)
          u(ij1) = f1( u1, u2 )
          u(ij2) = f2( u1, u2 )
          ij1 = ij1+1
          ij2 = ij2+1
   10   continue
   20 continue
      return
      end
c ----------------------------------------------------------------------
c note: The functions f1 & f2 define the "reaction part" of the system.
c ----------------------------------------------------------------------
      function f1( A, B )
      implicit none
      complex*16 f1, A, B
      real*8          Lx, Ly
      complex*16      c1, c2, c3, c4, c5, c6, c7
      common /params/ c1, c2, c3, c4, c5, c6, c7, Lx, Ly
      f1 = (c2 - c5*(dreal(A)*dreal(A)+imag(A)*imag(A))
     *         - c6*(dreal(B)*dreal(B)+imag(B)*imag(B)))*A + c7*conjg(B)
      return
      end
c ----------------------------------------------------------------------
      function f2( A, B )
      implicit none
      complex*16 f2, A, B
      real*8          Lx, Ly
      complex*16      c1, c2, c3, c4, c5, c6, c7
      common /params/ c1, c2, c3, c4, c5, c6, c7, Lx, Ly
      f2 = (c2 - c5*(dreal(B)*dreal(B)+imag(B)*imag(B))
     *         - c6*(dreal(A)*dreal(A)+imag(A)*imag(A)))*B + c7*conjg(A)
      return
      end
c ----------------------------------------------------------------------
```

```
      subroutine readascii( nx, ny, neqs, u, t )
      implicit none
      integer nx, ny, neqs, n, i, ii, k
      real*8  u(*), t
      integer           node, nnodes, icontxt, ip(40)
      common /parallel/ node, nnodes, icontxt, ip

      open(4,file='/tmp/scratch/granzow/ascii.file')
      read(4,*) n, neqs
      ii = 2*n*n*neqs
      read(4,*) t, ( u(i), i=1, ii )
      close(4)

      nx = n
      ny = n
      ii = 2*n*n
      do 20 k = 1, neqs
        do 10 i = 1, ii/nnodes
          u((k-1)*ii/nnodes+i) = u((k-1)*ii+node*ii/nnodes+i)
   10   continue
   20 continue

      return
      end
c ----------------------------------------------------------------------
      subroutine writeascii( nx, ny, neqs, u, t )
      implicit none
      integer nx, ny, neqs, i, ii, kount
      real*8  u(*), t
      character*38 filename
      integer           node, nnodes, icontxt, ip(40)
      common /parallel/ node, nnodes, icontxt, ip
      data    kount /0/
      save    kount
      kount = kount + 1
      write(filename,'(a31,3i1,a,3i1)
     *  ')')'/tmp/scratch/granzow/ascii.node',
     *  node/100, mod(node,100)/10, mod(node,10), '.',
     *  kount/100, mod(kount,100)/10, mod(kount,10)
c      write(*,*) filename
      open(4,file=filename)
      if( node .eq. 0 ) write(4,*) nnodes
      write(4,*) nx, ny, neqs
```

```
      ii = 2*neqs*nx*ny/nnodes
      write(4,*) t, ( u(i), i = 1, ii )
      close(4)
      return
      end
c -----------------------------------------------------------------------
      subroutine writemovie( nx, ny, neqs, u, t )
      implicit none
      integer nx, ny, neqs, i, ii
      real*8  u(*), t, umin, umax, du
      integer          node, nnodes, icontxt, ip(40)
      common /parallel/ node, nnodes, icontxt, ip
      data ii/0/
      save ii

      if( ii .eq. 0 ) then
        write(1) nx, ny, neqs
        ii = 2*neqs*nx*ny/nnodes
      endif

      umin = u(1)
      umax = umin
      do 10 i = 1, ii
        umin = min( umin, u(i) )
        umax = max( umax, u(i) )
   10 continue
      du = ( umax - umin ) / 255
      write(1) sngl(t), sngl(umin), sngl(umax),
     *       ( char(int((u(i)-umin)/du)), i=1,ii )
      return
      end
c -----------------------------------------------------------------------
      subroutine finddefects( nx, ny, neqs, u )
c     NOTE: in this subroutine ny = ny/nnodes in the main program
      implicit none
      integer  m2
      parameter ( m2 = 2 )
      integer  nx, ny, neqs, i, j, k, iplus1, jplus1, ii, c !, count(m2)
      real*8   u(2,nx,ny,*), bl(2), br(2), tl(2), tr(2), m(2), b(2),
     *         x(4), y(4), xx, yy, s(2)
      logical  top, bottom, left, right,
     *         exclusiveor, negtopos(2), different, positiveexp,
     *         wasgt2
```

```
      real*8          Lx, Ly
      complex*16      c1, c2, c3, c4, c5, c6, c7
      common /params/ c1, c2, c3, c4, c5, c6, c7, Lx, Ly

      real*8        t, dt, dtover2, dtover3, dtover6
      common /time/ t, dt, dtover2, dtover3, dtover6

      integer           node, nnodes, icontxt, ip(40)
      common /parallel/ node, nnodes, icontxt, ip

      integer msg, sendid, recvid, jj
      data    msg / 0 /
      save    msg

      msg = msg + 1
      jj = neqs*ny+1
      call mp_send(u,nx*16,mod(node+nnodes-1,nnodes),msg,sendid)
      call mp_recv(u(1,1,jj,1),nx*16,mod(node+1,nnodes),msg,recvid)

      wasgt2 = .false.
      write(3,*) 't', sngl(t), sngl(Lx)

      k  = 1
c      do 50 k = 1, neqs
c        count(k) = 0
        do 40 j = 1, ny
          jplus1 = j + 1
          if( j .eq. ny ) then
            call mp_wait( recvid, nx*16 )
            jplus1 = jj
          endif
          do 30 i = 1, nx
            iplus1 = i + 1
            if( i .eq. nx ) iplus1 = 1
            do 10 c = 1, 2
              bl(c) = u(c,i,j,k)
              br(c) = u(c,iplus1,j,k)
              tl(c) = u(c,i,jplus1,k)
              tr(c) = u(c,iplus1,jplus1,k)
              if(abs(sign(1.d0,bl(c))+sign(1.d0,br(c))
     *              +sign(1.d0,tl(c))+sign(1.d0,tr(c))) .gt. 3.)
     *          go to 25
```

```
10      continue
        do 20 c = 1, 2
          top    = exclusiveor(tl(c).gt.0.d0,tr(c).gt.0.d0)
          bottom = exclusiveor(bl(c).gt.0.d0,br(c).gt.0.d0)
          left   = exclusiveor(bl(c).gt.0.d0,tl(c).gt.0.d0)
          right  = exclusiveor(br(c).gt.0.d0,tr(c).gt.0.d0)
          ii = 0
          if( left ) then
            ii = ii + 1
            x(ii) = 0.
            y(ii) = bl(c)/(bl(c)-tl(c))
            s(c)  = 4.-y(ii)
            negtopos(c) = tl(c) .lt. bl(c)
          endif
          if( top ) then
            ii = ii + 1
            x(ii) = tl(c)/(tl(c)-tr(c))
            y(ii) = 1.
            s(c)  = 3.-x(ii)
            negtopos(c) = tr(c) .lt. tl(c)
          endif
          if( right ) then
            ii = ii + 1
            x(ii) = 1.
            y(ii) = br(c)/(br(c)-tr(c))
            s(c)  = 1.+y(ii)
            negtopos(c) = br(c) .lt. tr(c)
          endif
          if( bottom ) then
            ii = ii + 1
            x(ii) = bl(c)/(bl(c)-br(c))
            y(ii) = 0.
            s(c)  = x(ii)
            negtopos(c) = bl(c) .lt. br(c)
          endif
          m(c) = (y(2)-y(1))/(x(2)-x(1))
          b(c) = y(1)-m(c)*x(1)
          if( ii.gt.2 .or. wasgt2 ) call possible
 *          (k,c,ii,x,y,m,b,s,wasgt2,negtopos,.false.)
20      continue
        xx = (b(2)-b(1)) / (m(1)-m(2))
        yy = m(1)*xx+b(1)
        if( xx.ge.0..and.xx.lt.1. .and. yy.ge.0..and.yy.lt.1. ) then
```

```
              different   = exclusiveor( negtopos(1), negtopos(2) )
              positiveexp = exclusiveor( s(1).lt.s(2), different )
c              if( k .eq. 1 ) then
                xx = ( dble(i-1)+xx )*Lx/nx
                yy = ( dble(j-1)+yy )*Ly/ny
                yy = (Ly*node+yy)/nnodes
                if( positiveexp ) then
                  write(3,*) 'A', sngl(xx), sngl(yy)
                else
                  write(3,*) 'a', sngl(xx), sngl(yy)
                endif
c              endif
c              count(k) = count(k) + 1
            endif
   25       continue
   30     continue
   40   continue
   50 continue

c      write(*,*) 't =', sngl(t), count
      call mp_wait( sendid, nx*16 )
      return
      end
c ----------------------------------------------------------------------
      subroutine possible( k, c, ii, x, y, m, b, s, calledc1, negtopos,
     *                     printing )
      implicit none
      integer k, c, ii, i, j, jj, iii, jjj, n
      real*8  x(4), y(4), m(2), b(2), s(2), mm(4), bb(4), ss(4), xx, yy
      logical calledc1, negtopos(2), printing
      save    mm, bb, ss

      if( c .eq. 1 ) then
        if( x(2)+y(3) .gt. y(1)+x(4) ) then
          mm(1) = -y(1)/x(4)
          mm(2) = (1.-y(3))/(x(2)-1.)
          ss(1) =  x(4)
        else
          mm(1) = (1.-y(1))/x(2)
          mm(2) = y(3)/(1.-x(4))
          ss(1) = 3.-x(2)
        endif
        bb(1) = y(1)
```

```
      bb(2) = y(3)-mm(2)
      ss(2) = 1.+y(3)
      calledc1 = .true.
      return
    endif

    n = 0

    if( ii .le. 2 ) then
      do 20 i = 1, 2
        xx = (b(2)-bb(i))/(mm(i)-m(2))
        yy = mm(i)*xx + bb(i)
        if( xx.ge.0..and.xx.lt.1. .and. yy.ge.0..and.yy.lt.1. ) then
          n  = n+1
          ii = i
        endif
20    continue
      if( n .eq. 1 ) then
        if( printing ) write(*,*) 'WARNING(1); Position is uncertain:'
        m(1) = mm(ii)
        b(1) = bb(ii)
        s(1) = ss(ii)
        if( ii .eq. 2 ) negtopos(1) = .not.negtopos(1)
      else
        m(1) =  0.
        b(1) = -1.
      endif
      calledc1 = .false.
      return
    endif

    if( x(2)+y(3) .gt. y(1)+x(4) ) then
      mm(3) = -y(1)/x(4)
      mm(4) = (1.-y(3))/(x(2)-1.)
      ss(3) = x(4)
    else
      mm(3) = (1.-y(1))/x(2)
      mm(4) = y(3)/(1.-x(4))
      ss(3) = 3.-x(2)
    endif
    bb(3) = y(1)
    bb(4) = y(3)-mm(4)
    ss(4) = 1.+y(3)
```

```
   if( .not.calledc1 ) then
     do 30 j = 3, 4
       xx = (bb(j)-b(1))/(m(1)-mm(j))
       yy = m(1)*xx + b(1)
       if( xx.ge.0..and.xx.lt.1. .and. yy.ge.0..and.yy.lt.1. ) then
         n  = n+1
         jj = j
       endif
30   continue
     if( n .eq. 1 ) then
       if( printing ) write(*,*) 'WARNING(2); Position is uncertain:'
       m(2) = mm(jj)
       b(2) = bb(jj)
       s(2) = ss(jj)
       if( jj .eq. 4 ) negtopos(2) = .not.negtopos(2)
     else
       m(2) =  0.
       b(2) = -1.
     endif
     return
   endif

   do 50 i = 1, 2
     do 40 j = 3, 4
       xx = (bb(j)-bb(i))/(mm(i)-mm(j))
       yy = mm(i)*xx + bb(i)
       if( xx.ge.0..and.xx.lt.1. .and. yy.ge.0..and.yy.lt.1. ) then
         n  = n+1
         ii = i
         jj = j
       else
         iii = i
         jjj = j
       endif
40   continue
50 continue
   if( n.eq.1 .or. n.eq.3 ) then
     if( n .eq. 1 ) then
       if( printing ) write(*,*) 'WARNING(3); Position is uncertain:'
     else
       if( printing ) write(*,*) 'WARNING(4); Position is uncertain:'
       ii = 1 + mod(iii,2)
```

```
        jj = jjj
      endif
      m(1) = mm(ii)
      b(1) = bb(ii)
      s(1) = ss(ii)
      if( ii .eq. 2 ) negtopos(1) = .not.negtopos(1)
      m(2) = mm(jj)
      b(2) = bb(jj)
      s(2) = ss(jj)
      if( jj .eq. 4 ) negtopos(2) = .not.negtopos(2)
    else
      m(1) =  1.
      b(1) =  1.
      m(2) =  0.
      b(2) =  0.
    endif
    calledc1 = .false.
    return
    end
c ----------------------------------------------------------------------
    function exclusiveor( a, b )
    logical  exclusiveor, a, b
    if( (a.or.b).and..not.(a.and.b) ) then
      exclusiveor = .true.
    else
      exclusiveor = .false.
    endif
    return
    end
c ----------------------------------------------------------------------
    subroutine eckhaus( nx, ny, neqs, u, epsilon )
    implicit none
    integer    nx, ny, neqs, i, j, k, ijk
    complex*16 u(*), iepsilon
    real*8     epsilon, x, y, twopi

    integer           node, nnodes, icontxt, ip(40)
    common /parallel/ node, nnodes, icontxt, ip

    if( node .eq. 0 ) write(*,*) 'epsilon =', epsilon
    iepsilon = dcmplx(0.d0,epsilon)
    twopi = 8.d0*datan(1.d0)
```

```
      ijk = 1
      do 30 k = 1, neqs
        iepsilon = -1.d0*iepsilon
        do 20 j = 1, ny/nnodes
          y = (node*ny/nnodes+(j-1))*twopi/ny
          do 10 i = 1, nx
            x = (i-1)*twopi/nx
            u(ijk) = u(ijk)*(1.d0-iepsilon*(1.d0-cos(y))*sin(x))
            ijk = ijk + 1
   10     continue
   20   continue
   30 continue

      return
      end
c ----------------------------------------------------------------------
```

Appendix D

Defect Tracking Program

This is the defect tracking program. It reads a defects file created by combining the defects files written by the program in appendix C and accumulates histogram data and statistics of the motion of the defects. The graphics subroutines called are from the vogle graphics library.

```
c ----------------------------------------------------------------------
c  Description:  Defect tracking program w/histograms
c       Author:  Glen Granzow
c         Date:  May 5, 1997
c      Version:  Allows user to specify time interval.
c                Generates six histograms:
c                  00 - Number of defects in a loop.
c                  01 - Defect life times.
c                  02 - Maximum displacement of defects.
c                  03 - X direction bubble span.
c                  04 - Y direction bubble span.
c                  05 - Number of defects.
c                Normalizes histogram file data.
c                Zero probabilities are output as 1.e-15
c                Reads either formatted or unformatted defects file.
c                Reads more than one file for continued runs.
c ----------------------------------------------------------------------
      program main
      implicit none
      integer m3
      parameter ( m3 = 500 )
      integer   n(2), i, flag, backbuffer, checkkey, option
      real      x(m3,2), y(m3,2), xx, yy, L, radius, tstart, tstop
      character recordtype, device*12, filename*80, response
      logical   successfull, error, eof, existingfile

      real    criterion1, criterion2, criterion3, L2, t
```

```
      logical graphics
      common  criterion1, criterion2, criterion3, L2, t, graphics
      data    criterion1, criterion2, criterion3 / .05, .1, .1 /
      data    graphics / .false. /

      integer        counter1, counter2, error1, error2, error3
      common /bound/ counter1, counter2, error1, error2, error3
      data           counter1, counter2, error1, error2, error3 /5*0/

      data n / 2*0 /

      call histogram(0,1,0.,0.5,1.,0,0)
      call histogram(1,1,0.,-.5,1.,0,0)
      call histogram(2,1,0.,-.5,1.,0,0)
      call histogram(3,1,0.,-.5,1.,0,0)
      call histogram(4,1,0.,-.5,1.,0,0)
      call histogram(5,1,0.,-.5,1.,0,0)

      print *, 'INPUT FILE'
    1 call openfile(1,successfull)
      if( .not. successfull ) go to 1
      print *
      error = .false.
      eof   = .false.

      call readfile(1,recordtype,t,L,error,eof)
      if( eof .or. (recordtype.ne.'t') ) then
        print *, '*** ERROR reading first record *** ', recordtype
        stop
      endif
      radius = L/100.
      L2 = L*L
      write(*,*) 'Enter criteria: ( .05, .1, .1 )'
      read (*,*) criterion1, criterion2, criterion3
      criterion1 = criterion1*criterion1*L2
      criterion2 = criterion2*criterion2*L2
      criterion3 = criterion3*criterion3*L2

      print *
      print *, 'First time read is:', t
      print *, 'Enter time interval to be processed:'
      read(*,*) tstart, tstop
      print *
```

```
      if( .not. graphics ) then
 2      write(*,*) '<<<< Device options >>>>'
        write(*,*) ' 0: no graphics'
        write(*,*) ' 1: X11'
        write(*,*) ' 2: ppostscript'
        write(*,*) ' 3: pcps'
        write(*,*) ' 4: Enter another device'
        write(*,*) 'Enter device option number'
        read (*,*,err=2) option
        if( option .eq. 1 ) device = 'X11'
        if( option .eq. 2 ) device = 'ppostscript'
        if( option .eq. 3 ) device = 'pcps'
        if( option .eq. 4 ) read(*,*) device
        if( option .gt. 1 ) then
 4        write(*,*) 'Enter filename: (',filename,')'
          read(*,*,err=4) filename
          inquire(file=filename,exist=existingfile)
          if( existingfile ) then
 6          write(*,*) 'Overwrite? (y/n)'
            read (*,*,err=6) response
            if( response .eq. 'n' ) go to 4
            if( response .ne. 'y' ) go to 6
          endif
          call voutput(filename)
        endif
        graphics = option .gt. 0

        if( graphics ) then
          call prefposition(550,275)
          call prefsize(600,600)
          call vinit(device)
          call ortho2(0.,L,0.,L)
          call circleprecision((8))
c          call polyfill(.true.)
          if( device .eq. 'X11' ) i = backbuffer()
          call color(0)
          call clear()
          if( device .ne. 'X11' ) call fillbackground()
          call textsize( L/30., L/30. )
c          call centertext(.true.)
          if( device .eq. 'X11' ) call swapbuffers()
        endif
```

```
      endif

   10 call readfile(1,recordtype,xx,yy,error,eof)
      if( error ) then
        print *, '*** error reading file ***'
        print *, 'Final time read:', t
        recordtype = 'E'
      endif
      if( eof .and. .not. error ) then
        write(*,*) '*** end of file ***'
        print *, 'Final time read:', t
        recordtype = 't'
      endif

      if( recordtype .eq. 't' ) then
c          write(*,*) 'time =', t, n(1), n(2)
        if( t.gt.tstart ) then
          call histogram(5,2,.5*float(n(1)+n(2)),0.,0.,0,0)
          call trackdefects( n, x, y, L, t, flag )
          if( flag .ne. 0 ) go to 35
          if( graphics ) then
            call swapbuffers()
            if( device.eq.'X11' .and. (checkkey().ne.0 .or. eof) ) then
              write(*,*) 'time =', t, n(1), n(2)
              write(*,*) 'Press <Return>'
              read (*,*,err=25)
            endif
   25       call color(0)
            call clear()
            if( device .ne. 'X11' ) call fillbackground()
          endif
        endif
        t = xx
        n(1) = 0
        n(2) = 0
      else
        if( t.lt.tstart ) go to 10
        i = 0
        if( recordtype .eq. 'A' ) i = 1
        if( recordtype .eq. 'a' ) i = 2
        if( i .eq. 0 ) then
          print *,
     *      '*** ERROR: unknown record type (', recordtype, ') ***'
```

```
        else
          n(i) = n(i) + 1
          if( n(i) .gt. m3 ) then
            print *, 'ERROR: too many defects', i, n(i)
            print *, '       increase parameter m3 in program'
            stop
          endif
          x(n(i),i) = xx
          y(n(i),i) = yy
          if( graphics ) then
            call color(i)
            call circle(xx,yy,radius)
          endif
        endif
      endif

      if( (t.le.tstop) .and. (.not.eof) ) go to 10

   35 close(1)
      print *, 'Error counters:'
      print *, 'ERROR #1: (unequal + and - defects)', error1
      print *, 'ERROR #2: (single defect created)  ', error2
      print *, 'ERROR #3: (lost old defect)        ', error3
   40 print *, 'Continue with another file? (y/n)'
      read (*,*,err=40) response
      if( response .eq. 'y' ) go to 1
      if( response .ne. 'n' ) go to 40
      call defectloops(L)
      print *, 'collisions between   bound defects:', counter1
      print *, 'collisions between unbound defects:', counter2
      print *
      print *, 'Number of defects in a loop distribution:'
      call histogram(0,3,0.,0.,0.,0,99)
      print *
      print *, 'Defect life time distribution:'
      call histogram(1,3,0.,0.,0.,0,99)
      print *
      print *, 'Maximum defect displacement distribution:'
      call histogram(2,3,0.,0.,0.,0,99)
      print *
      print *, 'X direction bubble span distribution:'
      call histogram(3,3,0.,0.,0.,0,99)
      print *
```

```
      print *, 'Y direction bubble span distribution:'
      call histogram(4,3,0.,0.,0.,0,99)
      print *
      print *, 'Number of defects distribution:'
      call histogram(5,3,0.,0.,0.,0,99)
      stop
      end
c -----------------------------------------------------------------------
      subroutine fillbackground()
      call pushmatrix()
      call ortho2(0.,1.,0.,1.)
      call polyfill(.true.)
      call rect(0.,0.,1.,1.)
      call polyfill(.false.)
      call popmatrix()
      return
      end
c -----------------------------------------------------------------------
      subroutine trackdefects( nnew, xnew, ynew, L, time, flag )
      implicit none
      integer m3
      parameter ( m3 = 500 )
      integer nnew(2), flag, nold(2), numbernew(m3,2), numberold(m3,2),
     *        nextn, inew, iold, iclosest, j, i1, i2, iinew, nprint, n
      real    xnew(m3,2), ynew(m3,2), L, time, xold(m3,2), yold(m3,2),
     *        distance, d, dmin, t0old(m3,2), t0new(m3,2),
     *        x0old(m3,2), y0old(m3,2), x0new(m3,2), y0new(m3,2),
     *        d0old(m3,2), d0new(m3,2)
      logical assigned(m3,2)
      character   s(2)
      character*3 string
      save    nold, nextn, s, numberold, xold, yold,
     *        t0old, x0old, y0old, d0old, nprint
      data    nold, nextn, nprint, s / 0,0,1,1000,'+','-' /

      real    criterion1, criterion2, criterion3, L2, t
      logical graphics
      common  criterion1, criterion2, criterion3, L2, t, graphics

      integer        counter1, counter2, error1, error2, error3
      common /bound/ counter1, counter2, error1, error2, error3

      integer ksize
```

```
      parameter( ksize=100000 )
      integer ndefects, killer(ksize), xwrap(ksize,2), ywrap(ksize,2)
      real    xmin(ksize), xmax(ksize), ymin(ksize), ymax(ksize)
      common /bubbles/
     *        ndefects, killer, xwrap, ywrap, xmin, xmax, ymin, ymax

      if( nnew(1) .ne. nnew(2) ) error1 = error1 + 1

c  The "assigned" array refers to the old defect numbers:

      do 20 j = 1, 2
        do 10 iold = 1, nold(j)
          assigned(iold,j)  = .false.
   10   continue
   20 continue

c  Assign defect numbers to new defects that are close to old defects:

      do 60 j = 1, 2
        do 50 inew = 1, nnew(j)
          numbernew(inew,j) = 0
          dmin = L2
          do 30 iold = 1, nold(j)
            d = distance( xold(iold,j), yold(iold,j),
     *                    xnew(inew,j), ynew(inew,j), L )
            if( d .lt. dmin ) then
              iclosest = iold
              dmin = d
            endif
   30     continue
          if( dmin .lt. criterion1 ) then
            if( assigned(iclosest,j) ) then
              do 40 iinew = 1, inew-1
                if( numbernew(iinew,j) .eq. numberold(iclosest,j) ) then
                  d = distance( xold(iclosest,j), yold(iclosest,j),
     *                          xnew(iinew,j),    ynew(iinew,j), L )
                  if( dmin .lt. d ) then
                    numbernew(iinew,j) = 0
                    n = numberold(iclosest,j)
                    call setwrap(xnew(iinew,j),xold(iclosest,j),L,
     *                           xwrap(n,j))
                    call setwrap(ynew(iinew,j),yold(iclosest,j),L,
     *                           ywrap(n,j))
```

```
              go to 45
            else
              go to 50
            endif
          endif
40        continue
        endif
45      numbernew(inew,j) = numberold(iclosest,j)
        t0new(inew,j) = t0old(iclosest,j)
        x0new(inew,j) = x0old(iclosest,j)
        y0new(inew,j) = y0old(iclosest,j)
        d = distance(  xnew(inew,j),  ynew(inew,j),
  *                   x0new(inew,j), y0new(inew,j), L )
        d0new(inew,j) = max(d,d0old(iclosest,j))
        n = numbernew(inew,j)
        call setwrap(xold(iclosest,j),xnew(inew,j),L,xwrap(n,j))
        call setwrap(yold(iclosest,j),ynew(inew,j),L,ywrap(n,j))
        xmin(n) = min( xmin(n), xnew(inew,j)+xwrap(n,j)*L )
        xmax(n) = max( xmax(n), xnew(inew,j)+xwrap(n,j)*L )
        ymin(n) = min( ymin(n), ynew(inew,j)+ywrap(n,j)*L )
        ymax(n) = max( ymax(n), ynew(inew,j)+ywrap(n,j)*L )
        assigned(iclosest,j) = .true.
      endif
50    continue
60  continue

c  Check for collisions between old defects:

    do 80 i1 = 1, nold(1)
      if( .not. assigned(i1,1) ) then
        dmin = L2
        do 70 i2 = 1, nold(2)
          if( .not. assigned(i2,2) ) then
            d = distance( xold(i1,1), yold(i1,1),
  *                       xold(i2,2), yold(i2,2), L )
            if( d .lt. dmin ) then
              iclosest = i2
              dmin = d
            endif
          endif
70      continue
        if( dmin .lt. criterion2 ) then
c          write(*,*) 'Collision:',numberold(i1,1),s(1)
```

```
c     *                             ,numberold(iclosest,2),s(2)
            if( numberold(i1,1) .eq. numberold(iclosest,2) ) then
              counter1 = counter1 + 1
            else
              counter2 = counter2 + 1
            endif
            killer( numberold(i1,1) ) = numberold(iclosest,2)
            call histogram(1,2,time-t0old(i1,1),0.,0.,0,0)
            call histogram(1,2,time-t0old(iclosest,2),0.,0.,0,0)
            call histogram(2,2,sqrt(d0old(i1,1)),0.,0.,0,0)
            call histogram(2,2,sqrt(d0old(iclosest,2)),0.,0.,0,0)
            assigned(i1,1) = .true.
            assigned(iclosest,2) = .true.
            n = numberold(i1,1)
            call setwrap(xold(i1,1),xold(iclosest,2),L,xwrap(n,1))
            call setwrap(yold(i1,1),yold(iclosest,2),L,ywrap(n,1))
          endif
        endif
   80 continue

c  Any old defects which have not been identified are "Lost":

      do 100 j = 1, 2
        do 90 iold = 1, nold(j)
          if( .not. assigned(iold,j) ) then
c            write(*,*) 'Lost old:',numberold(iold,j),s(j)
c            call histogram(1,2,time-t0old(iold,j),0.,0.,0,0)
c            call histogram(2,2,sqrt(d0old(iold,j)),0.,0.,0,0)
            error2 = error2 + 1
          endif
   90   continue
  100 continue

c  New defect pairs are identified:

      do 130 i1 = 1, nnew(1)
        if( numbernew(i1,1) .eq. 0 ) then
          dmin = L2
          do 120 i2 = 1, nnew(2)
            if( numbernew(i2,2) .eq. 0 ) then
              d = distance( xnew(i1,1), ynew(i1,1),
     *                      xnew(i2,2), ynew(i2,2), L )
              if( d .lt. dmin ) then
```

```
              iclosest = i2
              dmin = d
            endif
          endif
 120    continue
        if( dmin .lt. criterion3 ) then
          if( nextn .gt. ksize ) go to 999
c          write(*,*) 'Pair created:', nextn
          numbernew(i1,1) = nextn
          numbernew(iclosest,2) = nextn
          t0new(i1,1) = time
          x0new(i1,1) = xnew(i1,1)
          y0new(i1,1) = ynew(i1,1)
          d0new(i1,1) = 0.
          t0new(iclosest,2) = time
          x0new(iclosest,2) = xnew(iclosest,2)
          y0new(iclosest,2) = ynew(iclosest,2)
          d0new(iclosest,2) = 0.
          n = nextn
          xwrap(n,1) = 0
          xwrap(n,2) = 0
          ywrap(n,1) = 0
          ywrap(n,2) = 0
          call setwrap(xnew(iclosest,2),xnew(i1,1),L,xwrap(n,1))
          call setwrap(ynew(iclosest,2),ynew(i1,1),L,ywrap(n,1))
          xmin(n) = min( xnew(i1,1)+xwrap(n,1)*L, xnew(iclosest,2) )
          xmax(n) = max( xnew(i1,1)+xwrap(n,1)*L, xnew(iclosest,2) )
          ymin(n) = min( ynew(i1,1)+ywrap(n,1)*L, ynew(iclosest,2) )
          ymax(n) = max( ynew(i1,1)+ywrap(n,1)*L, ynew(iclosest,2) )
          nextn = nextn+1
        endif
      endif
 130 continue

c  Any new defects which have not been identified are numbered here
c  and all "new" information is moved to the "old" arrays:

     do 150 j = 1, 2
       do 140 inew = 1, nnew(j)
         if( numbernew(inew,j) .eq. 0 ) then
           if( nextn .gt. ksize ) go to 999
c           write(*,*) 'Single created:',nextn,s(j)
           numbernew(inew,j) = nextn
```

```
          t0new(inew,j) = time
          x0new(inew,j) = xnew(inew,j)
          y0new(inew,j) = ynew(inew,j)
          d0new(inew,j) = 0.
          xmin(nextn) = xnew(inew,j)
          xmax(nextn) = xnew(inew,j)
          ymin(nextn) = ynew(inew,j)
          ymax(nextn) = ynew(inew,j)
          xwrap(nextn,j) = 0
          ywrap(nextn,j) = 0
          nextn = nextn+1
          error3 = error3 + 1
        endif
        numberold(inew,j) = numbernew(inew,j)
        xold(inew,j)      = xnew(inew,j)
        yold(inew,j)      = ynew(inew,j)
        t0old(inew,j)     = t0new(inew,j)
        x0old(inew,j)     = x0new(inew,j)
        y0old(inew,j)     = y0new(inew,j)
        d0old(inew,j)     = d0new(inew,j)
        if( graphics ) then
          write(string,1000) mod(numbernew(inew,j),1000)
          call move2( xnew(inew,j), ynew(inew,j) )
          call color(j)
          call drawstr(string)
        endif
140   continue
      nold(j) = nnew(j)
150 continue

    ndefects = nextn - 1
    if( ndefects .ge. nprint ) then
      print *, ndefects, ' defects, t =', t
      nprint = nprint+1000
    endif
    flag = 0
    return

999 print *, 'WARNING:  Too many defects'
    print *, '          Increase parameter ksize in program'
    ndefects = nextn - 1
    flag = 1
    return
```

```
 1000 format(i3)
      end
c ----------------------------------------------------------------------
      function distance( x1, y1, x2, y2, L )
      implicit none
      real distance, x1, y1, x2, y2, L, dx, dy
      dx = abs(x1-x2)
      dy = abs(y1-y2)
      dx = min(dx,L-dx)
      dy = min(dy,L-dy)
      distance = dx*dx+dy*dy
      return
      end
c ----------------------------------------------------------------------
      subroutine setwrap( xold, xnew, L, wrap)
      implicit none
      real     xold, xnew, L
      integer  wrap
      if( xnew.lt..25*L .and. xold.gt..75*L ) wrap = wrap + 1
      if( xnew.gt..75*L .and. xold.lt..25*L ) wrap = wrap - 1
      return
      end
c ----------------------------------------------------------------------
      subroutine openfile( unitnumber, successfull )
      implicit none
      integer   unitnumber
      logical   successfull, error
      character filename*60, recordtype
      real      x, y

      logical           formatted
      common /filetype/ formatted

      successfull = .true.
      write(*,*) 'Enter filename:'
      read (*,*,err=20) filename

      formatted = .false.
      error     = .false.
      open(unit=unitnumber,file=filename,status='old',form='u',err=10)
      call readfile(unitnumber,recordtype,x,y,error,error)
      if( .not. error ) then
```

```
        rewind(unitnumber)
        print *, 'This is an UNFORMATTED file'
        return
      endif
      close(unitnumber)

   10 formatted = .true.
      error     = .false.
      open(unit=unitnumber,file=filename,status='old',form='f',err=20)
      call readfile(unitnumber,recordtype,x,y,error,error)
      if( .not. error ) then
        rewind(unitnumber)
        print *, 'This is a FORMATTED file'
        return
      endif
      close( unitnumber )

   20 successfull = .false.
      write(*,*) '* * * * * * * * * * * * * * * * * * * * * *'
      write(*,*) '*  ERROR:  Unable to open ', filename
      write(*,*) '* * * * * * * * * * * * * * * * * * * * * *'
      return
      end
c ----------------------------------------------------------------------
      subroutine readfile( unitnumber, recordtype, x, y, error, eof )
      implicit  none
      integer   unitnumber
      character recordtype, string*30
      real      x, y
      logical   eof, error

      logical           formatted
      common /filetype/ formatted

      if( formatted ) then
        read(unitnumber,'(a30)',err=10,end=20) string
        read(string(1:2), *,err=10) recordtype
        read(string(3:30),*,err=10) x, y
      else
        read(unitnumber,err=10,end=20) recordtype, x, y
      endif
      return
```

```
   10 error = .true.
   20 eof   = .true.
      return
      end
c ======================================================================
c   Description:  Construct defect loops.
c        Author:  Glen Granzow
c          Date:  April 17, 1997
c ----------------------------------------------------------------------
      subroutine defectloops(L)
      implicit  none
      integer   i, j, kount, error1, error2, xshift, yshift
      real      L, xminloop, xmaxloop, yminloop, ymaxloop
      data      error1, error2 / 0, 0 /

      integer ksize
      parameter( ksize=100000 )
      integer ndefects, killer(ksize), xwrap(ksize,2), ywrap(ksize,2)
      real    xmin(ksize), xmax(ksize), ymin(ksize), ymax(ksize)
      common /bubbles/
     *        ndefects, killer, xwrap, ywrap, xmin, xmax, ymin, ymax

      logical   found(ksize)
      data      found / ksize*.false. /

      do 40 i = 1, ndefects
        if( found(i) ) go to 40
        found(i) = .true.
        kount = 1
        xminloop = xmin(i)
        xmaxloop = xmax(i)
        yminloop = ymin(i)
        ymaxloop = ymax(i)
        if( killer(i) .ne. i ) then
          j = i
          xshift = 0
          yshift = 0
   25     kount = kount + 1
          if( killer(j).le.0 .or. killer(j).gt.ndefects ) then
c            print *, 'ERROR #1: (inappropriate defect number)',
c     *                          j, killer(j)
            error1 = error1 + 1
            go to 40
```

```
          endif
          if( found(killer(j)) ) then
c            print *, 'ERROR #2: (defect in two loops)', j, killer(j)
            error2 = error2 + 1
            go to 40
          endif
          xshift = xshift + xwrap(j,1) - xwrap(killer(j),2)
          yshift = yshift + ywrap(j,1) - ywrap(killer(j),2)
          j = killer(j)
          found(j) = .true.
          xminloop = min( xminloop, xmin(j) + xshift*L )
          xmaxloop = max( xmaxloop, xmax(j) + xshift*L )
          yminloop = min( yminloop, ymin(j) + yshift*L )
          ymaxloop = max( ymaxloop, ymax(j) + yshift*L )
          if( killer(j) .ne. i ) go to 25
        endif
        call histogram(0,2,float(kount),0.,0.,0,0)
        call histogram(3,2, xmaxloop-xminloop, 0.,0.,0,0)
        call histogram(4,2, ymaxloop-yminloop, 0.,0.,0,0)
   40 continue

      print *, 'Highest defect number is', ndefects
      print *, 'Error counters:'
      print *, 'ERROR #1: (inappropriate defect number)', error1
      print *, 'ERROR #2: (defect in two loops)        ', error2
      return
      end
c ======================================================================
c   Description:  Generic histogram subroutine.
c        Author:  Glen Granzow
c          Date:  May 3, 1997
c         Usage:  option = 1: initialize
c                 option = 2: accumulate data
c                 option = 3: calculate statistics and histogram
c          Note:  minbucket and bucketsize are only used when option = 1
c                 value is only used when option = 2
c                 plotoption and fileunit are only used when option = 3
c       Version:  Writes statistics file (when option=3 & fileunit>0)
c ----------------------------------------------------------------------
      subroutine histogram
     *  (dataset,option,value,minbucket,bucketsize,plotoption,fileunit)
      implicit none
      integer  dataset, option, plotoption, fileunit
```

```
      real     value, minbucket, bucketsize

      integer   nbuckets, ndatasets
      parameter ( nbuckets = 1000, ndatasets = 5 )
      integer   n(0:ndatasets), toosmall(0:ndatasets),
     *          toobig(0:ndatasets), hstgrm(0:ndatasets,0:nbuckets),
     *          bucket, peak, k, mink, maxk, k1, i, sum3, median
      real      minbucketarray(0:ndatasets),
     *          bucketsizearray(0:ndatasets),
     *          minvalue(0:ndatasets), maxvalue(0:ndatasets),
     *          sum1(0:ndatasets), sum2(0:ndatasets), mean, variance,
     *          peakvalue, medianvalue
      save      n, toosmall, toobig, hstgrm,
     *          minbucketarray, bucketsizearray, minvalue, maxvalue,
     *          sum1, sum2
      character a(50), filename*17
      data      a / 50*']' /

      if( dataset .gt. ndatasets ) then
        print *, 'ERROR IN SUBROUTINE HISTOGRAM:  dataset =', dataset
        print *, '     is larger than parameter ndatasets =', ndatasets
        stop
      endif

      if( option .eq. 1 ) then

        n(dataset) = 0
        toosmall(dataset) = 0
        toobig(dataset) = 0
        do bucket = 0, nbuckets
          hstgrm(dataset,bucket) = 0
        enddo
        minvalue(dataset) =  1.e38
        maxvalue(dataset) = -1.e38
        sum1(dataset) = 0.
        sum2(dataset) = 0.
        minbucketarray(dataset)  = minbucket
        bucketsizearray(dataset) = bucketsize

      elseif( option .eq. 2 ) then

        n(dataset) = n(dataset) + 1
        bucket=(value-minbucketarray(dataset))/bucketsizearray(dataset)
```

```
        if( bucket .lt. 0 ) then
          toosmall(dataset) = toosmall(dataset) + 1
        elseif( bucket .gt. nbuckets ) then
          toobig(dataset) = toobig(dataset) + 1
        else
          hstgrm(dataset,bucket) = hstgrm(dataset,bucket) + 1
        endif
        minvalue(dataset) = min(value,minvalue(dataset))
        maxvalue(dataset) = max(value,maxvalue(dataset))
        sum1(dataset) = sum1(dataset) + value
        sum2(dataset) = sum2(dataset) + value*value

      elseif( option .eq. 3 ) then

        peak = 0
        sum3 = toosmall(dataset)+hstgrm(dataset,0)
        median = 0
        do bucket = 1, nbuckets
          if( hstgrm(dataset,bucket) .gt. hstgrm(dataset,peak) )
     *      peak = bucket
          if( sum3 .lt. n(dataset)/2 ) median = bucket
          sum3 = sum3 + hstgrm(dataset,bucket)
        enddo

        peakvalue =
     *    minbucketarray(dataset)+(.5+peak)*bucketsizearray(dataset)
        medianvalue =
     *    minbucketarray(dataset)+(.5+median)*bucketsizearray(dataset)

        mean = sum1(dataset)/real(n(dataset))
        variance = sum2(dataset)/n(dataset)-mean*mean

        print *, '       n:', n(dataset)
        print *, '     min:', minvalue(dataset)
c        print *, '    peak:', peakvalue,
c     *    '  (',hstgrm(dataset,peak),' occurances, ',
c     *    'probability:',real(hstgrm(dataset,peak))/real(n(dataset)),' )'
c        if( median .lt. nbuckets )
c     *    print *, '  median:', medianvalue
        print *, '     max:', maxvalue(dataset)
        print *, '    mean:', mean
c        print *, 'variance:', variance
        print *, ' std dev:', sqrt(variance)
```

```
      if( toosmall(dataset) .ne. 0 )
     *   print *, 'WARNING: ', toosmall(dataset),
     *            ' values were too small to be included in histogram'

      if( toobig(dataset) .ne. 0 )
     *   print *, 'WARNING: ', toobig(dataset),
     *            ' values were too big to be included in histogram'

      mink = (minvalue(dataset)-minbucketarray(dataset))
     *       /bucketsizearray(dataset)
      mink = max(0,mink)
      maxk = (maxvalue(dataset)-minbucketarray(dataset))
     *       /bucketsizearray(dataset)
      maxk = min(nbuckets,maxk)

      if( plotoption .eq. 1 ) then
        do k = mink, maxk
          k1 = (hstgrm(dataset,k)*50)/hstgrm(dataset,peak)
          write(*,100) k, (a(i),i=1,k1)
        enddo
      endif
      print *,
     * '------------------------------------------------------------'

      if( fileunit .gt. 0 ) then
        write(filename,200) dataset/10, dataset
        print *, 'Writing ', filename
        open(fileunit,file=filename,err=99)
        do k = mink, maxk
          write(fileunit,*,err=99)
     *      minbucketarray(dataset)+(.5+k)*bucketsizearray(dataset),
     *      max( 1.e-15, real(hstgrm(dataset,k))/real(n(dataset)) )
        enddo
        close(fileunit)
        write(filename,300) dataset/10, dataset
        open(fileunit,file=filename,err=99)
        write(fileunit,*,err=99) '       n:', n(dataset)
        write(fileunit,*,err=99) '     min:', minvalue(dataset)
        write(fileunit,*,err=99) '     max:', maxvalue(dataset)
        write(fileunit,*,err=99) '    mean:', mean
        write(fileunit,*,err=99) 'variance:', variance
        write(fileunit,*,err=99) ' std dev:', sqrt(variance)
        if( toosmall(dataset) .ne. 0 )
```

```
     *      write(fileunit,*,err=99) 'WARNING: ', toosmall(dataset),
     *        ' values were too small to be included in histogram'
          if( toobig(dataset) .ne. 0 )
     *      write(fileunit,*,err=99) 'WARNING: ', toobig(dataset),
     *        ' values were too big to be included in histogram'
          close(fileunit)
        endif

      endif
      return
 99   print *, 'WARNING:  Error writing file ', filename
      close(fileunit)
      return
100   format(i3,': ',50a1)
200   format('histogram.data.',2i1)
300   format('statistics.',2i1)
      end
c ======================================================================
```